Final Report

FDOT Contract No.: BDK75 977-23
UF Contract No.: 00083426

Development of Variable LRFD ϕ Factors for Deep Foundation Design Due to Site Variability

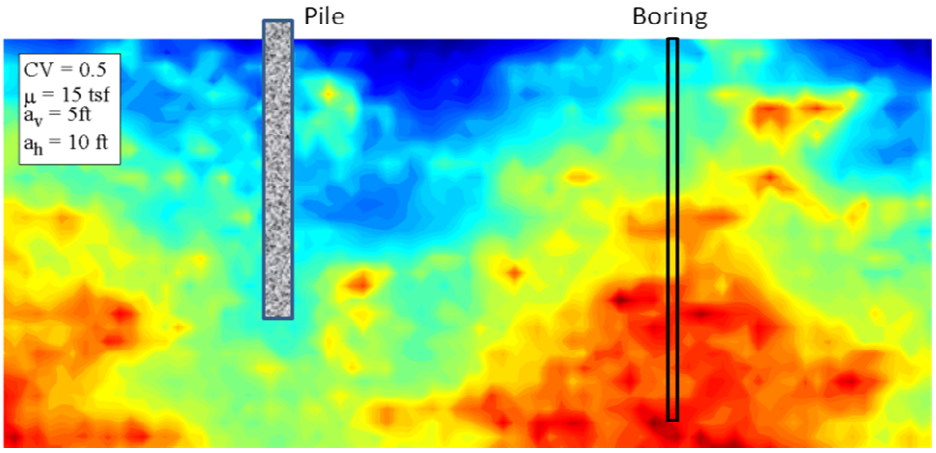

Principal Investigators: Michael C. McVay
Harald Klammler
Graduate Research Assistants: Michael A. Faraone
Krishnarao Dase
Chris Jenneisch

Department of Civil and Coastal Engineering
Engineering School of Sustainable Infrastructure and Environment
University of Florida
P.O. Box 116580
Gainesville, Florida 32611-6580

Developed for the

Peter Lai, P.E., and Rodrigo Herrera, P.E., Project Managers

June 2012

DISCLAIMER

The opinions, findings, and conclusions expressed in this publication are those of the authors and not necessarily those of the Florida Department of Transportation or the U.S. Department of Transportation.

Prepared in cooperation with the State of Florida Department of Transportation and the U.S. Department of Transportation.

SI (MODERN METRIC) CONVERSION FACTORS (from FHWA)

APPROXIMATE CONVERSIONS TO SI UNITS

SYMBOL	WHEN YOU KNOW	MULTIPLY BY	TO FIND	SYMBOL
LENGTH				
in	inches	25.4	millimeters	mm
ft	feet	0.305	meters	m
yd	yards	0.914	meters	m
mi	miles	1.61	kilometers	km

SYMBOL	WHEN YOU KNOW	MULTIPLY BY	TO FIND	SYMBOL
AREA				
in^2	square inches	645.2	square millimeters	mm^2
ft^2	square feet	0.093	square meters	m^2
yd^2	square yard	0.836	square meters	m^2
ac	acres	0.405	hectares	ha
mi^2	square miles	2.59	square kilometers	km^2

SYMBOL	WHEN YOU KNOW	MULTIPLY BY	TO FIND	SYMBOL
VOLUME				
fl oz	fluid ounces	29.57	milliliters	mL
gal	gallons	3.785	liters	L
ft^3	cubic feet	0.028	cubic meters	m^3
yd^3	cubic yards	0.765	cubic meters	m^3
NOTE: volumes greater than 1000 L shall be shown in m^3				

SYMBOL	WHEN YOU KNOW	MULTIPLY BY	TO FIND	SYMBOL
MASS				
oz	ounces	28.35	grams	g
lb	pounds	0.454	kilograms	kg
T	short tons (2000 lb)	0.907	megagrams (or "metric ton")	Mg (or "t")

SYMBOL	WHEN YOU KNOW	MULTIPLY BY	TO FIND	SYMBOL
TEMPERATURE (exact degrees)				
°F	Fahrenheit	5 (F-32)/9 or (F-32)/1.8	Celsius	°C

SYMBOL	WHEN YOU KNOW	MULTIPLY BY	TO FIND	SYMBOL
ILLUMINATION				
fc	foot-candles	10.76	lux	lx
fl	foot-Lamberts	3.426	candela/m^2	cd/m^2

SYMBOL	WHEN YOU KNOW	MULTIPLY BY	TO FIND	SYMBOL
FORCE and PRESSURE or STRESS				
Lbf*	poundforce	4.45	newtons	N
kip	kip force	1000	pounds	lbf
lbf/in^2	poundforce per square inch	6.89	kilopascals	kPa

APPROXIMATE CONVERSIONS TO SI UNITS

SYMBOL	WHEN YOU KNOW	MULTIPLY BY	TO FIND	SYMBOL
		LENGTH		
mm	millimeters	0.039	inches	in
m	meters	3.28	feet	ft
m	meters	1.09	yards	yd
km	kilometers	0.621	miles	mi

SYMBOL	WHEN YOU KNOW	MULTIPLY BY	TO FIND	SYMBOL
		AREA		
mm^2	square millimeters	0.0016	square inches	in^2
m^2	square meters	10.764	square feet	ft^2
m^2	square meters	1.195	square yards	yd^2
ha	hectares	2.47	acres	ac
km^2	square kilometers	0.386	square miles	mi^2

SYMBOL	WHEN YOU KNOW	MULTIPLY BY	TO FIND	SYMBOL
		VOLUME		
mL	milliliters	0.034	fluid ounces	fl oz
L	liters	0.264	gallons	gal
m^3	cubic meters	35.314	cubic feet	ft^3
m^3	cubic meters	1.307	cubic yards	yd^3

SYMBOL	WHEN YOU KNOW	MULTIPLY BY	TO FIND	SYMBOL
		MASS		
g	grams	0.035	ounces	oz
kg	kilograms	2.202	pounds	lb
Mg (or "t")	megagrams (or "metric ton")	1.103	short tons (2000 lb)	T

SYMBOL	WHEN YOU KNOW	MULTIPLY BY	TO FIND	SYMBOL
		TEMPERATURE (exact degrees)		
°C	Celsius	1.8C+32	Fahrenheit	°F

SYMBOL	WHEN YOU KNOW	MULTIPLY BY	TO FIND	SYMBOL
		ILLUMINATION		
lx	lux	0.0929	foot-candles	fc
cd/m^2	candela/m^2	0.2919	foot-Lamberts	fl

SYMBOL	WHEN YOU KNOW	MULTIPLY BY	TO FIND	SYMBOL
		FORCE and PRESSURE or STRESS		
N	newtons	0.225	poundforce	lbf
kPa	kilopascals	0.145	poundforce per square inch	lbf/in^2

*SI is the symbol for International System of Units. Appropriate rounding should be made to comply with Section 4 of ASTM E380.
(Revised March 2003)

TECHNICAL REPORT DOCUMENTATION PAGE

1. Report No.	2. Government Accession No.	3. Recipient's Catalog No.

4. Title and Subtitle	5. Report Date
Development of Variable LRFD ϕ Factors for Deep Foundation Design Due to Site Variability	April 2012
	6. Performing Organization Code
7. Author(s) Michael C. McVay, Harald Klammler, and Michael A. Faraone, Krishnarao Dase, Chris Jenneisch	8. Performing Organization Report No.
9. Performing Organization Name and Address University of Florida – Dept. of Civil and Coastal Engineering Engineering School of Sustainable Infrastructure & Environment 365 Weil Hall – P.O. Box 116580 Gainesville, FL 32611-6580	10. Work Unit No. (TRAIS)
	11. Contract or Grant No. BDK75 977-23
12. Sponsoring Agency Name and Address Florida Department of Transportation 605 Suwannee Street, MS 30 Tallahassee, FL 32399	13. Type of Report and Period Covered Final Report 9/1/10 – 5/1/12
	14. Sponsoring Agency Code

15. Supplementary Notes

16. Abstract

The current design guidelines of Load and Resistance Factor Design (LRFD) specifies constant ϕ values for deep foundation design, based on analytical method selected and degree of redundancy of the pier. However, investigation of multiple sites in Florida reveals significant variability of soil/rock properties from site to site (costal conditions) suggesting the introduction of variable ϕ values based on reliability-based design approach. Building on previous work (**BD545-76**) a geostatistical (variograms) approach was developed to quantify the spatial uncertainty for site specific conditions. As a result, ϕ values are evaluated due to both a site's measured spatial uncertainty and error associated with a particular analytical method.

This report summarizes subsequent efforts to further expand the applicability of the reliability design to the analytical models currently available in the FB-DEEP software program. For the geostatistical analysis, a simple yet robust graphical user interface (GUI) was developed, which considers two design scenarios: 1) conditioning to nearby boring data, and 2) unconditional mean site data. For either scenario the GUI generates thousands of potential data sets, which are evaluated by FB-DEEP to asses mean pile/shaft resistance and spatial uncertainty at a pier location. Spatial uncertainty is then combined with the design method error associated with the selected FB-DEEP model to asses ϕ. For demonstration of the application of the GUI, standard penetration test (SPT) and laboratory strength data were collected from seven FDOT projects and subsequent ϕ values were evaluated. The ϕ values ranged from 0.3 to 0.7 depending upon amount of subsurface data, measure summary statistics, and degree of spatial correlation. The report concludes with recommendations (in situ measurements, load testing, etc.) on improving the computed ϕ on a site-by-site basis.

17. Key Words	18. Distribution Statement
Deep Foundations, LRFD ϕ, Spatial Variability, Method Error, and Case Studies	No restrictions.

19. Security Classif. (of this report)	20. Security Classif. (of this page)	21. No. of Pages	22. Price
Unclassified	Unclassified	134	

Form DOT F 1700.7 (8-72) Reproduction of completed page authorized

ACKNOWLEDGMENTS

The researchers would like to thank the Florida Department of Transportation (FDOT) for the financial support to carry out this research, as well as the input of the central office geotechnical engineers in the collection of site data (spreadsheets, load test reports, and borings) for Jewfish Creek, CR12A, MIC, and MIC station. In addition, this research could not have been completed without the aid of the State Materials Office (SMO), which was instrumental in conducting additional laboratory/field testing at a number of bridge sites (Dixie Highway, 17th Street, and Keystone Heights). Also, the districts were of great help in locating and ensuring that the field testing occurred near the identified load test shaft plans.

EXECUTIVE SUMMARY

Current load and resistance factored design (LRFD) codes (Florida Department of Transportation (FDOT); and American Association of State Highway and Transportation Officials (AASHTO) list resistance factor, ϕ, values for a variety of deep foundation design approaches e.g., [standard penetration test blow count (SPT N), cone penetration test(CPT), rock compressive strength (q_u)]. All of the reported values were established from comparison of load test resistance with predictions from nearby borings. However, none of the evaluations accounted for the inherent spatial variability that exists from site-to-site or from layer-to-layer on a site. This site or layer variability may be represented by coefficient of variation, CV, or the variance of the soil/rock properties divided by the mean value. For example, variability(CV) varies from 0.4 to 0.8 for rock and 0.3 to 0.7 for SPT N for soils in Florida.

Besides point variability (CV), the soil/rock properties are generally spatially correlated, i.e., transition from weak to strong or vice versa as a function of distance. Examples of correlation length vary from 3 ft up to 15 ft for Florida soils and rocks. Depending on the site's correlation structure, as well as point variability (CV), the uncertainty of a pile or shaft axial resistance will vary. Also contributing to the pile or shaft's total uncertainty of resistance and the resulting LRFD ϕ, is the uncertainty of the method σ_ϵ^2, which is associated with the prediction method, construction practices, etc. The use of databases, or more recently the use of load testing, on the site allows the evaluation of σ_ϵ^2 on a site-by-site basis.

The first research to account for site-specific variability in LRFD ϕ was FDOT research project **BD545-76**. Specifically, site-specific ϕ was developed from total uncertainty σ_R^2, which was found as the sum of both the spatial uncertainty σ_s^2 and method uncertainty σ_ϵ^2. Since this work focused on only skin friction of drilled shafts, there was great interest to extend this work to include end bearing, other types of foundations (e.g., piles), other in situ methods (CPT) and

boring locations, as well as automation, i.e., assisting the engineer in assessing site characteristics (layering, summary statistics, and correlation structure).

To assist the engineer with the development of LRFD ϕ on a site-by-site basis for any foundation type, a graphical user interface (GUI) was developed independently of pile/shaft analysis software (e.g., FB-DEEP). Using the GUI, the engineer reads in all boring (SPT and rock strength) data and laboratory data for the site for a geostatistical analysis. Specifically, they will break the site into zones and layers to determine point variability of each CV, as well as spatial correlation structure (vertical and horizontal variograms). Next, using kriging techniques, the GUI allows the engineer to estimate boring data with uncertainty (unconditional-all borings, or conditional-nearest boring) from which the design software (e.g., FB-DEEP) may be run to assess both the mean pile/shaft resistance, as well its spatial uncertainty. Subsequently, the GUI allows the engineer to add either site-specific method uncertainty or default values to determine total uncertainty CV_R from which site specific LRFD ϕ and recommended design resistance $\phi \bullet R_N$ as a function of depth is found.

The developed design approach, geostatistical (GUI) in combination with FB-DEEP, was subsequently used on seven bridge sites throughout Florida with variable amounts of field in situ, laboratory and field test results. The investigation revealed that LRFD ϕ varied from a low of 0.17 to a high of 0.8 over the sites as a function of depth, site investigation, and load testing. For instance, sites with minimal knowledge on vertical correlation (i.e., a_v) and samples (e.g., 18 rock core samples) had a ϕ value of 0.39, whereas another site with both vertical and horizontal in situ information had a ϕ value of 0.7. The research concludes with a discussion of recommendations to assist design engineers in assessing ϕ for a site, as well as recommendations on increasing ϕ on a site-by-site basis.

TABLE OF CONTENTS

page

LIST OF TABLES

LIST OF FIGURES

CHAPTER 1
INTRODUCTION

1.1 Background

The supports for most Florida Department of Transportation (FDOT) structures (bridges, elevated roadways, signage, etc.) are deep foundations (piles, drilled shafts, etc.). Generally, the dimensions of the foundation elements have gone from small to large (e.g., 18-inch to 30-inch pile, 42-inch to 84-inch drilled shaft); having fewer elements to reduce the size of the foundation's footprint (right-of-way issues) as well as lower costs. Unfortunately, fewer larger elements with higher volume-to-surface-area ratios result in higher variance of axial pile/shaft resistances. In addition, coastal bridge sites have observed large variability of soil properties. For example standard penetration test blow count (SPT N), cone penetration test (CPT), rock compressive strength (q_u) can have coefficient of variation (CV) range between 0.3 and 0.8, which can also be spatial correlated. Spatial variability is shown in Figure 1-1 for rock strength (cohesion) for 17th Street Bridge in Fort Lauderdale and Fuller Warren Bridge, Jacksonville.

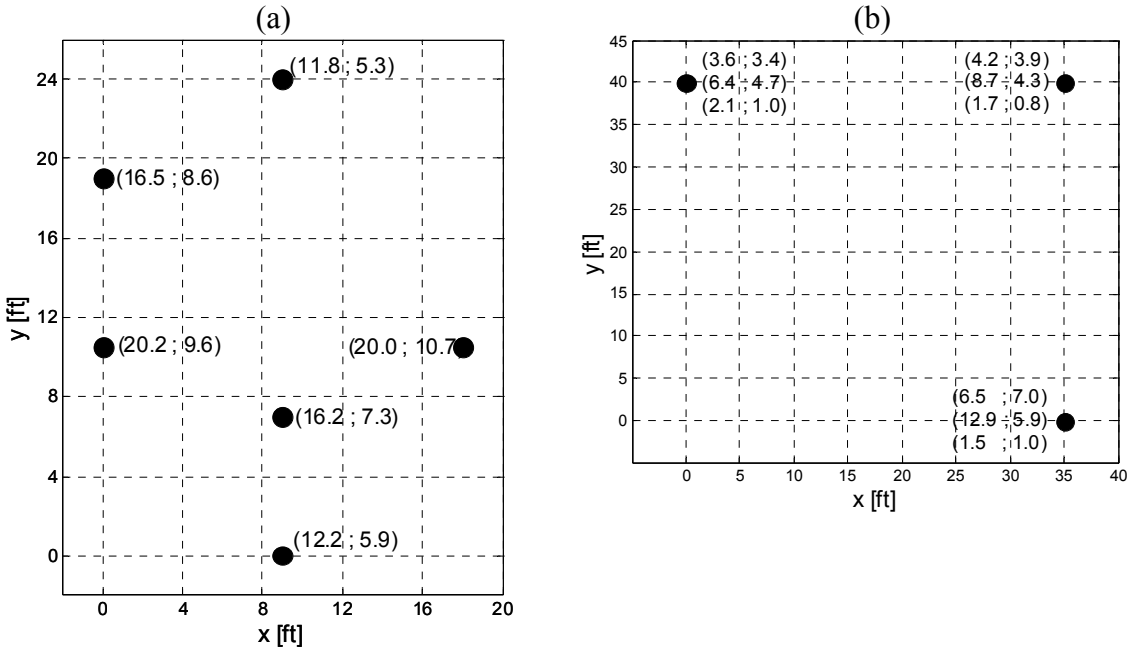

Figure 1-1. Mean and standard deviation of rock strength in boreholes: (a) 17th Street Bridge, Fort Lauderdale; and (b) Fuller Warren, Jacksonville.

The values next to each borehole are the mean and standard deviation in units of tons per square foot (tsf; 1 tsf =95.8 kPa) of the rock cohesion (c) over the depth of the borehole. In the case of Fuller Warren, two separate layers are present with the bottom two sets representing each layer value and the top set corresponding to the combined or single borehole value. Evident from both sites, significant difference in mean values exists from boring to boring (maximum 200%) over finite separation distances (from 15 ft to 40 ft separating). Unfortunately, the spatial borehole mean uncertainty translates into similar pile/shaft axial capacity uncertainty.

To account for uncertainty, the FDOT, Federal Highway Administration (FHWA), etc., have moved away from allowable stress design (ASD) to load and resistance factored design (LRFD) for deep foundations. Since LRFD models both the loads and the resistances on the pile/shaft as random variables, the resistance factors (ϕ) are assessed based on a reliability analysis (i.e., probability of load being greater than resistance). Using a database of load tests with adjacent boring/laboratory tests in Florida, the FDOT established LRFD resistance factors based on reliability indices of 2.5 to 3.0 (probability of failure 1/100 to 1/1000). For instance, shown in Figure 1-2 are current FDOT resistance factors for drilled shafts embedded in Florida limestone.

Unfortunately, at the time of the original FDOT LRFD development McVay et al. (1998), the databases contained load test results with a single boring (nearest) and little, if any, site spatial information. A recent FDOT study **BD545-76** revealed that Florida site variability (CV) ranges from 0.3 to 0.8 for soil/rock data, and the soil/rock properties are spatially correlated, e.g., Figure 1-1. Consequently, FDOT **BD545-76** separated total uncertainty of pile/shaft resistance into spatial and method (e.g., FB-DEEP, etc.) uncertainty. In the case of spatial uncertainty, plots of variance reduction (α) for borings in the footprint (Figure 1-3) or unconditional (all borings, Figure 1-4) were developed for drilled shafts founded in Florida limestone. For

instance, knowing the mean and CV_c of the rock strength and correlation lengths (a_v, a_h) with shaft dimensions (L, D), the shaft's resistance uncertainty due to spatial variability $\sqrt{\alpha}CV_q$ may be assessed from Figure 1-3 or 1-4. Adding the spatial variance to method error variance, the total uncertainty of the shaft resistance (CV_R) may be assessed using American Association of State Highway and Transportation Officials (AASHTO 2004) first order second moment (FOSM) approach, Figure 1-5. The LRFD ϕ for the design may be determined as function of reliability (β), or probability of failure.

3.6.3 Resistance Factors [10.5.5] ***(01/06)***[33]

Delete ***LRFD*** Table 10.5.5-3 and substitute ***SDG*** Table 3.5 for drilled shafts.

Table 3.5 Resistance Factors for Drilled Shafts (Bridge Foundations)

Loading	Design Method	Construction QC Method	Resistance Factor,φ	
			Redundant	Non-redundant[6]
Compression	For soil: FHWA alpha or beta method[1]	Std Specifications	0.60	0.50
	For rock socket: McVay's method[2] neglecting end bearing	Standard Specifications	0.60	0.50
	For rock socket: McVay's method[2] including 1/3 end bearing	Standard Specifications	0.55	0.45
	For rock socket: McVay's method[2]	Statnamic Load Testing	0.70	0.60
	For rock socket: McVay's method[2]	Static Load Testing	0.75	0.65
Uplift	For soil: FHWA alpha or beta method[1]	Std Specifications	Varies[1]	Varies[1]
	For rock socket: McVay's method[2]	Std Specifications	0.50	0.40
Lateral[3]	FBPier[4]	Std Specifications Or Lateral Load Test[5]	1.00	0.90

1. Refer to FHWA-IF-99-025, soils with N<15 correction suggested by O'Neill.
2. Refer to ***FDOT*** ***Soils and Foundation Handbook***.
3. Extreme event.
4. Or comparable lateral analysis program.
5. When uncertain conditions are encountered.
6. As defined in SDG 3.6.9.

Commentary: LRFD resistance factors are based on the probability of failure (Pf) of an element or group of elements resisting structural loads. When resistance factors were calibrated, the state of practice utilized redundant drilled shaft

Figure 1-2. Resistance factors table for drilled shafts socketed into limestone from *FDOT Structural Design Manual*.

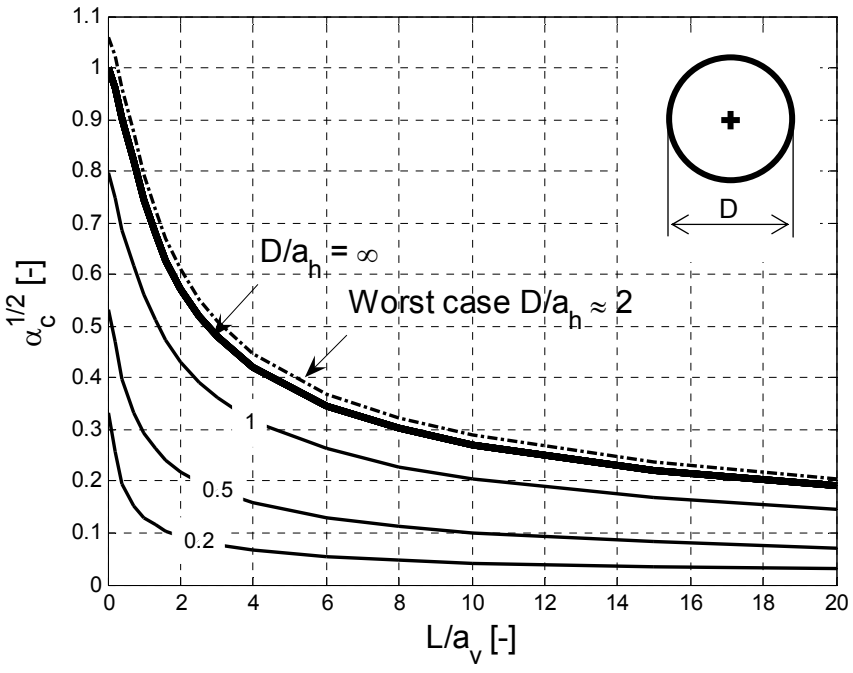

Figure 1-3. Variance reduction α as function of shaft length L, diameter D, and vertical a_v and horizontal a_h correlation lengths, boring in footprint.

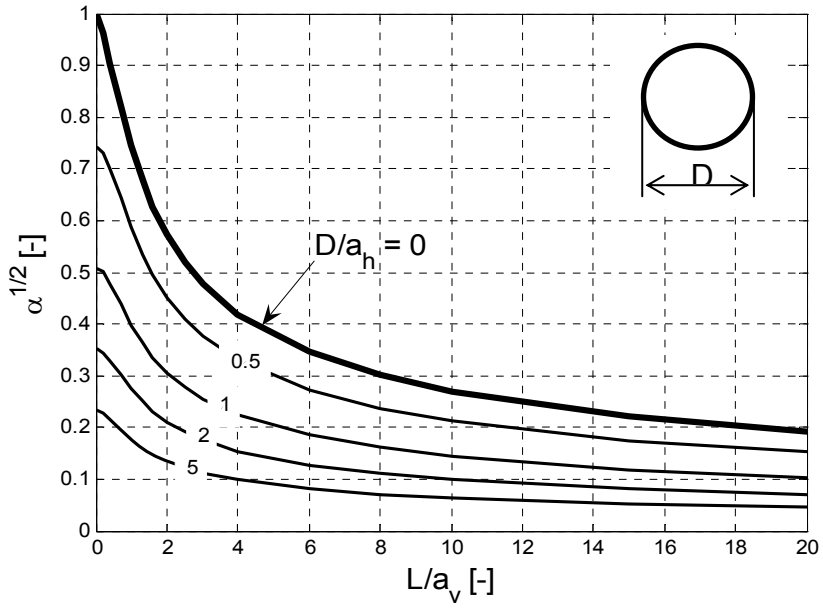

Figure 1-4. Unconditional variance reduction α as function of shaft length L, diameter D, and vertical a_v and horizontal a_h correlation lengths.

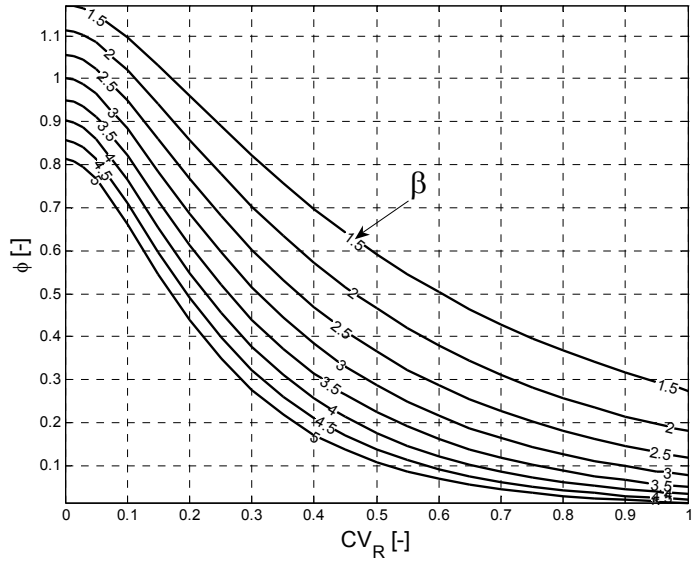

Figure 1-5. AASHTO (2004) LRFD ϕ as function of CV_R and reliability β.

1.2 Objective and Supporting Tasks

Of great interest was the extension of FDOT **BD545-76** LRFD ϕ assessment to other foundation types (piles), boring locations (i.e., conditioning), as well as in situ measurements (e.g., SPT and CPT). Also to assist the engineer, software (graphical user interface or GUI) to assess layer statistics (i.e., mean and variance) and spatial correlation (e.g., a_v and a_h) was required. Moreover, the GUI had to interface with axial capacity assessment software (e.g., FB-DEEP) to assess spatial uncertainty which had to be added to method error to obtain pile/shaft uncertainty and LRFD ϕ as a function of depth. To achieve this goal, the following four tasks were completed.

1.2.1 Task 1 – Collection of Boring and Static Load Test Data

For the verification, implementation, etc., it is important that static load tests on piles and shafts be obtained with site boring information. For design without load testing, boring data around the pile/shaft are acceptable to assess layer summary statistics (mean and variance), as well as spatial correlation (e.g.. a_v and a_h) and spatial uncertainty. The latter combined with a

conservative estimate of method error based on prior load testing may be used to assess LRFD ϕ. However with load testing, the relationship between mean load test results and predicted boring resistance may be established on a specific site (bias correction). The latter requires SPT or CPT boring in the footprint (removes spatial uncertainty) of the test piles/shafts. Besides Jewfish Creek, data from other sites with load testing and borings within the footprint must be collected.

1.2.2 Task 2 – Development of LRFD ϕ for Combined Side and Tip Resistance

As identified earlier, this effort is to extend **BD545-76** LRFD ϕ assessment to other deep foundation types. For piles and short shafts founded in strong soils/rock, a significant portion of total pile/shaft capacity will be provided by tip resistance. Consequently, the work must be extended to include total pile/shaft capacity, i.e., side resistance plus tip resistance. Like side resistance, the work must identify the variance reduction for tip resistance. For example, FB-DEEP assesses tip resistance by considering the blow count 3.5 diameters below the pile and 8 diameters above it. Specifically, each SPT N value within this zone is converted to a tip resistance and, subsequently, averaged. The latter averaging process results in a variance reduction in the estimated tip resistance and must be considered in assessing total capacity variance. Similarly within the bearing layer, the skin friction is adjusted based on tip resistance (i.e., friction ratio R_f) which introduces the covariance (i.e., variance of side resistance as a function of tip resistance) and must be considered. The work should consider the typical design approaches used by FDOT, such as the FB-DEEP method for pile design based on SPT or CPT.

1.2.3 Task 3 – Development of Expected Measured Load Test Resistance versus Predicted Boring Resistance Relationships with Uncertainty of Method σ_{ε}^2

Using the load test data collected in Task 1, the bias λ_R (measured divided by predicted) in AASHTO (2004) LRFD assessment will be replaced by mean predicted resistance $\mathbf{m_L}$, which is

estimated from the mean borehole resistance $\mathbf{m_B}$ through linear regression coefficients **a** (intercept) and **b** (slope). Conservative values of the **a** and **b** coefficients as well as uncertainty of method (σ^2) must be established for each of the design methods of interest, e.g., FB-DEEP SPT or CPT for cases where no load test data are available for site specific LRFD ϕ assessment. The work will also investigate the separate treatment of side and tip resistance (separate assessment of method error), as well as total pile capacity. The latter is needed for skin friction piles (i.e., uplift loads). Also, the work will consider Davisson and ultimate capacities of the piles.

1.2.4 Task 4 – Development of Nomographs or Spreadsheets for LRFD ϕ Implementation

To assist with the design verification, simple nomographs or spread sheets were originally planned to automatically compute variance reduction (e.g., Figure 1-3) for single pile/shafts or multiple pile/shafts along with LRFD ϕ assessment. In addition, for the covariance (i.e., correlation lengths a_v and a_h), a simple generic spreadsheet, which considered SPT N or CPT q_c values, was planned. However, during the completion of the work it was realized that the SPT N data may not be evenly spaced and the tip averaging is greatly influenced on strength of soil above the bearing layer, thus, conditioning from boring not in the footprint but within the correlation length a_h should be considered.

Therefore, it was decided to develop GUI that reads in all the borings on the site. Then the user defines layers, detrending of data (Kitanidis, 1997, bias removal), and the GUI computes each layer's summary statistics (mean and variance), and with user input it establishes spatial correlation parameters (a_v and a_h). Next, the user identifies the type of deep foundation (e.g., pile or drilled shaft) and type of analysis (unconditional using all borings or conditional using specific boring), and then the GUI generates thousands (e.g., 2 to 5 thousand) of boring profiles.

All of the latter boring profiles are run automatically through FB-DEEP (batch mode), and the GUI assesses the spatial uncertainty of side, tip, and total capacity. Subsequently, the method error is added to the spatial uncertainty, and the GUI computes total uncertainty (CV_R), the LRFD ϕ, and the recommended design resistance ϕ•Rn as a function of depth.

1.2.5 Task 5 – Case Studies of LRFD ϕ Assessment Considering Spatial Variability

Very important in the development and acceptance of LRFD ϕ with spatial soil/rock variability with load testing is a comparison with existing practice. Since Task 1 involves the collection of load testing results with boring data, the proposed pile/shaft design process (i.e., GUI) was used on multiple FDOT sites. The comparison considered both with and without load testing, as well as boring within the footprint or nearby. Multiple foundation types were investigated (i.e., piles and shafts), as well as multiple sites with different soil/rock conditions (i.e., number of borings, establishing horizontal spatial correlation, etc.). Also identified suggestions to improve a given site design. For instance, the discussion considered load testing or collecting more vertical or horizontal boring data.

1.2.6 Task 6 – Addition of Site Specific Data to the FDOT Database

Task 6 concerns the recovery and storage of all the static load test results, boring data (SPT/CPT), and laboratory strength data in the FDOT database for future use of FDOT. All of the data (SPT, CPT and laboratory data) were uploaded into the FDOT database using "in situ" and "lab test" Excel sheets located at (fdot.ce.ufl.edu/applications.html). Seven FDOT sites were uploaded and analyzed for this project.

CHAPTER 2
SPATIAL VARIABILITY ANALYSIS

2.1 Introduction

In the evaluation of the effects of spatial variability on LRFD ϕ factors of a deep foundation, in situ data (i.e., SPT-N, CPT-q_t, rock strength-q_u) must be obtained for capacity assessment. Depending on the calculation method (FB-DEEP), one or more in situ properties may be required. In a statistical sense this will require either a univariate (one variable) or multivariate analysis for multiple random variables that may be correlated. Additionally, these in situ parameters will also have an associated location in space (x-longitude, y-latitude, z-elevation). Depending on their separation distance, the values of the information may also be related (i.e., spatially correlated).

The study of spatially correlated random data started in the 1950s in the mining industry. It has experienced strong theoretical and practical developments with a number of introductory texts for engineers by Isaaks and Srivastava (1989) and Deutsch (2002). It has been expanded and applied to other fields, including agriculture, petroleum industry, environmental and other natural resources. Tools developed in this field can be readily applied to evaluate spatial variability of any site for the design of deep foundations. A discussion of the application of these tools follows.

2.2 Description of Site with a Random Variable

In a geostatistical analysis, any in situ measurement (e.g., SPT-N, CPT-q_c, etc.) becomes the random variable of interest over a spatial domain. To define this random variable requires a univariate analysis to determine the probability density function (PDF), which accounts for its mean, variance, and distribution type (i.e., normal, log-normal, etc.). Additionally, any apparent

spatial correlation must also be quantified. When performing a geostatistical analysis, it is assumed that the PDF and spatial correlation are constant throughout the spatial domain (i.e., layer) of interest. This is referred to as stationarity, a requirement needed for a geostatistical analysis.

The geostatistical analysis of a site begins with the determination of sub domains, layers, which are generally identified by inspection of in situ data as a function of depth. For instance, the delineation of a layer is either by constant or trending (i.e., higher or lower) mean over a specific depth interval. Examples of this process are shown in Figure 2-1, where Part A represents a site with two separate layers which have significant different mean values. Part B has two layers where Layer I is identified by a linear trend over its depth interval, and Layer II by a constant mean.

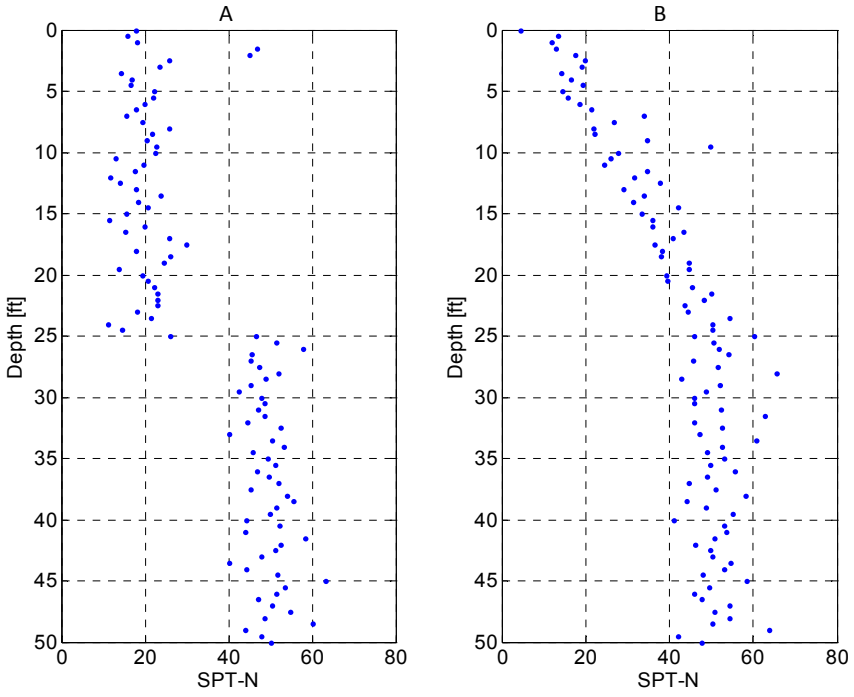

Figure 2-1. Example of layer identification.

Note when analyzing project sites, it is not unusual to encounter a strength profile that increases or decrease with depth. However, such a trend violates the requirement of stationarity

(i.e., fixed mean with depth). For a layer with a visible trend, the analysis should begin by fitting the apparent trend with a polynomial (recommended up to a 2nd order) as a function of depth. Next, the in situ properties for the layer are decomposed into two parts, the mean trend (polynomial function) and the random residual about that trend. An illustration of this can be seen in Figure 2-2, where the two components are added to obtain the representative behavior of the layer. Then, the trend is subtracted from the observed data to determine the spatial fluctuation about the trend. This component is used in the geostatistical analysis (i.e., identification of spatial correlation, etc.), and it meets the requirement of stationarity. Again, it is important to note that the observed trend information must be saved and added to the results of the spatial variability analysis (discussed later).

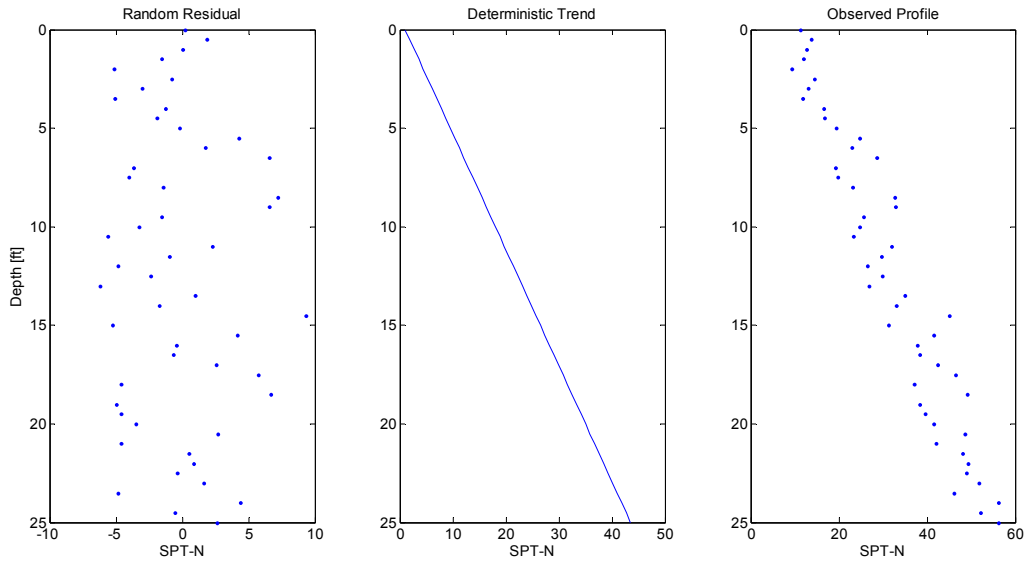

Figure 2-2. Separation of random residual from deterministic trend.

2.2.1 Histogram, Mean and Variance

After dividing the site into layers or zones and detrending the data for stationarity requirements, the data for each layer or zone need to be plotted in histogram form. The histogram allows the engineer to see the frequency ranges of data as well as its distribution (e.g., mode and mean align, etc.). Also, the histogram can be used to assess whether multiple

distributions are present within the zone or layer by the presence of multiple peaks or modes shown within the histogram.

In addition to the histogram, both the mean and variance of the data set (e.g., q_i) should be found,

$$\mu = \frac{1}{n}\sum_{i=1}^{n} q_i \quad \text{Eq. 2.1}$$

$$\sigma^2 = \frac{1}{n-1}\sum_{i=1}^{n}(q_i - \mu)^2 \quad \text{Eq. 2.2}$$

With these summary statistics, the coefficient of variation (CV) can be calculated as

$$CV = \frac{\sigma}{\mu} \quad \text{Eq. 2.3}$$

CV is a dimensionless quantity that represents the spread or dispersion of the data about the mean.

Based on the shape of the histogram's distribution, as well as summary statistics (mean vs. mode, etc.), an engineer should select the best PDFs that represent the measured data (e.g., normal, log-normal, etc.). Note, most soil properties (e.g., strength, modulus, etc.) have no negative values and have large ranges in values giving rise to significant differences in mode (most frequent) versus mean values and are best characterized through log-normal distributions.

2.2.2 Spatial Correlation and Variogram

In many instances, engineers fail to realize that geotechnical data are spatially variable, which may lead to unsafe foundation designs. A good indicator of spatial variability is simple evaluation of mean boring values within a zone or layer. For example, evaluation of mean strengths (e.g., cohesion or unconfined compression) from one boring to another at 17th Street Bridge in Fort Lauderdale (< 50-ft spacing), and Fuller Warren Bridge in Jacksonville (< 75-ft spacing) exhibit changes of 165% and 200%, respectively. This difference is directly attributed to spatial variability across a site and will result in similar variability in deep foundation axial

capacities. Moreover, since spatial variability generally possesses a certain degree of correlation, which decays with distance, the recommended LRFD resistance values for foundation design from data within the footprint or outside the footprint will be quite different.

The approach to assess spatial correlation is to plot pair values at prescribed separation distances. For example, all data pairs may be selected at a separation distance of 3 ft from one another (e.g., vertically) and plotted in a scatter plot, i.e., a figure where one data value q_i of the pair is on the x-axis and the other value q_j (located lag distance, h = 3 ft from q_i) on the y-axis. Other separation distances, called lag (h), may be selected and plotted from which correlation may be assessed. Shown in Figure 2-3 are the scatter plots for increasing lag distances, where the 45° line represents perfect correlation $q_i = q_j$. It can be seen that the least amount of scatter is present in (a), which has the smallest h. As h increases, it can be seen that the scatter about the 45° line increase from (b) to (c) grows, resulting in decreased correlation.

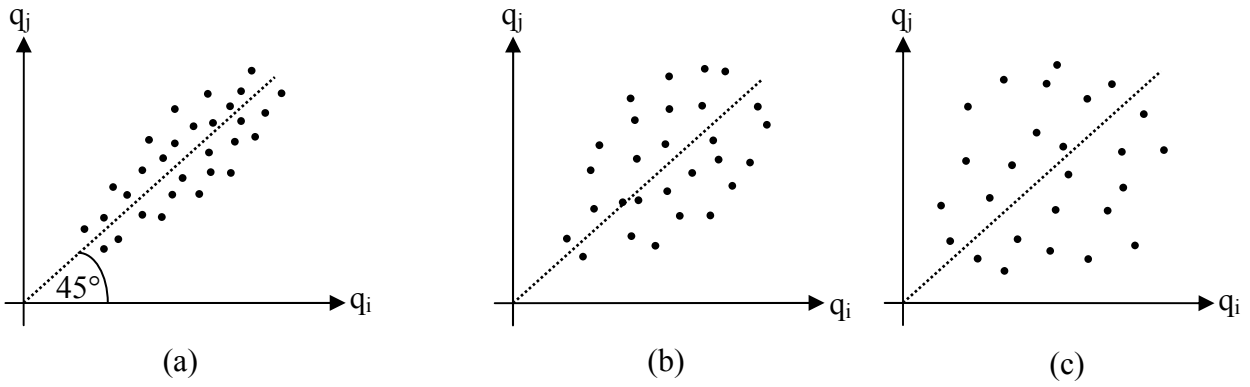

Figure 2-3. Data scatterplots for different separation (lag) distances of data pairs (q_i, q_j): Sequence of (a), (b), and (c) represents increasing separation distance and decreasing correlation. Dashed line is 45° and represents perfect correlation ($q_i = q_j$ or zero separation distance)(McVay et al. 2009).

To quantify the correlation for any lag distance h, the covariance may be computed as

$$C(h) = \frac{1}{n}\sum_{i,j=1}^{n}(q_i - \mu)(q_j - \mu) \qquad \text{Eq. 2.4}$$

where q_i and q_j are the data pairs separated by distance h and n is the number of these data pairs. For perfectly correlated data (i.e., $q_i = q_j$), C(h) is equal to the variance (Eq. 2.1). In the case of no correlation, C(h) = 0 (i.e., the product of the terms is both plus and minus and sums to zero). A dimensionless representation of the data's correlation is through the correlation coefficient

$$\rho(h) = \frac{C(h)}{\sigma^2} \qquad \text{Eq. 2.5}$$

with limits of zero and one ($0 < \rho(h) < 1$) representing no correlation and perfect correlation, respectively.

Another characterization of spatial correlation in geostatistics is the semi-variogram $\gamma(h)$ (referred to as variogram herein), which is given as

$$\gamma(h) = \frac{1}{2n}\sum\left(q_i - q_j\right)^2 \qquad \text{Eq. 2.6}$$

The covariance C(h) may be found from the variogram $\gamma(h)$ from the variance of the data σ^2 as

$$\gamma(h) = \sigma^2 - C(h) \qquad \text{Eq. 2.7}$$

Typical examples of C(h), $\rho(h)$ and $\gamma(h)$ as a function of h are shown in Figure 2-4. Evident from the figure, each function indicates a decreasing correlation with increasing h. At a distance, h = a (called the range), the correlation function goes to zero, or the data pairs become uncorrelated. In the case of the variogram Eq. 2.7, $\gamma(h=a) = \sigma^2$ [C(h) = 0] and its upper value or sill is reached. Generally, a function (e.g., spherical Eq. 2.8 or exponential Eq. 2.9) is fitted to the variogram or covariance data and is used to describe spatial correlation.

$$\gamma(h) = \begin{cases} \sigma^2\left(1.5\frac{h}{a} - 0.5\left(\frac{h}{a}\right)^3\right) & for\ h < a \\ \sigma^2 & for\ h \geq a \end{cases} \qquad \text{Eq. 2.8}$$

$$\gamma(h) = \sigma^2\left(1 - exp\left(\frac{-0.3|h|}{a}\right)\right) \qquad \text{Eq. 2.9}$$

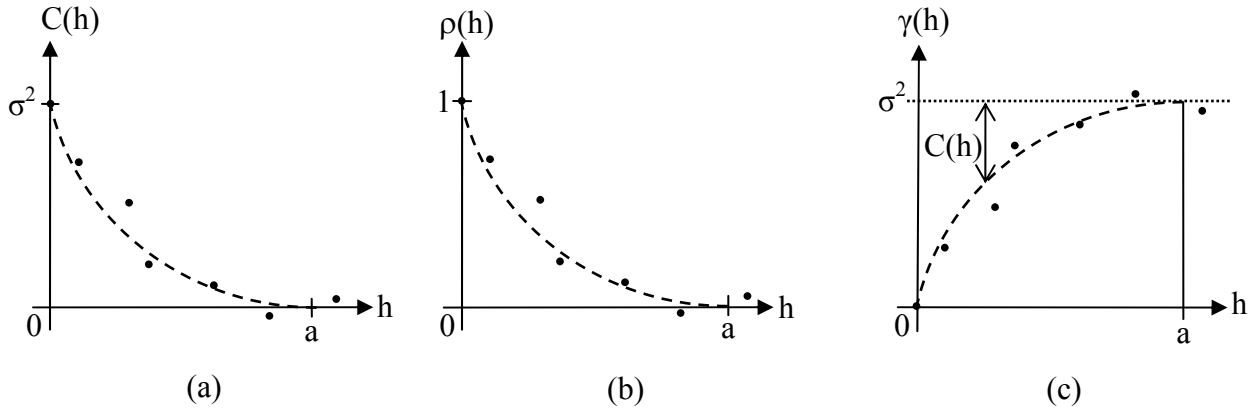

Figure 2-4. Graphical examples: (a) Spatial covariance function C(h); (b) Spatial correlation function $\rho(h)$; and (c) Variogram $\gamma(h)$. Dots represent experimental values derived from site data and Eq. 2.5, 2.6, and 2.7, respectively, while dashed lines represent variogram model fits of range a (McVay et al. 2009).

When generating variograms, it is recommended that large enough numbers of pairs $n \geq 30$ be used to obtain a reliable estimate of $\gamma(h)$. Also, since measured data can be irregularly spaced, a limited number of available pairs may ensue, unless the size of the search domain at a specific lag distance h is increased. This is illustrated in Figure 2-5 where the gray area represents the search domain that finds pairs used in Eq. 2.6. This search area is defined by parameters typically referred as the tolerance (tol) and bandwidth.

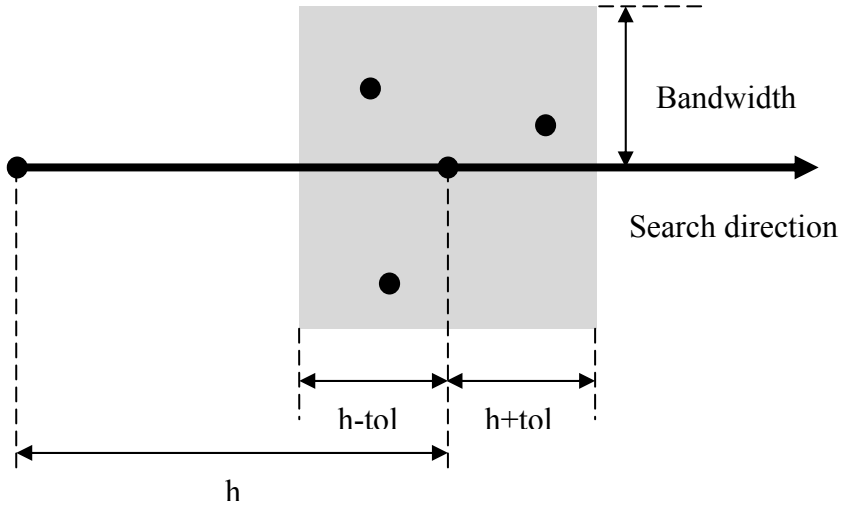

Figure 2-5. Tolerance and bandwidth selection for variogram.

The final variogram may have to be characterized as the sum of multiple individual variograms (i.e., nested) to represent the observed random function. An example of this is shown in Figure 2-6 for two structures that are defined by different ranges a_1 and a_2. For instance in Figure 2-6c, the horizontal dashed line with correlation length $a_1 = 0$ represents a "nugget effect" from either measurement errors or lack of data (i.e., smallest sampling distance), which is added to the a_2 variogram to represent the composite variogram (continuous line).

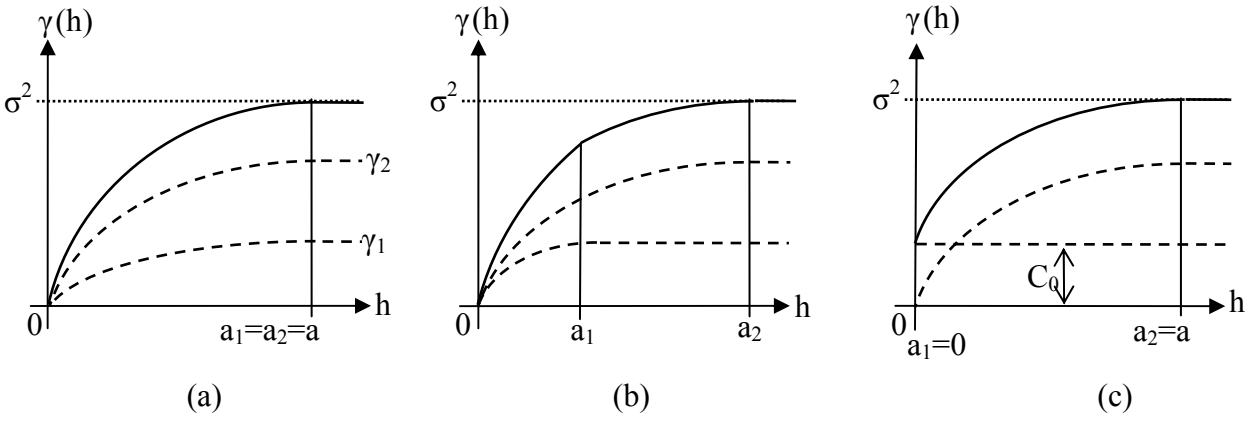

Figure 2-6. Examples of nested (composite) variograms: (a) Equal ranges $a_1 = a_2 = a$; (b) $a_1 < a_2$; and (c) $a_1 = 0$ representing a nugget effect of variance C_0 (McVay et al. 2009).

Also identified within the variograms are different forms of anisotropy. Geometric anisotropy refers to different correlation lengths in the vertical and horizontal direction. For instance, Figure 2-7a shows longer correlation length a_h in the horizontal direction than a_v in the vertical direction. Zonal anisotropy refers to different sills in the vertical and horizontal variances, i.e., $\sigma^2_v \neq \sigma^2_h$. For instance, Figure 2-7b shows higher variance σ^2_v in the vertical direction than the horizontal σ^2_h direction and may be generally attributed to random layering. Figure 2-7c shows higher variance in the horizontal versus the vertical direction (random areal trend), as well as geometric anisotropy (e.g., $a_v \neq a_h$). Note, it is very important to identify the

zonal anisotropy since its variance component, i.e., $\sigma^2_h - \sigma^2_v$, is not reduced through spatial averaging when estimating LRFD Φ values from boring data that is spaced far apart.

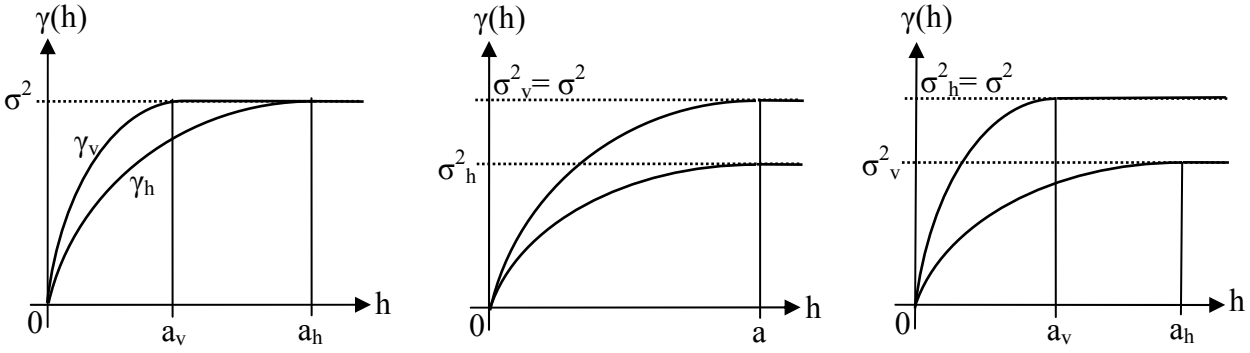

Figure 2-7. Examples of anisotropic variograms: (a) Geometric anisotropy with $a_h > a_v$; (b) Zonal anisotropy with $\sigma^2_h < \sigma^2_v$; and (c) Mix of geometric and zonal anisotropies with $a_h > a_v$ and $\sigma^2_h < \sigma^2_v$ (McVay et al. 2009).

2.3 Upscaling, Kriging and Change of Support Size

The estimation of the axial resistance of a deep foundation is typically determined by converting in situ measurements (e.g., SPT N, CPT q_c, etc.) to soil resistance (side – f_s & tip – q_t) and averaging the values over a domain (surface area – side friction, 3.5D below & 8D above – tip resistance). Any process associated with averaging of a spatially random variable,

$$\overline{f_s} = \frac{1}{\bar{n}} \sum_i^{\bar{n}} f_{s_i} \qquad \text{Eq. 2.10}$$

over a region (e.g., surface, line, etc.) that is spatially correlated will result in a variance reduction. This is typically referred to as "upscaling," i.e., going from in situ measurements at a point scale to resistance values for the whole pile or shaft foundation. The uncertainty (i.e., variance) of the mean over the region may be expressed as

$$\sigma^2_{\overline{f_s}} = \alpha_{\overline{f_s}} \sigma^2_{f_s} \qquad \text{Eq. 2.11}$$

Using the correlation function (Eq. 2.5), the reduction can be evaluated for any specified size of domain A, as

$$\alpha_{\overline{f_s}} = \frac{1}{A^2}\int_A\int_A \rho(h)\, dA_1 dA_2 \qquad \text{Eq. 2.12}$$

Generally, this equation can be solved numerically by averaging the correlation matrix (i.e., summing of elements and dividing by the number of elements) corresponding to a finite number of grid points located over the domain of interest (e.g., shaft surface)

$$\alpha_{\overline{f_s}} = \frac{1}{\bar{n}^2}\ \sum_i^{\bar{n}}\sum_j^{\bar{n}} \rho_{ij} \qquad \text{Eq. 2.13}$$

where $\bar{n}$ is the number of discrete grid points uniformly distributed over A_s. The use of $\alpha_{\overline{f_s}}$ in spatial variability analysis could be explored in FDOT phase 1 design where in situ samples are obtained; however, relative location of a foundation is unknown. In such analysis it is assumed that adequate in situ sampling occurs to quantify the mean, variance, and correlation structure of associated layers. An implementation of this analysis was conducted by Klammler et al. (2010a), for the evaluation of side friction of a shaft, which results in a mean resistance equal to the mean of the site and variance equal to the site variance reduced by $\alpha_{\overline{f_s}}$. Presented in Figure 2-8 Klammler et al. (2010a) is the solution of Eq. 2.12 for $\sqrt{\alpha_{\overline{fs}}}$ [$\sigma_{\overline{fs}}$] using an exponential form of covariance function in Eq. 2.5 [i.e., C(h)] as a function of foundation length L, diameter D, and spatial correlation lengths a_v (vertical) and a_h (horizontal).

In the case of FDOT phase 2 design, additional in situ samples are taken and foundation locations are known. In this case, the engineer can take advantage of having a boring located in the footprint or nearby which "conditions" the prediction. The geostatistical tool provided for this task is called ordinary kriging or best linear unbiased estimation. For instance, in the case of boring data SPT N or CPT q_c, a foundation's estimated average skin friction (after converting N$\rightarrow$$fs_i$ or $q_c \rightarrow fs_i$) may be given as

$$\widehat{f_s} = \frac{1}{\hat{n}}\sum_{i=1}^{\hat{n}} w_i f_{s_i} \qquad \text{Eq. 2.14}$$

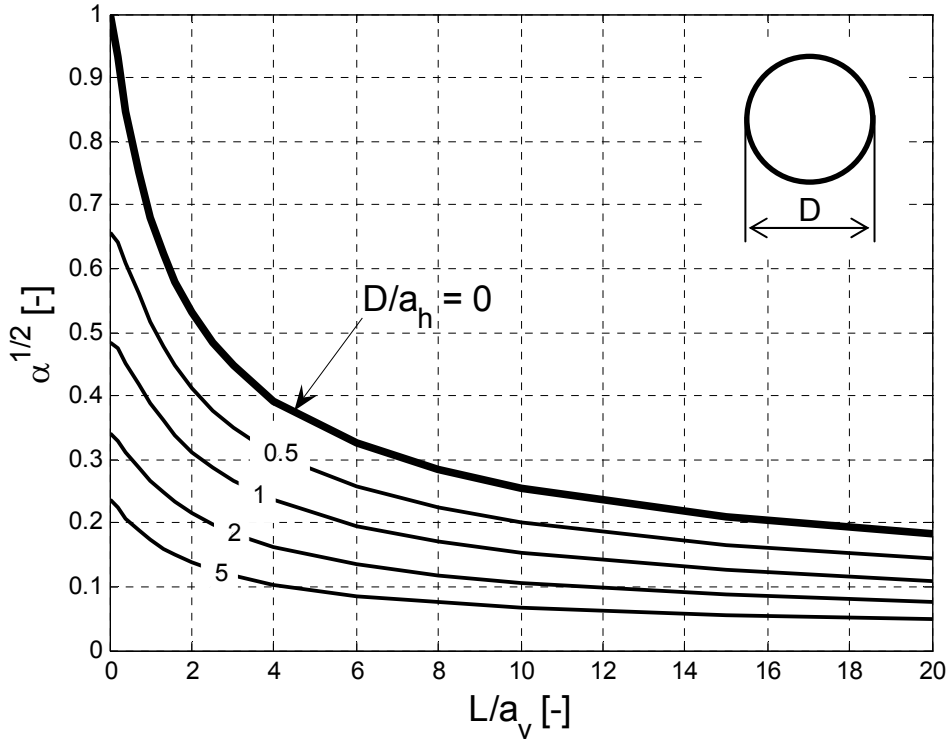

(b)

Figure 2-8. Term $\alpha^{1/2}$ as a function of L/a_v and D/a_h (Eq. 2.8) for single shafts with exponential covariance model (Klammler et al. 2010a).

where $\hat{n}$ may be the number of data within the borings, and w_i are weighting functions ($\sum w_i$) for individual borings. In the case of a single boring, $w_i = 1$. In the case of multiple borings, the weighting functions w_i are solved by minimizing the uncertainty of prediction σ_R^2 expressed as,

$$\sigma_R^2 = \sigma_{\overline{f_s}}^2 + \sigma_{\widehat{f_s}}^2 - 2COV\left(\overline{f_s}, \widehat{f_s}\right) \qquad \text{Eq. 2.15}$$

The first term on the right, $\sigma_{\overline{fs}}$, is again given by Eq. 2.11 and represents the uncertainty of the pile/shaft resistance from location A to B, assuming fs_i values are known on the surface of the shafts. The second term represents the uncertainty of the mean due to too few data (e.g., one boring with 10 values versus 10 borings with 20 values in each). Note, with sufficient data $\sigma_{\widehat{fs}}^2$, will go to zero. The third term in Eq. 2.15 represents the reduction (minus sign) in prediction mean shaft uncertainty due to boring data within the spatial correlation length (e.g., a_h) of the

foundation's surface. The weighting constants w_i (Eq. 2.14) may be solved from the following equations (Isaaks, 1989) as

$$\begin{bmatrix} \rho_{11} & \cdots & \rho_{1\hat{n}} & 1 \\ \vdots & \ddots & \vdots & \vdots \\ \rho_{\hat{n}1} & \cdots & \rho_{\hat{n}\hat{n}} & 1 \\ 1 & \cdots & 1 & 0 \end{bmatrix} * \begin{bmatrix} \omega_1 \\ \vdots \\ \omega_{\hat{n}} \\ \lambda \end{bmatrix} = \begin{bmatrix} \bar{\rho}_{1A_s} \\ \vdots \\ \bar{\rho}_{\hat{n}A_s} \\ 1 \end{bmatrix} \qquad \text{Eq. 2.16}$$

where ρ_{ij} represents the correlation function (Eq. 2.5) between boring i and boring j; $\bar{\rho}_{iA_s}$ is the correlation between boring measured values and the deep foundation surface A_s; and λ is a constant to ensure all the weights w_i sum to one. Once the weights are known, the uncertainty of prediction σ_R^2 (Eq. 2.15) may be solved (Isaaks, 1989) in terms of the weighting constants as

$$\sigma_R^2 = \sigma_{f_s}^2 \left[\alpha_{\bar{f}_s} + \sum_{i=1}^{\hat{n}} \sum_{j=1}^{\hat{n}} \omega_i \, \omega_j \rho_{ij} - 2 \sum_{i=1}^{\hat{n}} \omega_i \rho_{iA}\right] = \sigma_{f_s}^2 \alpha_c \qquad \text{Eq. 2.17}$$

Note, the terms in the bracket express the three terms in Eq. 2.15, and the total variance reduction of the boring variability $\sigma_{f_s}^2$) may be represented as α_c. In the case of a single boring within the footprint of the footing, the value of $\alpha_c^{1/2}$ as a function of footing length L, diameter D, and correlation lengths a_v and a_h, is given in Figure 2-9 (Klammler et al. 2010a). An examination of the figure reveals the worst case scenario (i.e., highest value of $\alpha_c^{1/2}$) occurs for the case of $D/a_h = 2$ (spatial correlation, $a_h = D/2$), which is just outside the foundation boundary or no reduction due to correlation, i.e., the third term (Eq. 2.15) is zero. Also, the uncertainty of mean due to limited data in the single boring (second term, Eq. 2.17) results in slightly higher total uncertainty($\alpha_c^{1/2}$) compared to variance reduction of fs_i by averaging over the shaft surface($\alpha_{\bar{f}_s}$ i.e., first term in Eq. 2.17) represented as the thick solid line in Figure 2-9.

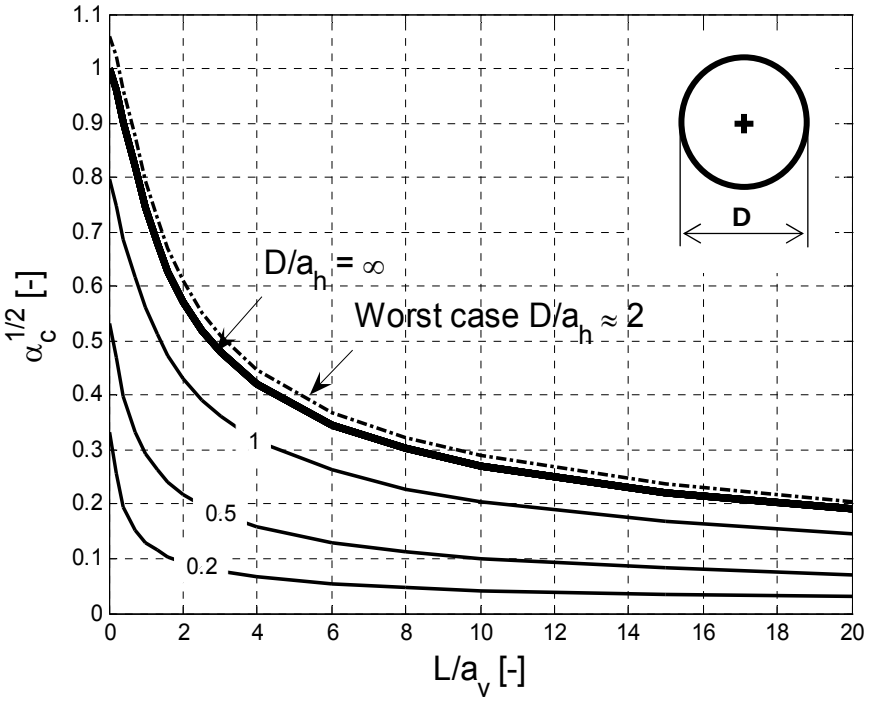

The thick continuous line for $D/a_h = \infty$ is identical to α_0 (line shaft approximation). The dash dotted line for $D/a_h \approx 2$ represents maximum values of $\alpha_c^{1/2}$ for a given L/a_v, while thin continuous lines indicate $\alpha_c^{1/2}$ for $D/a_h < 2$.

Figure 2-9. Term $\alpha_c^{1/2}$ for a single shaft with one single boring (cross) at the center as a function of L/a_v and D/a_h (Klammler et al. 2010a).

2.4 Estimation of the Effects of Spatial Variability by Stochastic Simulation

To assist an engineer in accounting for spatial uncertainty with any type of analysis (e.g., linear or nonlinear skin and tip resistance), a geostatistical method called stochastic simulation may be used. This process involves the generation of many realizations of point values on a specified grid that honor a given PDF and correlation structure. These realizations then can be used in capacity calculation (e.g., FB-DEEP, FB-MultiPier, etc.), which results in a distribution of capacities that quantifies the effects of spatial variability. When implementing the stochastic simulation process, the two cases discussed previously, i.e., complete site knowledge with an unknown foundation location and conditioning to a boring, need to be considered. The case of

complete site knowledge is analogous to unconditional simulations. In this process, values of a random variable are generated on a specified grid (i.e., line of points, shaft surface, volume) that reproduce the PDF and correlation structure of the site. An example of this can be seen in Figure 2-10 for the generation of unit side friction along the surface of a square pile. The case of conditioning to a boring is analogous to conditional simulations where the generated values at the grid points reproduce measured values at their locations (e.g., SPT N values).

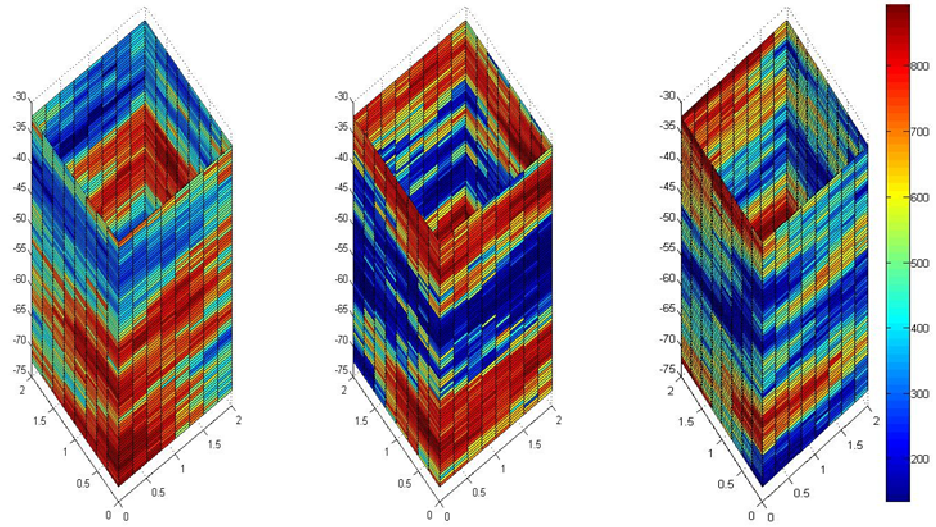

Figure 2-10. Example of realization of unit side friction along pile surface.

For the simulation, the LU decomposition algorithm was selected. The LU approach has the advantage of being able to generate a random field that represents the mean, variance, and correlation structure for both conditional and unconditional characterizations. In addition, the LU algorithm can generate points on a one-dimensional line (i.e., boring – pile assessment), two-dimensional surface (i.e., shaft surface area), or any volume of interest.

The simulation begins with the definition of grid points needed (i.e., volume, shaft surface, or boring). For k grid points in a Cartesian coordinate system, a k × k covariance matrix is created from the covariance function established from the variogram model. Next, the

covariance matrix is decomposed into upper U and lower L triangular matrices. The need for matrix decomposition brings the additional requirement that the covariance matrix be positive definite. To ensure that the covariance matrix generated is positive definite can be accomplished by the selection of the variogram model used as well as ensuring that no two grid points are identical. The lower triangular matrix L can be used in Eq. 2.18, where η is a vector of k independent standard normal deviates (mean = 0 and standard deviation = 1).

$$y = L\eta \qquad \text{Eq. 2.18}$$

The simulated grid y values are normally distributed and still need to meet the requirement of the target distribution from a measured data set. For this purpose, the simulated data are transformed by use of the normal score transformation process. This transformation uses cumulative distribution functions "CDF" of the measured data and a standard normal distribution to map the simulated y values onto its corresponding value in the target distribution. An example of this can be seen in Figure 2-11 where a value of a log-normal distribution is mapped

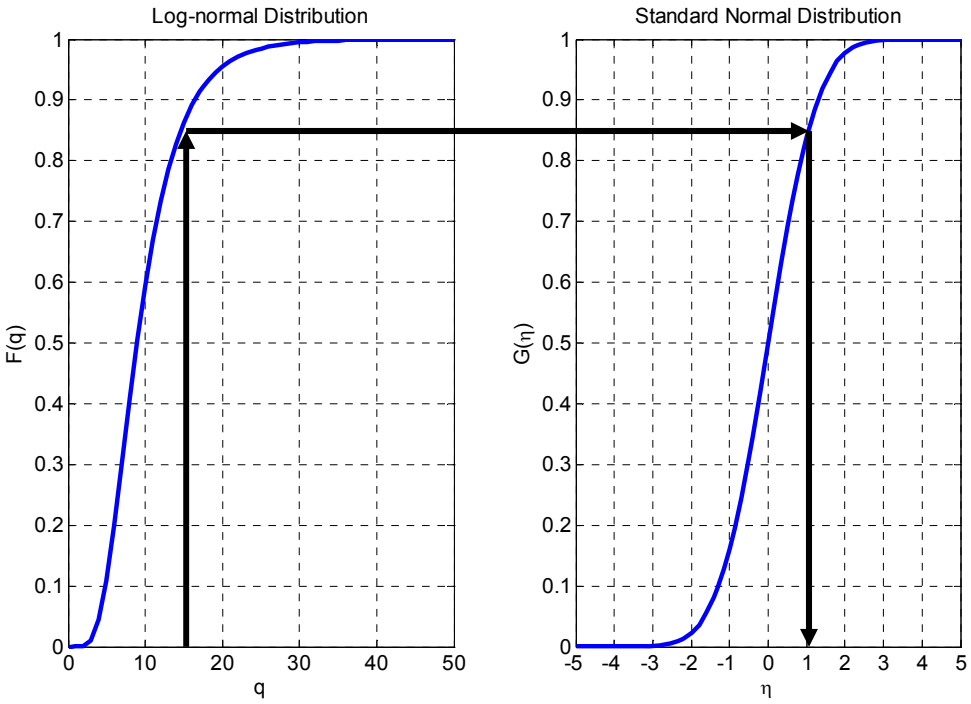

Figure 2-11. Normal score transform using CDFs.

onto a corresponding standard normal value using the CDFs of both distributions. It is also recommended that when analyzing semi-variograms for the project site that the measured data first be transformed to a standard normal distribution.

If an engineer wants to take advantage of having a boring located in the footprint or nearby the location of a foundation, the LU algorithm can be modified to achieve conditioning. As suggested by Emery (2007), the algorithm begins with generating the unconditional values at both the measured data location (u_α, α=1,…,n) and the grid points of interest using Eq. 2.18. Then, to simulate a conditional value at location u on the grid points, the following is used,

$$Y_{cs}(u) = y^{OK}(u) + U_s(u) - U_s^{OK}(u) \quad \text{Eq. 2.19}$$

$$y^{OK}(u) = \sum_{\alpha=1}^{m} \omega_\alpha^{OK}(u) y(u_\alpha) \quad \text{Eq. 2.20}$$

$$U_s^{OK}(u) = \sum_{\alpha=1}^{m} \omega_\alpha^{OK}(u) U_s(u_\alpha) \quad \text{Eq. 2.21}$$

where y^{OK} is ordinary kriging prediction; U_s is the unconditional simulated value at location of interest; and U_s^{OK} is the ordinary kriging predicted value using unconditional simulated value at measured data locations. Equation 2.19 is repeated for all the grid points with their corresponding ω_α^{OK} weights.

A comparison was made with the stochastic simulation (LU algorithm) for spatial uncertainty and the associated variance reductions, i.e., alpha charts from BD-545-76. For the LU algorithm, a grid of points was generated that represented the surface of a cylindrical shaft. A comparison was made for both the unconditional and conditional cases with comparisons shown in Tables 2-1 through 2-3. It can be seen from these tables that the LU algorithm replicates the variance reduction for linear side friction models. Consequently, the LU algorithm would be appropriate to use for other capacity models (non-linear and end bearing).

Table 2-1. Comparison between LU Algorithm and α from Figure 2-8.

$D/a_h = 1$		
L/a_v	$\alpha^{1/2}$ LU SIM	BD-545-76 $\alpha^{1/2}$
2	0.300	0.31
4	0.228	0.22
6	0.182	0.18
8	0.161	0.16
10	0.140	0.14
20	0.130	0.10

Table 2-2. Comparison between LU Algorithm and α from Figure 2-9.

$D/a_h = 1$		
L/a_v	$\alpha^{1/2}$ LU SIM	BD-545-76 $\alpha^{1/2}$
2	0.4139	0.43
4	0.3107	0.32
6	0.2588	0.26
8	0.2272	0.22
10	0.2080	0.20
20	0.1561	0.15

Table 2-3. Comparison of Nested Structures LU Algorithm and α from Figure 2-9.

$D/a_h = 1$ Sill_h=1 Sill_v=0.8 Nugget=.2		
L/a_v	$\alpha^{1/2}$ LU SIM	BD-545-76 $\alpha^{1/2}$
2	0.480	0.480
4	0.426	0.432
6	0.410	0.411
8	0.397	0.392
10	0.394	0.386

2.5 Worst Case Spatial Uncertainty Scenarios

The use of the LU algorithm requires inputs for the variogram models (horizontal and vertical) for each layer for the simulation analyses. However due to the nature of in situ testing, sufficient borings in proximity to one another may result in an inability to characterize the horizontal variograms. For such situations, a selection of worst case scenarios must be made. Here the worst case scenario is considered as the capacity prediction, which results in the highest spatial variance, the lowest LRFD ϕ value, and thus, longer piles/shafts.

For the case of unconditional simulation, the alpha chart shown in Figure 2-8 can give an insight into which spatial correlation parameters will result in the most unfavorable scenario. A majority of FB-DEEP's capacity calculations use some sort of arithmetic averaging domain (e.g., 8D above to 3.5 D below for end bearing, etc.) and the alpha chart is also for the arithmetic averaging for side friction of a cylindrical shaft. Using the alpha chart of Figure 2-8, it can be seen the worst case (largest resulting α) a_h is for $a_h >> D$, i.e., the dashed contour. If a_v cannot be identified from the experimental variograms, then a value of $a_v >> L$ should be used.

In the case of conditional simulation, the alpha chart shown in Figure 2-9 can give an insight into which spatial correlation parameters will result in the worst case. Shown in Figure 2-9 is the evaluation of α for a boring located in the footprint of the shaft. The worst case can be seen where $a_h \approx D/2$ and $a_v >> L$. This can be further expanded to the case of a boring located outside a footprint at horizontal distance (d) from the shaft. In this case, it has been found the largest α are for $a_h \approx d$ and $a_v >> L$.

CHAPTER 3
EVALUATION OF UNCERTAINTY OF METHOD

3.1 Introduction

In the evaluation of LRFD ϕ values for any design method, the total uncertainty of its design resistance CV_R needs to be assessed. CV_R is comprised of spatial variability (σ_S^2) and the inherent design method error (σ^2) associated with the given method or approach. Chapter 2 discussed the use of geostatistical tools to quantify spatial variability (σ_S^2) for any site. This chapter focuses on the evaluation of method error (σ^2) for most FDOT design approaches using predicted and measured resistances.

The method error (σ^2) used herein, represents the total difference between the predicted design resistance versus its corresponding measured load tested value. Sources of error contributing to σ^2 can be associated with measurement error of in situ testing, specific empirical relationships used to develop design calculations, spatial variability of properties used to predict resistance (non-collocated boring), and construction methods (deviations from geometry or poor construction). This work uses many early FDOT studies that reported measured and predicted deep foundation results. However, unlike AASHTO (2004), the study uses a best fit regression between the measured and predicted response in order to assess the method error σ^2. Finally, this chapter discusses ways to reduce σ^2 through the use of site specific load testing and the use of future borings within the footprint of load tests. A discussion of regression concepts is presented before evaluation of method error.

3.2 Review of Regression Analysis Concepts

To quantify the error of a calculation method, a regression analysis of measured versus predicted capacities is needed. Figure 3-1 is an example plot of measured versus predicted

resistance fitted with a linear trend. A linear regression is fitted to the data (Eq. 3.1) where p_i and m_i are the predicted and measured values; a and b are coefficients of the linear regression (a = intercept, and b = slope); and ε is a random residual with mean of 0 and variance σ^2. The residual ε represents the random error of the method.

$$m_i = a + bp_i + \varepsilon \qquad \text{Eq. 3.1}$$

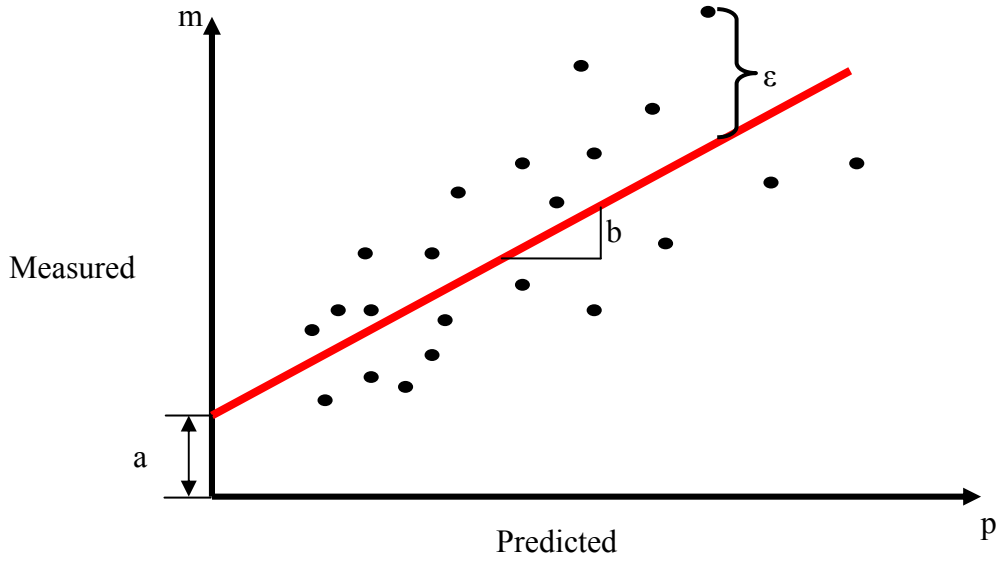

Figure 3-1. Measured versus predicted resistance.

The coefficients a and b in Eq. 3.1 represent a systematic bias that is imparted by the prediction model (i.e., consistent under or over prediction). These coefficients are determined by Eq. 3.2 and 3.3, where ρ is the correlation coefficient between the measured and predicted values; σ_m is the standard deviation of measured data about its mean ($\overline{m}$); and σ_p is the standard deviation of predicted data about its mean ($\overline{p}$). Most regression analysis gives the coefficient of determination R^2 which is equal to ρ^2, as an indicator of the proportion of σ_m^2 that is described by the linear regression. The proportion of σ_m^2 that is not described by the linear regression equals to σ^2. In essence, R^2 is a measure of how well the resistance calculation predicts the true measured resistance. Its relationship to σ^2 is shown in Eq. 3.4. For example, if the measured

and predicted values were perfectly correlated ($R^2 = 1$), then the data points would all fall on the regression line, $\sigma^2 = 0$ would equal zero (Eq. 3.4), and the predicted value, p_i, would be a perfect estimator of the measured value, m_i. Conversely, if there is zero correlation ($R^2 = 0 \rightarrow \sigma^2 = \sigma_m^2$), then p_i is inappropriate as an estimator of m_i.

$$b = \rho \frac{\sigma_m}{\sigma_p} \quad \text{Eq. 3.2}$$

$$a = \overline{m} - b\overline{p} \quad \text{Eq. 3.3}$$

$$\sigma^2 = \sigma_m^2(1 - R^2) \quad \text{Eq. 3.4}$$

3.3 Regression Analysis for Drilled Shafts in Rock

To estimate the value of σ^2, data used in previous FDOT reports for reliability design of different foundation types were collected and analyzed. The data collected encompass all calculation methods found in FB-DEEP and can be separated into two categories. The first category concerns data which characterize unit skin friction (tsf) separate from unit end bearing (tsf) and the second is total measured versus predicted capacities (tons). Note, separate evaluation of LRFD ϕ for pullout (e.g., tension pile), uncertainty of calculation method σ^2 for skin separate from tip with corresponding CV_R for a pile (i.e., all soils, layers, etc.) would be required. Similarly for top down compression, uncertainty of calculation method σ^2 for side or tip separate or together may be used to evaluate CV_R of a pile.

For bias assessment, the regression analyses showed in Figure 3-1, Eqs. 3.1 to 3.4 were used. However, the identified regression does not account for number of data points, n, used in the assessment. For limited data, the best linear estimate is obtained by taking the expectation and variance of Eq. 3.1. Equation 3.5 is the best estimate of $\hat{m}$ or the bias-corrected prediction. Similar to equation 3.4, equation 3.6 represents the variance about the fitted linear trend.

Equation 3.7 represents the estimation error of $\hat{m}$ due to a limited number n of data pairs. In this equation, p_i is the predicted pile resistance, and $\bar{p}$ is the mean of the predictions of the data set. Equation 3.7 reflects that uncertainty increases as less data are available (n smaller) and moves away from the mean of the data cloud ($p_i - \bar{p}$ larger). The terms from Eq. 3.6 and 3.7 can be summed to find the error of a calculation method ,σ^2, shown in Eq. 3.8. For large n value, Eq. 3.7 approaches zero, and Eq. 3.6 and 3.8 are one and the same as Eq. 3.4.

$$\hat{m} = a + bp_i \qquad \text{Eq. 3.5}$$

$$\sigma_{LF}^2 = \frac{n-1}{n-2}\sigma_m^2(1 - R^2) \qquad \text{Eq. 3.6}$$

$$\sigma_{\hat{m}}^2 = \sigma_{LF}^2\left[\frac{1}{n} + \frac{(p_i-\bar{p})^2}{(n-1)\sigma_p^2}\right] \qquad \text{Eq. 3.7}$$

$$\sigma^2 = \sigma_{\hat{m}}^2 + \sigma_{LF}^2 \qquad \text{Eq. 3.8}$$

Data collected were sorted by calculation method as a function of foundation and soil type. For drilled shafts in Florida limestone data was compiled from FDOT Report BC354-08. The data available for measured and predicted responses were for unit resistance calculations. The regression analysis for the data is summarized in Table 3-1. This regression analysis incorporates a number of samples in the assessment of σ^2 as discussed previously. Note Eq. 3.8 suggests that σ^2 is also a function of p_i through Eq. 3.7. However, by limiting the range of validity of the regression model to the range of resistance value observed, the approximate assumption of a constant σ^2 value is justified (see Table 3-1 for both side and tip resistances). Bias corrections, as well as method error, are given in Table 3-1 with plots of measured versus predicted skin and tip resistances presented in Figures 3-2 and 3-3.

Table 3-1. Regression Analysis for Drilled Shafts in Limestone

Model	Resistance	n	σ^2 (tsf^2)	Regression (tsf)
McVay	Side	18	4.519	$0.9p + 0.898 \quad p \leq 20$
O'Neill	Tip	11	48.89	$0.773p + 20.5 \quad p \leq 160$

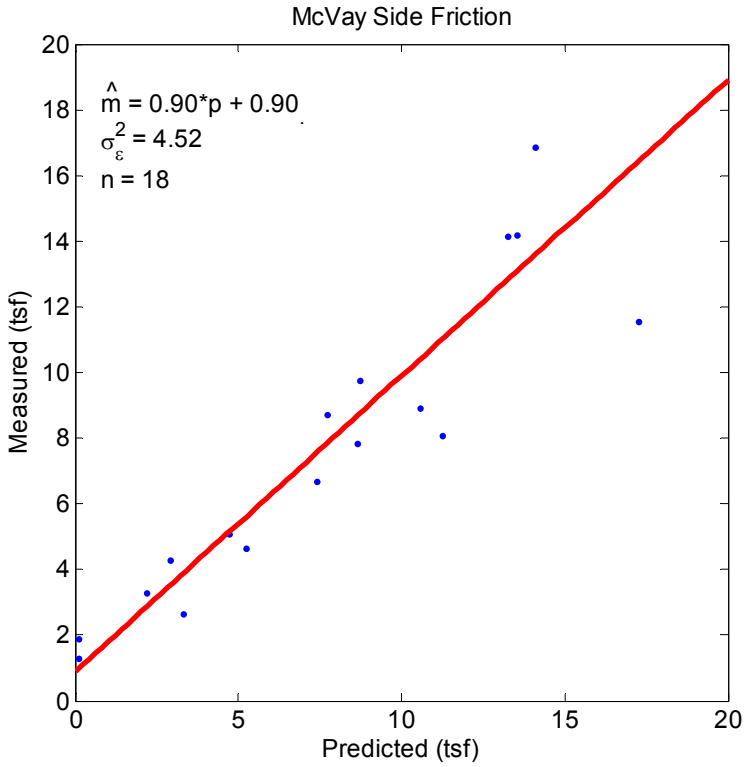

Figure 3-2. Regression analysis drilled shaft (McVay side friction).

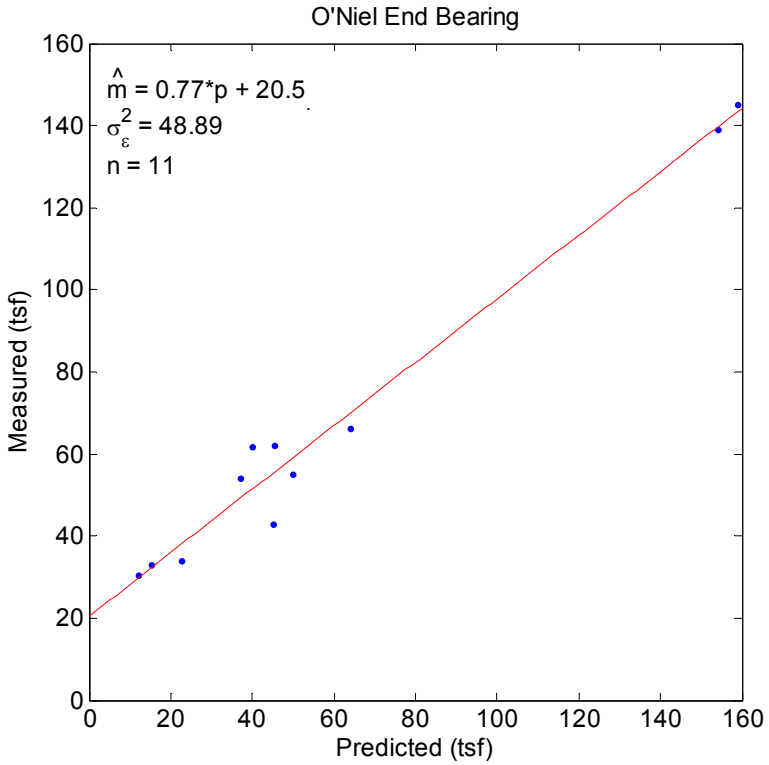

Figure 3-3. Regression analysis drilled shaft (O'Neill end bearing).

Data collected for method error assessment may have the borings outside of the footprint of the load tested shaft. Unless the borings show minimal spatial influences (e.g., similar means), the data used in the regression may result in a very conservative estimate of σ^2. This is due to the fact that the prediction from the boring located outside of the footprint of the load test pile/shaft will contain the additional error due to spatial variability. Thus, the values for $\sigma^2$and the linear trends are considered preliminary values used to get a sense of magnitude of variability that is contributed from the error of the calculation method. The current data sets shown in Table 3-1 will be considered for integration into future regression analyses, but for optimization of σ^2, borings used will be required to be sufficiently close to the load test shaft (e.g., inside the footprint).

Having established σ^2 for unit capacities, the total uncertainty (variance) of a foundation's resistance may be assessed. Equations 3.9 and 3.10 compute the variance for both side friction and end bearing. In both equations, the first term represents the measured variance of unit capacities, which are bias corrected (b) and reduced (α) for spatial averaging between support size of the data and full dimension of the shaft. The second term is the recently found method error σ^2 and the whole term is multiplied by the square of their corresponding areas to obtain total uncertainty for skin and tip. These variances are then used in Eq. 3.11 to determine the total uncertainty of the foundation resistance, which includes correlation (ρ) between skin and tip resistance.

$$\sigma_{Skin}^2 = A_s^2 \left(b_{fs}^2 \alpha_s^2 \sigma_{fs}^2 + \sigma^2{}_{fs} \right) \quad \text{Eq. 3.9}$$

$$\sigma_{Tip}^2 = A_t^2 \left(b_{qt}^2 \alpha_t^2 \sigma_{qt}^2 + \sigma^2{}_{qt} \right) \quad \text{Eq. 3.10}$$

$$\sigma_{TOTAL}^2 = \sigma_{Skin}^2 + \sigma_{Tip}^2 + 2\rho\sigma_{Skin}\sigma_{Tip} \quad \text{Eq. 3.11}$$

3.4 Regression Analysis for FB-DEEP Pile/Shaft Capacities

The regression analysis of unit capacities for drilled shafts in rock showed no change in error trend as a function of predicted resistance p_i (Figure 3-2). This is not the case when analyzing total FB-DEEP capacities. Shown in Figure 3-4 is the predicted versus measured total capacities (i.e., Davisson) for prestressed concrete piles. It is evident, the spread around the linear trend increases with an increasing resistance prediction. This proportionality suggests that the measured and predicted capacities are log normally distributed (Isaaks, 1989). Consequently, to assess σ^2, a log transform of the data was applied to allow regression analysis as described previously. Since the variance is proportional to p_i in normal space (i.e., without log transformation), $\sigma^2{}_{LN}$ from the log analysis is used to determine an approximately constant

coefficient of variation of error for normal space, shown in Eq. 3.12. In other words, instead of working with a prediction error $p_i - m_i$ and a constant value of σ as in the previous section, a prediction error p_i/m_i is used in combination with a constant value of CV_ε.

$$CV = \sqrt{\exp\left(\sigma^2_{LN}\right) - 1} \qquad \text{Eq. 3.12}$$

$$\hat{m} = \exp(a)\, p^b \qquad \text{Eq. 3.13}$$

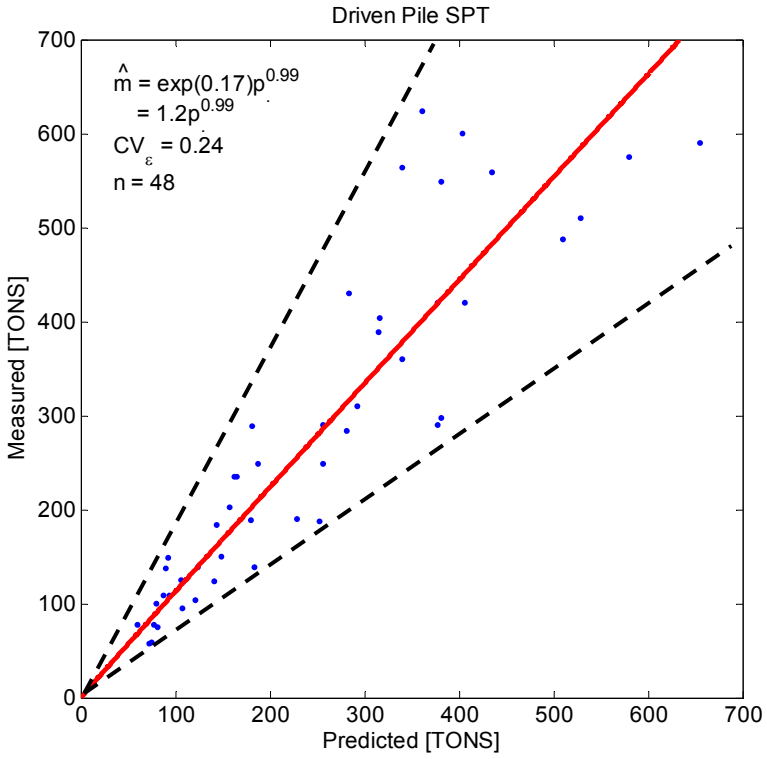

Figure 3-4. Regression analysis for concrete pile (FB-DEEP).

In the case of drilled shafts in clay and sand soil types, only the data for total capacities from NCHRP Report 507 (Paikowski, 2004) were available. The result of the regression analysis for total capacities is shown in Table 3-2 and plots are shown in Figures 3-5 and 3-6. For the analysis, data sets were first filtered prior to the regression analysis to remove any outliers. The filtering involved converting the data sets to ratios of measured over predicted

values, and then removing any ratio outside ±2 standard deviations from the mean as recommended by NCHRP 507. In this process, no more than 3 pairs (i.e., < 5%) were removed from the entire data set.

Table 3-2. Regression Analysis for Drilled Shafts in Clay and Sand (Total Resistance)

Soil Type	n	CV_ε	Regression (tons)
Clay	38	0.41	$\exp(0.73)p^{0.86} = 2.1p^{0.86} \quad p \leq 1000$
Sand	31	0.68	$\exp(0.66)p^{0.98} = 1.9p^{0.98} \quad p \leq 700$

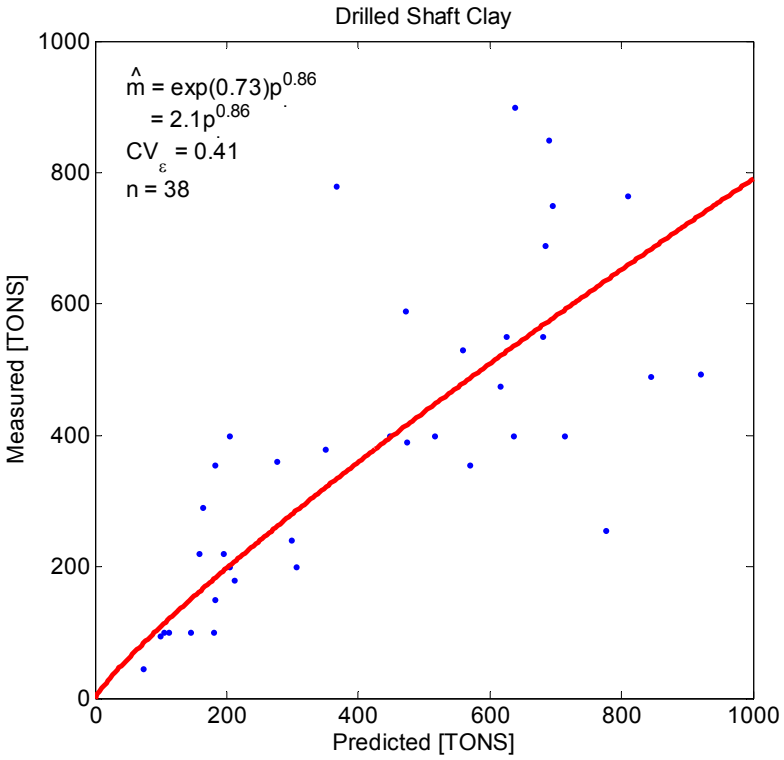

Figure 3-5. Regression analysis drilled shaft (clay model).

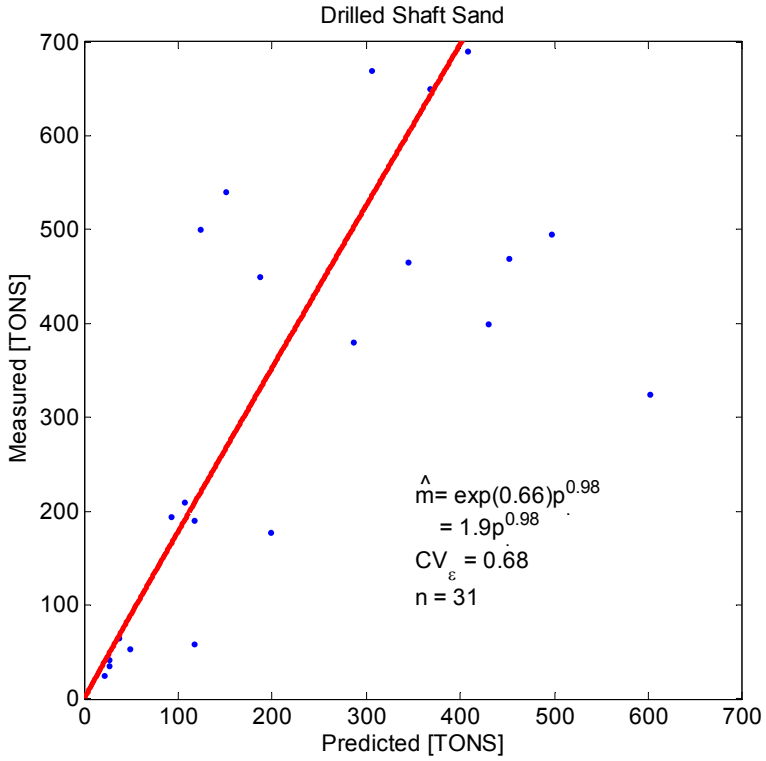

Figure 3-6. Regression analysis drilled shaft (sand model).

Evident in Table 3-2, the CVε for sand is significantly higher than that of the clay. This large difference may be attributed to constructability issues for drilled shafts in sand. In contrast to sands, drilled shafts in clay and rock are well suited to maintain the size and shape of the shaft specified. In sands, the problem of caving soils may result in irregular shaft shapes, which could significantly impact the resistance of shafts when load tested and may be a significant contribution to the higher CV_ε shown in Table 3-2. As discussed previously, the regression analysis for these models should be updated in future work.

Data for driven piles whose capacities were calculated from SPT N values were collected from a variety of sources listed in Table 3-3. The regression analysis was subsequently performed on the measured and predicted Davisson capacities. The data sets were also filtered for outliers as discussed above (±2 standard deviations).

Table 3-3. Regression Analysis for Davisson Resistance FB-DEEP Driven Piles (SPT) Tons

Pile Type	Source	Soil Type	n	CV_ε	a	exp(a)	b	limit
Concrete	BA 512	All	48	0.24	0.17	1.19	0.99	700
Concrete	NCHRP 507	Sand	33	0.43	0.74	2.10	0.88	500
Concrete	NCHRP 507	Mix	71	0.52	2.24	9.39	0.66	500
Small Dia. Steel Pipe	NCHRP 507	Clay	13	0.81	0.33	1.39	0.88	300
Small Dia. Steel Pipe	NCHRP 507	Sand	18	0.58	1.85	6.35	0.70	300
Small Dia. Steel Pipe	NCHRP 507	Mix	29	0.51	3.88	48.4	0.28	300
Large Dia. Steel Pipe	BC354 60	All	13	0.11	0.54	1.72	0.94	1300
Large Dia. Conc. Cyl.	BC354 60	All	8	0.19	1.93	6.89	0.75	1300

A review of Table 3-3 shows that calculated CV_ε for large diameter steel and concrete cylinder piles are significantly lower than that for the other foundation types. This difference is attributed to the fact that the regression analysis is based on data from the same report, which were used to create the resistance calculation models. That is, the same measured load test data were used to assess pile skin and tip resistance from measured SPT blow counts. Consequently, it is suggested that further validation from projects other than ones in the FDOT Report BC354-60 be undertaken for proper analysis of CV_ε for these pile types. Table 3-4 is a summary of regression analyses for FB-DEEP's CPT resistance calculation methods. The data used for this analysis came from FDOT Report BD545-43.

Table 3-4. Regression Analysis for Davisson Resistance FB-DEEP Driven Piles (CPT) Tons

Method	n	CV_ε	a	exp(a)	b	limit
UF[1]	21	0.29	–0.28	0.76	1.06	500
Schmertmann[2]	19	0.29	1.02	2.77	0.85	500
LCPC[3]	20	0.30	-0.06	0.95	0.98	500

1-McVay et al. (2004)
2-Schmertmann (1978)
3-Brustamante, M. & Gianeselli, L. (1982)

Again, once method error CV_ε is assessed for total pile capacities, the CV_R (Eq. 3.12) can be determined and the LRFD ϕ may be found. In Eq. 3.14, σ_ρ^2 is the total variance from the spatial analysis, i.e., the spatial variance about the predicted mean value p, and b is the bias correction. For the case of total capacities σ_ρ^2 can be determined from either LU simulations or analytical solutions using alpha charts (BD545-76).

$$CV_R = \frac{\sqrt{\exp(a)^2\sigma_\rho^2 + (CV_\varepsilon p)^2}}{\exp(a)p^b} \qquad \text{Eq. 3.14}$$

As discussed earlier, the data presented in Tables 3-2 through 3-4 are only being recommended as preliminary assessment of method error.

3.5 Load Testing and Borings within Footprint

In the previous evaluation of method error from previous projects, relative location of boring used for prediction is not discussed or given. Thus, it is possible that too much spatial error could be incorporated in the evaluation of the method error. It is typical practice to perform load testing on a project site. Thus with load test and corresponding boring located within the footprint, a site specific regression analysis can be used to evaluate both the method error and bias.

From various FDOT projects eleven load tests were collected; however, only eight of these tests have borings located within the footprint. Of these eight load tests, three of them were missing rock strength testing. A discussion of these projects and their site specific regression analysis follows.

Jewfish Creek has two load tested drilled shafts with borings in the footprint. This site is primarily limestone, and regression analysis for this site's data is shown in Figure 3-7. Measured versus predicted values were taken from BD545-76. In that report, a regression analysis was

performed to quantify the sites method error. However, in that analysis it did not account for number of samples n. In BD545-76, it lists $\sigma^2 = 3.975$ (tsf^2) for Jewfish Creek. This can be seen to be quite less when compared to $\sigma^2 = 7.45$ (tsf^2) shown in Figure 3-7. This illustrates the effect of a small amount of load testing samples on poor quantification of the method error. When comparing the regression results of Jewfish Creek to Table 3-1, it can be seen that Jewfish Creek has a higher σ^2 and different bias correction.

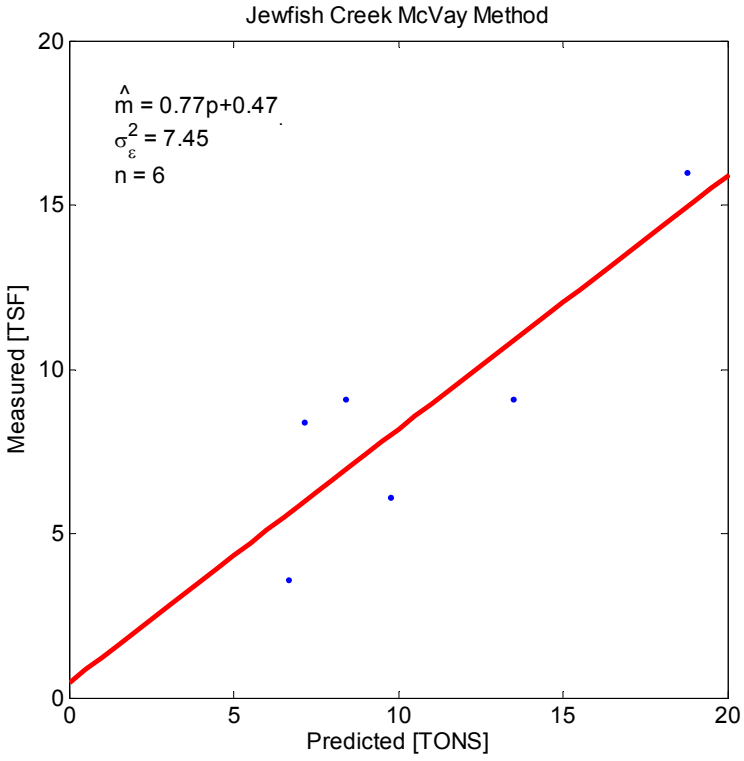

Figure 3-7. Regression analysis for Jewfish Creek (McVay method).

SR686 has two load tested drilled shafts with borings located within the foot print. For this site, mixed soils (sand and clay) and limestone are present. Due to lack of lab testing of the rock cores at limestone drilled shafts, evaluation of the method error for limestone is unavailable. Regression analysis was performed for sand and clay, however, some strain gauge intervals contain mixes of both sand and clay soils. For these cases, predominate soil layer over that interval is considered as the primary soil type for this analysis. Also, boring logs given for this

site gives mixed soil descriptors adding difficulty when determining which soil model to use in the resistance prediction.

The regression model for clay at SR-686 is shown in Figure 3-8. Of the 2 load tested shafts, only 6 segments could be used in the regression analysis for the clay modeling. With only 6 points available for analysis, a higher CV_ε resulted than the one given in Table 3-2, and the values for a and b are quite different. Results are not shown for the sand model due to only 4 points being available and resulting regression showing a very poor fit and negative slope (i.e., bias).

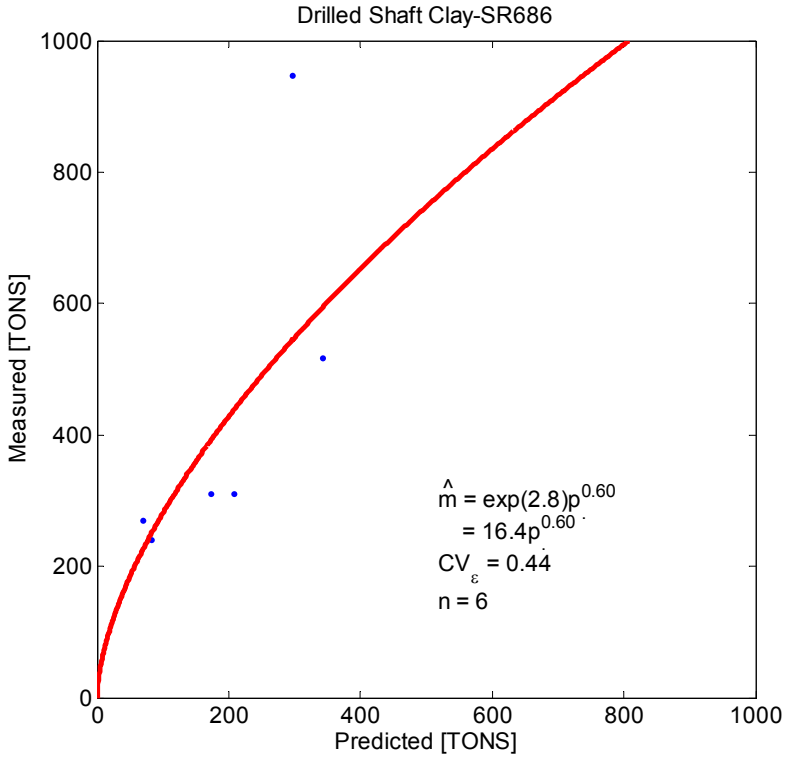

Figure 3-8. Regression analysis for SR-686 (clay model).

The regression model for Dixie Highway FB-DEEP driven piles is shown in Figure 3-9. The Dixie site has 3 load tested driven piles, 2 compression and 1 tension, with each having a boring located within the footprint and another located 2.5 feet away. This site is predominately sand over limestone. The two compression tested piles each have strain gauges placed at 4

different levels. This results in the ability to measure three side-friction resistances and one tip resistance for each compression-tested pile. In total, nine measured resistances are available for a regression analysis.

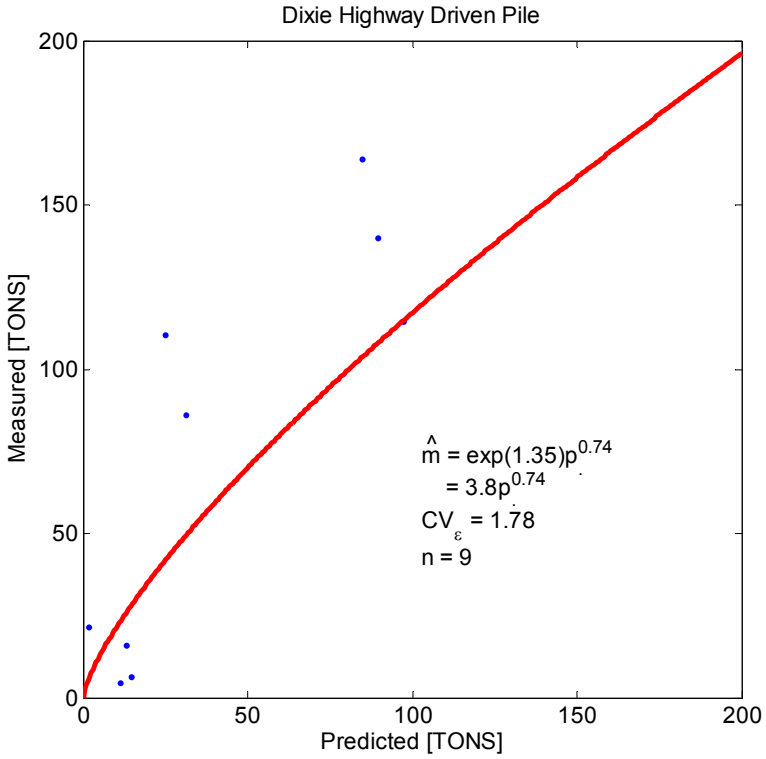

Figure 3-9. Regression analysis for Dixie Highway (FB-DEEP driven piles).

The result of load testing measurements is that only 6 data points are available for the regression analysis. With only 6 points available for analysis, a higher CV_ε resulted than one given in Table 3-3, and values for a and b are quite different.

The use of a reduction factor α_o with the evaluation of σ^2 was discussed in BD545-76. This reduction factor was needed when upscaling the side resistance from the support domain of load test intervals to the entire shaft. However, if load test intervals encompass the entire layer thickness, it is recommended that α_o not be used.

3.6 Normalized Resistance Factors

In AASHTO and NCHRP Report 507 (Paikowski, 2004) load and resistance factor design (LRFD) for deep foundations, Eq. 3.15 is used for deep foundation resistance. The determination of resistance factor ϕ (Eq. 3.16) requires knowledge of statistical distribution parameters of both the load Q and resistance R, as well as specified reliability index β. The selected β is equivalent to a target probability of failure p_f for the deep foundation being designed. Also, the statistical distributions for both Q and R are assumed to be log normal in the development of these equations.

$$\phi R \geq \gamma_D Q_D + \gamma_L Q_L \qquad \text{Eq. 3.15}$$

$$\phi = \frac{\lambda_R\left(\gamma_D \frac{Q_D}{Q_L} + \gamma_L\right)\sqrt{\frac{\left(1+CV_{QD}^2+CV_{QL}^2\right)}{\left(1+CV_R^2\right)}}}{\left(\lambda_{QD}\frac{Q_D}{Q_L}+\lambda_{QL}\right)exp\left\{\beta\sqrt{\ln\left[\left(1+CV_R^2\right)\left(1+CV_{QD}^2+CV_{QL}^2\right)\right]}\right\}} \qquad \text{Eq. 3.16}$$

For evaluation of ϕ, the resistance bias factor λ_R is determined as the mean value of the measured to predicted resistances. The coefficient of variation of resistance CV_R is determined from the distribution of the ratio of measured to predicted resistance about the mean, i.e., λ_R resistance bias factor. The remaining dimensionless parameters in Eq. 3.1 and 3.2 are chosen according to the FHWA/AASHTO recommended values (for load cases I, II, and IV),

Dead load factor:	γ_D	= 1.25
Live load factor:	γ_L	= 1.75
Dead to live load ratio:	Q_D/Q_L	= 2.00
Dead load bias factor:	λ_{QD}	= 1.08
Live load bias factor:	λ_{QL}	= 1.15
Dead load coefficient of variation:	CV_{QD}	= 0.128
Live load coefficient of variation:	CV_{QL}	= 0.18

The proposed LRFD characterization has undergone a number of improvements with respect to the AASHTO (2004) and NCHRP (Paikowski, 2004) representation. The limit state Eq. 3.15 is still used; however, the value of R is determined from mean of the spatial analysis (Chapter 2) and is biased corrected (Chapter 3) for the specified method used. The value of CV_R uses the mean value of the bias corrected R mentioned in the previously discussed sentence, but it also incorporates method and spatial uncertainty, i.e., σ_S^2 and σ^2. As a consequence, a normalized resistance factor $\overline{\phi}$ is proposed in Eq. 3.17, which no longer depends on prediction bias (i.e., normalized to $\lambda_R = 1$) and that is to be used in combination with the full form of CV_Q as suggested by Styler (2006) given in Eq. 3.18.

$$\overline{\phi} = \frac{\left(\gamma_D \frac{Q_D}{Q_L} + \gamma_L\right)\sqrt{\frac{\left(1+CV_Q^2\right)}{\left(1+CV_R^2\right)}}}{\left(\lambda_{QD}\frac{Q_D}{Q_L} + \lambda_{QL}\right) exp\left\{\beta\sqrt{\ln\left[\left(1+CV_R^2\right)\left(1+CV_Q^2\right)\right]}\right\}} \qquad \text{Eq. 3.17}$$

$$CV_Q^2 = \frac{\left(\lambda_{QD}\frac{Q_D}{Q_L}CV_{QD}\right)^2 + \left(\lambda_{QL}CV_{QL}\right)^2}{\left(\lambda_{QD}\frac{Q_D}{Q_L}\right)^2 + 2\frac{Q_D}{Q_L}\lambda_{QD}\lambda_{QL} + \lambda_{QL}^2} \qquad \text{Eq. 3.18}$$

3.7 Values from AASHTO LRFD ϕ for Comparison to $\overline{\phi}$

The computed $\overline{\phi}$ is evaluated for multiple case studies on both pile and drilled shaft sites in Chapters 4 and 5. A direct comparison of $\overline{\phi}$ with ϕ specified by AASHTO or the *Soils and Foundations Handbook* is not appropriate. This is due to λ_R used in Eq. 3.16, which can have a significant impact on ϕ. A more appropriate comparison for the calculated $\overline{\phi}$ would be with respect to ϕ/λ_R. Table 3-5 shows a collection of ϕs for multiple methods and corresponding ratios from previous FDOT and NCHRP research. However, in current practice the FDOT specifies values of ϕ that are slightly conservative when compared to Table 3-5. The more appropriate parameter ϕ/λ_R for comparison to $\overline{\phi}$ is shown in Table 3-6. This table of resistance

factors comes from the FDOT's *Structural Manual, Vol. I*, and uses the corresponding λ_R for its specific method in Table 3-5. In Table 3-6, ϕ/λ_R was not computed for design of side friction plus 1/3 end bearing. This is due to λ_R not being calculated for the combination of the two methods. Not shown in Table 3-6 are resistance factors for driven piles. The FDOT's *Structural Manual* does list factors for driven piles that include the use of dynamic testing. Resistance factors calculated in this project do not account for the use of dynamic testing, thus for comparison purposes, the value of ϕ/λ_R for driven piles should be used. For the FHWA alpha and beta methods, λ_R was found from the recommendation in the NCHRP Report 507, Table 29.

Table 3-5. Collections of ϕ from FDOT Reports

Design Method	CV_R	λ_R	ϕ for β listed			ϕ/λ_R for β listed			Report
			2.0	2.5	3.0	2.0	2.5	3.0	
Rock: Side friction	0.280	1.060	0.81	0.69	0.59	0.76	0.65	0.56	BC354-08, Table 8.5
Rock: O'Neill's end bearing (nearest boring approach)	0.290	1.400	0.86	0.71	0.60	0.61	0.51	0.43	BC354-08, Table 11.21
Rock: O'Neill's end bearing (random selection - Monte Carlo)	0.460	1.210	0.56	0.43	0.33	0.46	0.36	0.27	BC354-08, Table 11.22
Driven piles: SPT 94	0.246	1.172	0.81	0.69	0.59	0.69	0.59	0.50	510772, Tables 3.2 and 3.3

Table 3-6. Resistance Factor for Drilled Shafts (Bridge Foundations)

Design Method	Quality Control Method	ϕ		λ_R	ϕ/λ_R	
		Redundant	Non-redundant		Redundant	Non-redundant
For soil: FHWA alpha or beta method	Specs.	0.6	0.5	1.03	0.58	0.49
For rock socket: McVay's method, neglecting end bearing	Specs.	0.6	0.5	1.06	0.57	0.47
For rock socket: McVay's method, including 1/3 end bearing	Specs.	0.55	0.45	NA	NA	NA
For rock socket: McVay's method	Statnamic	0.7	0.6	1.06	0.66	0.57
For rock socket: McVay's method	Static	0.75	0.65	1.06	0.71	0.61

CHAPTER 4
DEVELOPMENT OF GRAPHICAL USER INTERFACE FOR DEEP FOUNDATION DESIGN

4.1 Introduction

Axially loaded deep foundation (piles or shaft) design is a function of the factored loads and the LRFD resistance factors. Controlling the LRFD $\overline{\phi}$ is total uncertainty of the design, which is a function of uncertainty of the construction method (e.g., deviations from design parameters), the design method (e.g., FB-DEEP), and spatial uncertainty of the in situ/laboratory data. Chapter 3 presented current assessment of uncertainty of the method based on legacy data, as well as recommended an approach to assess uncertainty of a method on a site-by-site basis (i.e., load testing). Chapter 2 identified the process of determining spatial uncertainty of a site based on nearest boring (i.e., conditioning) or all borings within an area (i.e., unconditional). Impacting the spatial uncertainty are identification of layers, summary statistics (mean and variance of in situ/laboratory data), spatial correlation (i.e., variogram, spatial correlation length), and dimensions of the pile/shaft. To assist with spatial uncertainty assessment, a graphical user interface (GUI) was written to aid the design engineer. Besides developing the expected mean and variance of in situ/lab data at the planned deep foundation (pile/shaft), the GUI writes/reads FB-DEEP files from which total uncertainty (method and spatial) is evaluated along with total pile/shaft capacities and LRFD $\overline{\phi}$ resistance factors as a function of depth. Presentation of the GUI is through the step-by-step process a design engineer would perform on two existing FDOT pile/shaft projects. The first is 17th Street Bridge (drilled shafts) in Fort Lauderdale, Florida, and the second is the Dixie Highway (driven piles) in Miami, Florida.

4.2 17th Street Bridge – Fort Lauderdale, Florida

A project site that is ideal for implementing a geospatial analysis for drilled shafts socketed in limestone is 17th Street Bridge, Fort Lauderdale. This project has small separation distances between borings and a large quantity of strength test performed for each boring. Closely spaced data results in the easy identification of the experimental variograms in the horizontal and vertical directions, as well as accurate assessments of layering and summary statistics (mean and variances). A discussion of spatial uncertainty assessment, method error, total uncertainty, LRFD $\overline{\phi}$, and recommended axial design capacity follows.

4.2.1 GUI: Start Tab

Shown in Figure 4-1, is the starting screen for the GUI. At the top of the GUI, Figure 4-1A are five tabs (start, profile, geostat, etc.) arranged in order for design. Each tab will be completed in sequence until the final axial design load as function of depth is obtained. The start tab is the starting point of the analysis where all project in situ data is imported to the GUI. Shown in Figure 4-1B is the XML button which loads all boring information from either the FDOT database (online) or from a file (hard drive) in XML format. For this example, borings from the 17th Street Bridge was loaded with spatial locations as shown in Figure 4-1C. This plot is presented in northing and easting (plan view) and shows borings relative to one another. The figure allows the user to see if the borings are located properly (used in variograms and conditional simulation). Also in the start tab is selection of foundation type, Figure 4-1D (drilled shaft or driven pile) which influences the required in situ parameters later in the GUI analysis. For this example, drilled shaft was selected.

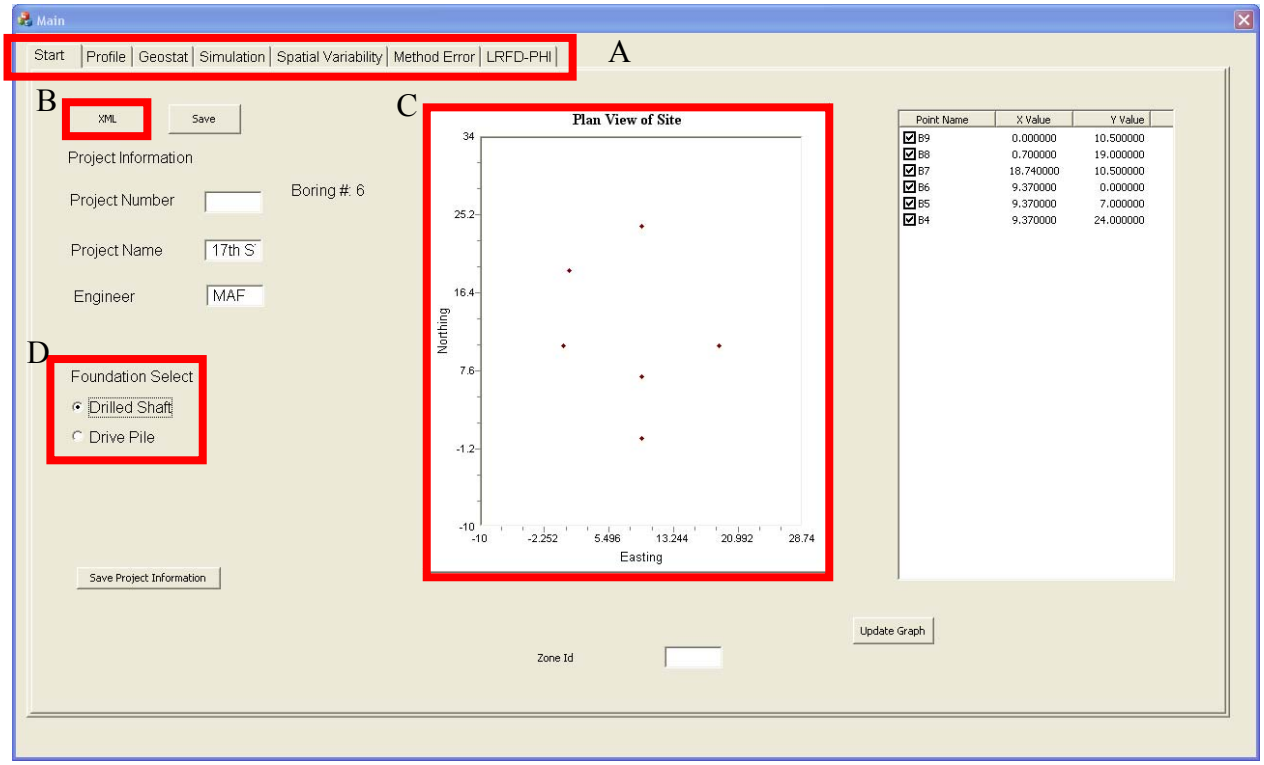

Figure 4-1. Start tab.

4.2.2 GUI: Profile Tab

The second tab is the profile tab shown in Figure 4-2. On this tab the user can see profiles (parameter values versus elevation) for SPT-N and unconfined compressive strength q_u. For the 17th Street Bridge, only rock strength data were collected and elevation versus q_u profile is displayed in Figure 4-2A. The graph to its left would show SPT-N profile, if data from the borings were available.

Profile data is very important for identification of layers and trends. To establish a layer boundary, an engineer simply clicks (mouse) at any elevation within the SPT or q_u profile. A horizontal blue line will appear in the graph at that location within both SPT and q_u profiles ,. The engineer may establish any number of layers within the profiles. Selection of layers should be based on either soil (e.g., sand, clay, etc.) or rock descriptions, or observed means and variances (scatter of data about mean).

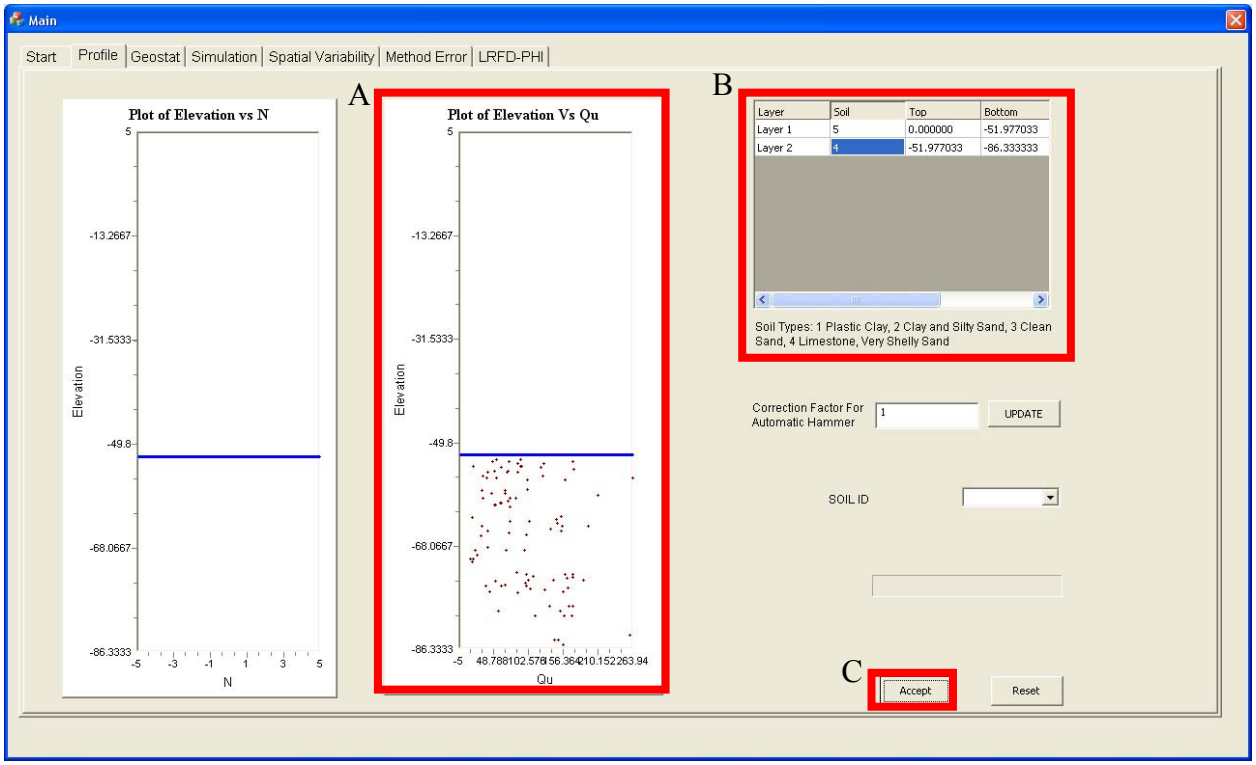

Figure 4-2. Profile tab.

With the profile separated into layers, the engineer must assign soil types in the upper right corner of the tab (Figure 4-2B). Since drilled shaft analysis was selected (start tab), by using the slide bar Figure 4-2B the user must also input mean and coefficient of variation (CV) of soil / rock unit weight for each layer. For the example, layer 2 was selected as a rock layer (soil type 4), and layer 1 was input as a void (soil type 5), since no SPT-N data were available. Note, both soil and rock may be considered simultaneously in design (SPT N data required). In the case of soil, the designer has the option of entering an energy correction value for automatic versus safety hammers. With profiles separated into layers (Figure 4-2A) and soil types with unit weight parameters inputted (Figure 4-2B), the user needs to click "Accept," Figure 4-2C, to advance to the next tab.

4.2.3 GUI: Geostat Tab

With the site or zone separated into layers, the user next moves to the Geostat tab (Figure 4-3) where the geostatistical analysis is performed. Specifically, this tab is used to determine summary statistics as well as measures of spatial correlation for each of the layers selected in the profile tab (Figure 4-2). Since the profile may be composed of multiple layers, the Geostat tab is displayed on a layer-by-layer basis.

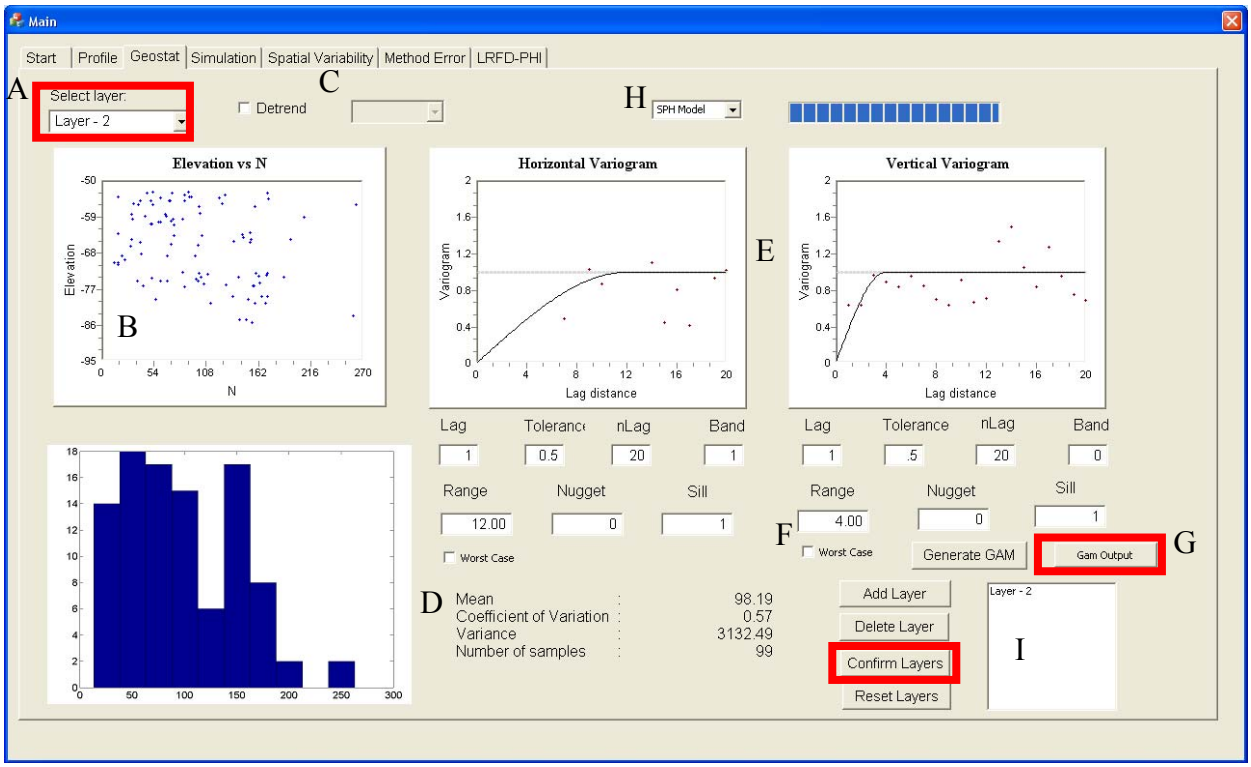

Figure 4-3. Geostat tab.

The analysis begins with a selection of a layer number from the pull down menu in Figure 4-3A. Layer-2 is shown, which shows the corresponding q_u values with elevation (profile) in Figure 4-3B. This plot allows the user to quickly identify whether the data have a trend (increasing or decreasing mean value with elevation). If the data were clustered around a mean, which changes with depth, the data need to be detrended. To detrend the data, the user needs to select the check box shown in Figure 4-3C. If selected, a drop box appears, and a linear or 2nd

order polynomial may be selected to detrend the data for any layer through regression fitting (examples presented in Dixie Highway). For the 17th Street Bridge data in Figure 4-3B, it can be seen that no detrending is needed. Displayed in Figure 4-3D is the mean (tsf), variance (tsf^2) and CV of the layer data. In the case of detrended data (check box, Figure 4-3C), the variance and CV of the detrended data are displayed. Shown to the left of Figure 4-3D is the histogram of the raw data, useful in identifying the distribution (e.g., normal, log-normal, etc.) of the data.

Two graphs on the right side of the tab (Figure 4-3E) plot the horizontal and vertical variograms of the layer data. To generate the variograms, the following search parameters (Figure 2-5) must be defined for Eq. 2.6: increment in lag distance (h); number of lags; and lag tolerance and bandwidth shown in Figure 4-3F. Variogram search parameters used in this analysis are shown in Table 4-1. Experimental variograms shown in Figure 4-3E are evaluated for data that are detrended (if selected) and that have undergone a normal score transformation. The normal score transform process is performed in the background by the GUI.

Table 4-1. Variogram Search Parameters

Search Direction	Lag(ft)	Tolerance(ft)	Number of Lags	Bandwidth (ft)
Horizontal	1	0.5	20	1
Vertical	1	0.5	20	0

To ensure that the calculated values in the displayed variograms are reliable for the various lag distances, the number of pairs used in the computation of Eq. 2.6 should be checked. Clicking on the (Vario)Gam Output button shown in Figure 4-3G results in the pop-up window of Figure 4-4. The window displays the variogram value γ and number of pairs for both the vertical and horizontal directions as function of lag distance. As identified in Chapter 2, the recommended number of pairs is $n > 30$. Evident in Figure 4-4, for the 17th Street Bridge, adequate numbers of pairs are available to estimate variograms in both directions.

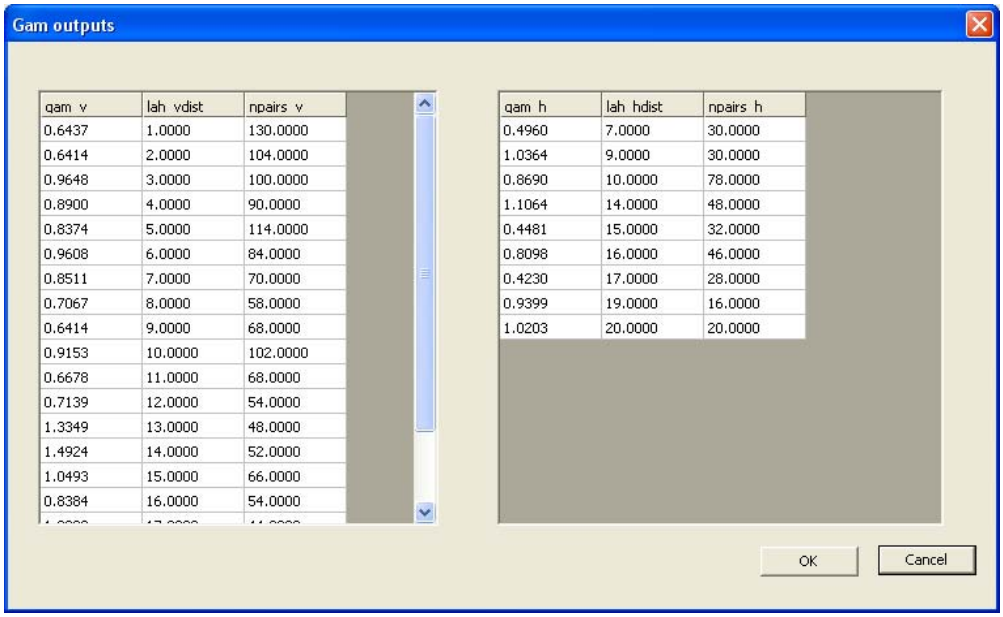

Figure 4-4. Variogram output.

With variograms generated, the user can now fit (Figure 4-3H) either an exponential or spherical model (Eq. 2.8) (Figure 4-3F), to the plots of vertical and horizontal variogram points. The user has the option of specifying the range, sill, and nugget for each direction (below plots, Figure 4-3H). Additionally for easier function fitting, the user can simply click within each graph and a model will be generated based on the x (range) and y (sill) position of the mouse click within the graph. For the 17th Street Bridge example, a spherical model was used with parameters shown in Table 4-2.

Table 4-2. Spherical Model Parameters

Direction	Nugget	Sill	Range, a (ft)
Horizontal	0	1	12
Vertical	0	1	4

For the case of when variograms cannot be constructed, i.e., limited data, then the engineer has the option of selecting the worst case scenario. This feature is selected in Figure 4-3F with a

check box which can be applied for either the vertical and horizontal directions. The worst cases (unconditional and conditional) have been identified and discussed in Chapter 2, Section 2.5.

After completing the geostatistical analysis of a layer, the user needs to click the "add layer" button on the bottom right corner of Figure 4-3I. The user must repeat the geostatistical analysis for each layer (Figure 4-3A) and subsequently add them to the completed list (Figure 4-3I). When all the layers have been added, the user needs to confirm (Figure 4-3I) before proceeding to the next phase of the design, the 'Simulation' tab. For this example (17^{th} Street Bridge), only layer 2 was considered, since layer 1 was the special case of a void with no data to analyze.

4.2.4 GUI: Simulation Tab

After completing the geostatistical analysis for each layer (Geostat tab), the expected boring/laboratory strength information at a planned pile/shaft location is generated using the LU algorithm. The simulation, i.e., generation of soil/rock boring profiles for FB-DEEP shaft/pile analyses, is controlled by the simulation tab (Figure 4-5). Summary statistics from the Geostat tab are also shown by layer (Figure 4-5A) for quick check of parameters controlling the LU process. Note the type of foundation, i.e., drilled shaft versus driven pile, has been preselected from the start tab (Figure 4-1).

The simulation process begins with the selection of the simulation type, either unconditional or conditional. (Figure 4-5C). If unconditional simulation (use of all values) is selected, no additional input is needed. In the case of conditional simulation, i.e., using the nearest boring(Figure 4-5C), the user needs to specify which boring to use with the pull down window (Figure 4-5C), as well as the position of the foundation. The position can be either inputted by its northing and easting, or by a general horizontal distance from the selected boring.

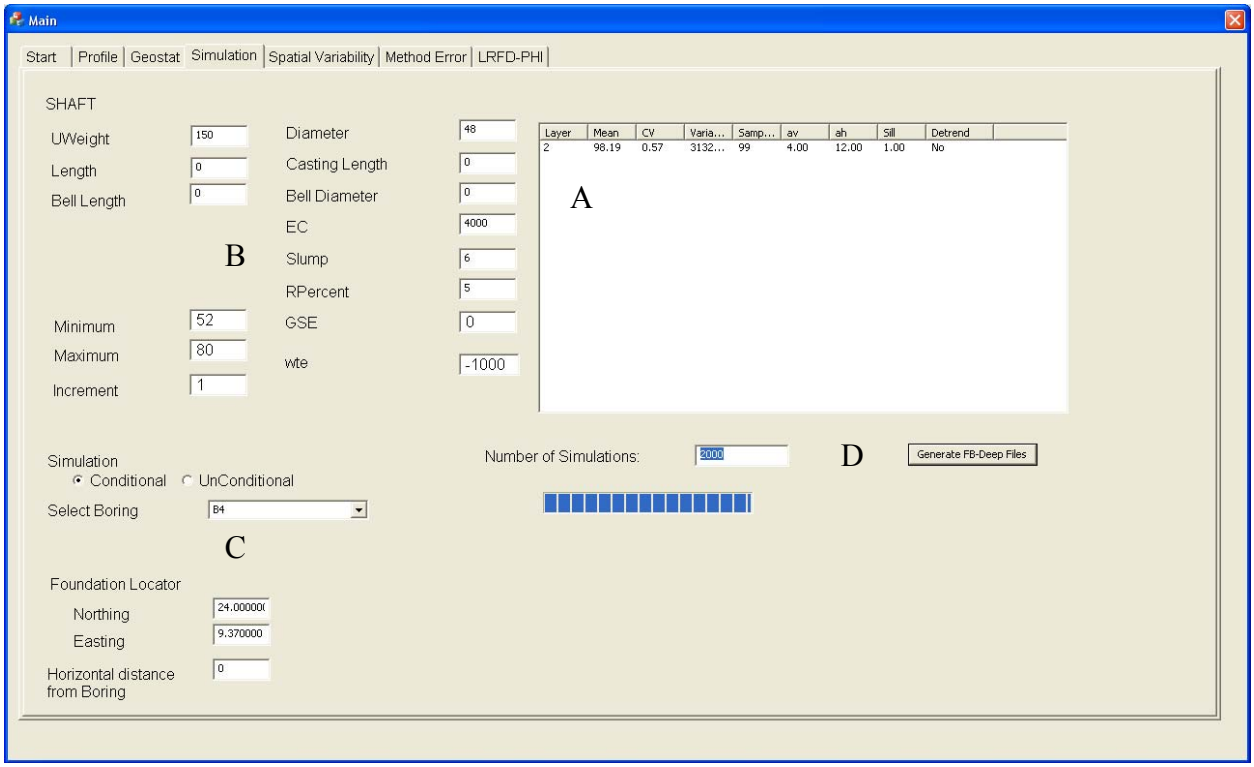

Figure 4-5. Simulation tab.

Other input parameters required in FB-DEEP for drilled shaft design (e.g., shaft dimensions, unit weight, casing length, slump, ground surface elevation [GSE], and water table elevation [wte], etc.) are entered in tab boxes shown in Figure 4-5B. After inputting all required parameters, input files for FB-DEEP may be generated. That is simply done by clicking the Generate Input Files located on the bottom right of the tab (Figure 4-5D). The user first enters the number of simulations of interest (e.g., 2000), and then clicks the "Generate FB-Deep Files" in Figure 4-5D. These files can be saved to any folder and are labeled "1.in" to "2000.in," where each file represents a single realization of parameter values in a boring. Any number of simulations may be considered; over 1000 simulations are suggested to obtain reliable estimates of both the mean and variability of predicted pile/shaft capacity. Prior to presentation of FB-DEEP output, however, the handling of other input data paired to q_u (i.e., q_t, E_m, etc.) in order to meet FB-DEEP requirements will be discussed.

4.2.4.1 FB-DEEP q_t versus q_u. For limestone, soil type 4, FB-DEEP requires inputs for q_u and q_t at the same specified depth. However, within a core run, corresponding samples are sized and tested for q_u and q_t at various locations, i.e., depths different from one another. Therefore, to meet FB-DEEP requirements, a relationship between properties in the form of linear regression is proposed based on the rock formation's cohesion

$$C = 0.5\sqrt{q_u}\sqrt{q_t} \qquad \text{Eq. 4.1}$$

To find a site specific relationship between q_u and q_t, pairs of tested samples (i.e., cohesion, Eq. 4.1) must be determined. Generally, the positions (elevation within the boring) of the samples within the 5-ft core run are not recorded, but cannot exceed 5 ft. An example of lab results for a rock core is shown in Table 4-3 from 17th Street Bridge. This particular core run is from a depth of 57 to 62 ft and has a measured recovery (REC) of 90% and rock quality designation (RQD) of 48%. It is assumed for the collected data, as well as recommended for future projects, that the samples listed in the database are in

Table 4-3. Sample of FDOT Rock Results 17th Street Bridge Boring 4 Core 2

SAMP. NO.	LENGTH (in)	DIA. (in)	MAX. LOAD (lbs)	S. T. STRENGTH (psi)	q (u) (psi)	DISPL. @ FAIL. (in)	STRAIN @ FAIL. (%)
1T	2.495	2.399	1414.2	150.3842		0.1128	
2U	4.376	2.383	1978.9		439.014	0.0355	0.811243
3T	2.621	2.381	1262.1	128.7227		0.0891	
4T	2.492	2.403	3328.0	353.7287		0.0556	
5U	3.913	2.356	2030.7		454.679	0.0354	0.904677
6T	2.473	2.343	2302.1	252.8827		0.0906	
7T	2.404	2.399	2290.3	252.7647		0.0901	
8T	2.658	2.395	2816.1	281.5633		0.0969	
9U	4.811	2.382	3170.6		711.509	0.0553	1.14933

order from top to bottom of the core. The selected pairs to be used in the regression analysis, i.e., q_u and q_t values are assumed to be in sequential order. An illustration for pairs selected from Core 2 is shown in Figure 4-6. Even though Core 2 did have REC and RQD less than 100%, it is still assumed that these pairs were located next to one another.

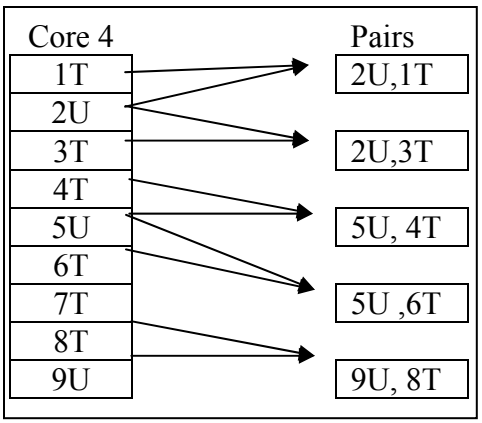

Figure 4-6. Illustration of pair matching.

With pairs of q_u and q_t selected, a regression analysis was used to determine the relationship between both parameters. Shown in Figure 4-7 is a plot of q_t vs q_u for the 17th Street Bridge, where red squares represent measured values and gray values were simulated. Evident from the figure, increasing q_u results in more scatter in the predicted q_t. The increase may be attributed to both distributions being log-normal functions. Consequently, to replicate the trend or the scatter shown in Figure 4-7, a log transformation of data prior to regression was performed.

Shown in Figure 4-8 is a plot of the pairs of the log (q_t) versus log (q_u). A linear regression of the data (intercept and slope) is also shown in Figure 4-8.

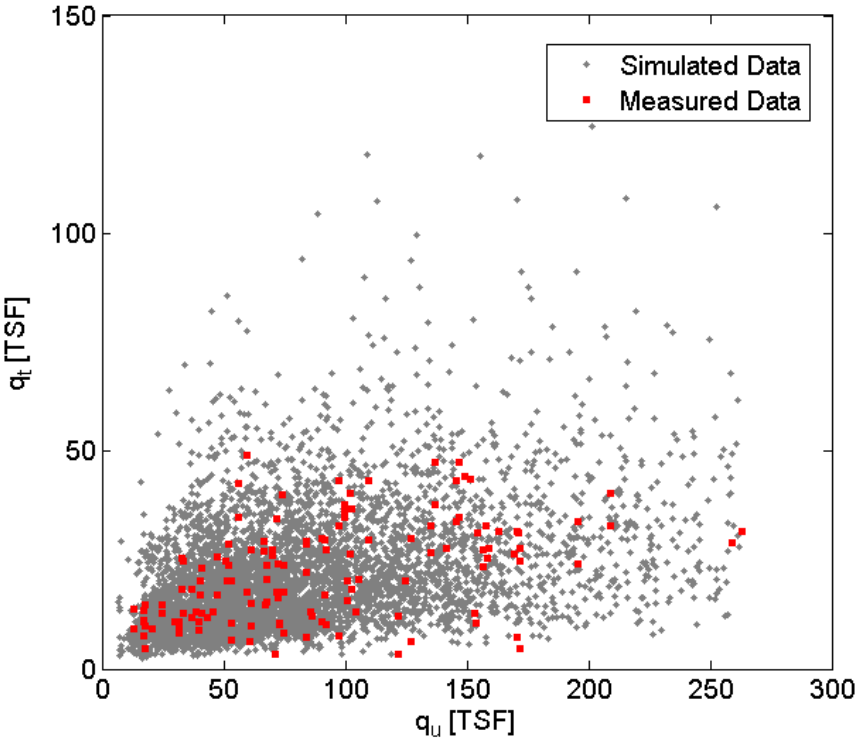

Figure 4-7. Measured and simulated q_t versus q_u.

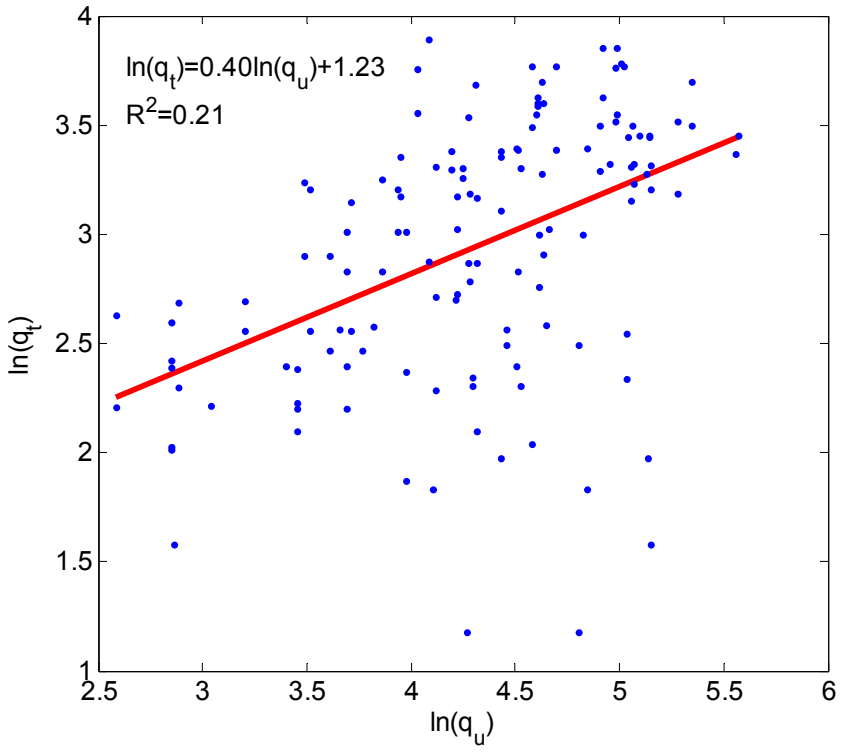

Figure 4-8. Regression of log transformed data [$\ln(q_t)$ vs $\ln(q_u)$].

Having established the relationship between q_u and q_t (Figure 4-8), the required pairs of values for FB-DEEP (Section 4.14) analysis may be generated. First q_u values are generated by the LU algorithm (Section 4.14: conditional or unconditional). Then the simulated q_{u_sim} values are used in Eq. 4.2 (exponentiation to convert back from log transform) with regression parameters (a and b from Figure 4-8) as

$$q_{t\_sim} = exp\left(a \ln q_{u\_sim} + b + \varepsilon\right) \quad \text{Eq. 4.2}$$

In addition, a random residual term ε (Eq. 4.2) was added for the uncertainty, which has a mean value of 0 and variance of σ^2 given by

$$\sigma^2 = (1 - R^2)\sigma^2_{\ln(qt)} \quad \text{Eq. 4.3}$$

where the correlation coefficient R is given in Figure 4-8, and $\sigma^2_{ln(qt)}$ is the variance of transformed (natural log) q_t data. Figure 4-7 shows the simulated q_{t_sim} versus q_{u_sim} values (gray circles) versus the measured values (red dots).

Note, each site will have its own correlation (Eq. 4.2 and Figure 4-8) established between q_u and q_t. Input of q_u and q_t data, as well as modulus E_i and recovery, are through the XML button shown in Figure 4-1. The format of the XML data, as well as the data itself, may be generated from the in situ and lab test Excel sheets used for the FDOT database (fdot.ce.ufl.edu/applications.html).

4.2.4.2 FB-DEEP E_m versus q_u. The relationship between q_u and intact Young's modulus E is much easier to obtain, since the modulus is computed from the unconfined compression test data directly (no pair matching required). For this analysis, the secant modulus E_{sec} (D_f – displacement at failure / L – Length of specimen times stress at failure) was used. Shown in Figure 4-9 (red squares) are the recorded in situ/lab results for the 17th Street Bridge.

Similar as for q_u versus q_t, Section 4.1.4.1, a log transformation was performed with regression coefficients a = 7.32 and b = 9.8, and correlation coefficient $R^2 = 0.57$). Evident from the plot, E_{sec} and q_u are more correlated (i.e., larger R^2) than q_t and q_u. This was attributed to the samples being collocated and less influenced by spatial variability.

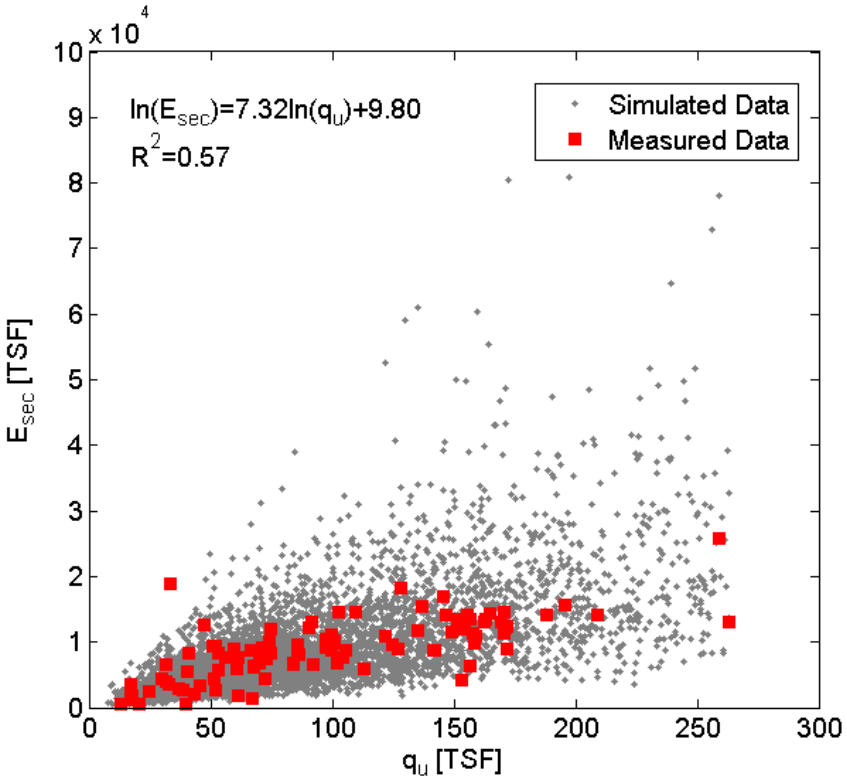

Figure 4-9. 17th Street Bridge E_{sec} versus q_u for Florida limestone.

Like q_t, the FB-DEEP software needs the Young's modulus E_m for corresponding q_u at a specified depth for tip assessment. As discussed in Section 4.1.4.1, first the q_u data are generated by the LU algorithm (Section 4.14: conditional or unconditional). Then the simulated q_{u_sim} values (same ones used to determine q_{t_sim}) are used in Eq. 4.2 with regression parameters (a and b from Figure 4-9) to generate the simulated Young's Modulus E_{sec_sim}. The random residual term ε was found from Eq. 4.3 with $\sigma^2_{ln(qt)}$ and replaced by $\sigma^2_{ln(Esec)}$. Shown in Figure 4-9 are the measured (red dots) and simulated (gray dots) secant Young's modulus for the 17th Street Bridge.

4.2.4.3 FB-DEEP recovery versus q_u. Also needed for FB-DEEP for each q_u are RQD and recovery (REC) values. For this research, the relationship between q_u and RQD/REC for a number of sites (e.g., 17th, Jewfish Creek) was investigated. However, no relationship between q_u and RQD/REC was found as has been reported in the FDOT report **BC354-08**. Therefore when generating the boring data (conditional or unconditional), the RQD/REC values are randomly selected from distribution data inputted for a site (Figure 4-1). Shown in Figure 4-10 is the RQD distribution for the 17th Street Bridge from which data will be randomly selected.

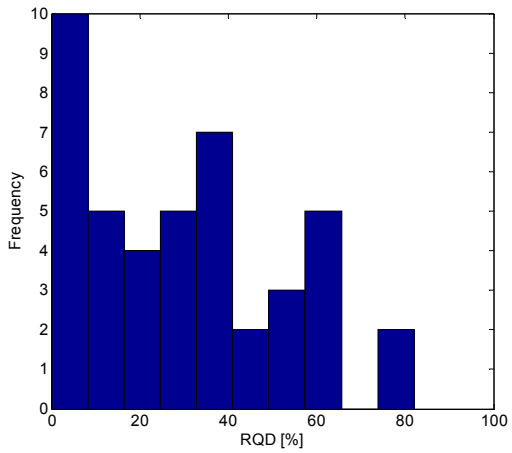

Figure 4-10. Histogram of RQD for 17th Street Bridge.

Having simulated both the RQD and intact rock secant modulus, the O'Neill's mass modulus E_m for FB-DEEP can be determined using the trend line shown in Figure 4-11.

4.2.4.4 FB-DEEP drilled shaft soil properties. Besides rock strength and modulus, unit weight of soil (sand and clay) and the undrained strength of clay Cu are needed for drilled shaft analysis. For most projects, inadequate amounts of unit weight measurements are recorded and predicted values have some variability or variance. For this work, the unit weight will be assumed to be log-normally distributed and a mean and CV will be available as user input. During the simulation process (conditional or unconditional), the unit weight will be randomly

selected for each generated input for FB-DEEP based on user supplied mean and CV. Evidently, the smaller the user supplied CV, the smaller the variability in generated unit weights.

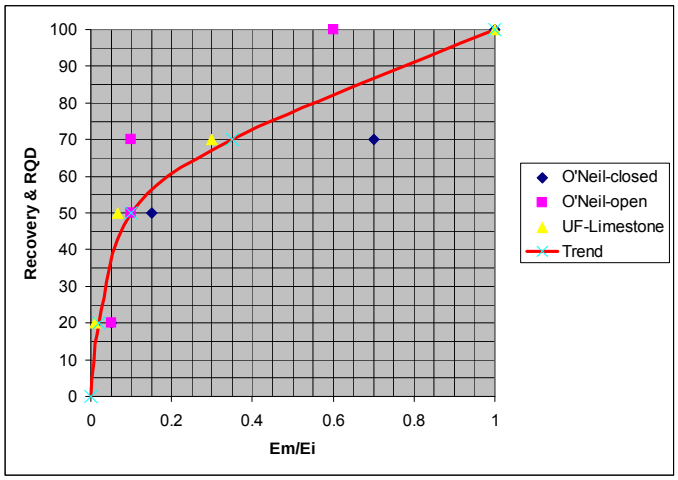

Figure 4-11. O'Neill E_m/E_i versus RQD and UF E_m/E_i versus recovery (McVay et al. 2009).

For FB-DEEP's drilled shafts in clayey soil input (FB-DEEP types1 and 2) of undrained shear strength, Cu is needed. Since little, if any, undisturbed sampling is reported in the soil boring plan sheets for FDOT sites, Cu values will be correlated to SPT "N". Thus for clay layers, a default model by Terzaghi and Peck (1976) will be used, which is Cu = 0.06 N (tsf). This model was selected because the method error assessment for drilled shafts in clay (Chapter 3) was collected from the NCHRP Report 507 and was used in the predictions. Note, the user has the option of choosing alternative models (e.g., linear or power) for converting SPT-N to Cu. The only condition for this is that the user must also use regression parameters for method error (Chapter 3) at the method error tab (Figure 4-5). This will ensure that any errors from the user specified model are appropriately considered.

4.2.5 GUI: Simulation Tab –FB-DEEP Analyses

After generating all soil/rock parameters (conditional or unconditional) for drilled shaft analysis, the user must open FB-DEEP separately from the GUI to analyze the data sets. With

FB-DEEP open, the user must select "Batch Mode" process under the "Show" icon displayed in Figure 4-12. From batch mode, the user then clicks "Incremental Selection" which allows the user to enter the beginning (1.in) and end (2000.in) file. FB-DEEP will analyze each file and generate a corresponding output file from "1.out" to "2000.out" with capacity calculations outputted in each.

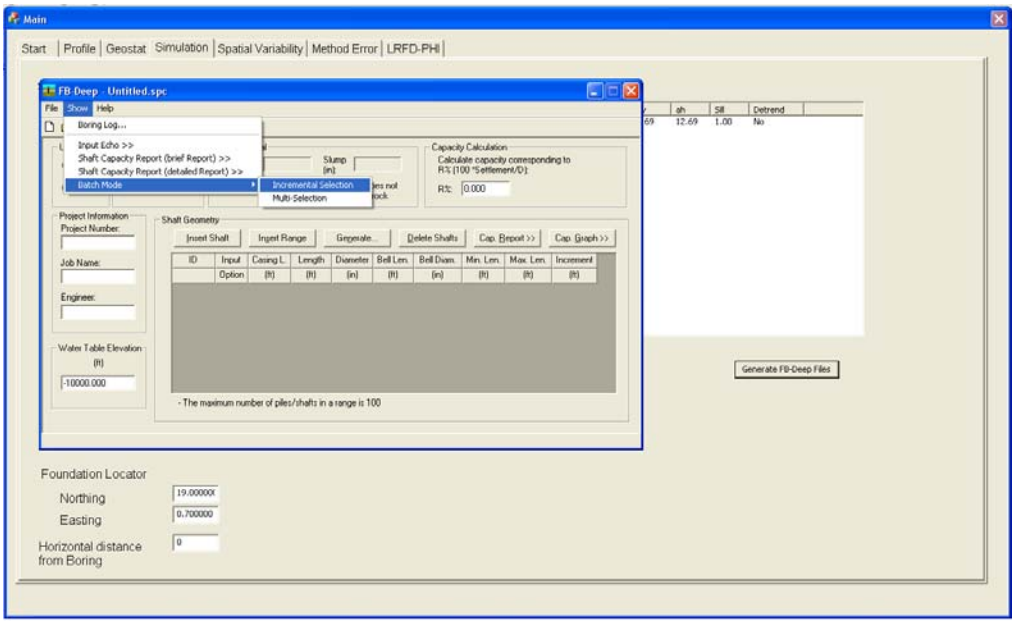

Figure 4-12. FB-DEEP batch mode.

4.2.6 GUI: Spatial Variability Tab

After analyses of all the simulated data sets (e.g., 2000) in FB-DEEP, the output of each is read back into the GUI and analyzed. Shown in Figure 4-13 on the spatial variability tab is the icon "Import FB-DEEP Output," where the user imports the ".out" files generated by FB-DEEP. The GUI analyzes the results of the simulations and computes the mean, variance, CV, and $\overline{\phi}$, which are displayed in the four graphs as a function of depth. It is important to note that at this stage of the analysis, the results are for spatial variability only; method error has not yet been incorporated into the evaluation. The user has the option of selecting skin, tip, or total (radio

buttons). The case of skin alone is for limestone, where tip resistance is neglected. As expected, the mean and variance of the resistance increase with depth due to increased surface area of the shaft. However, the CV (standard deviation / mean) decreases, resulting in increasing $\overline{\phi}$ with depth.

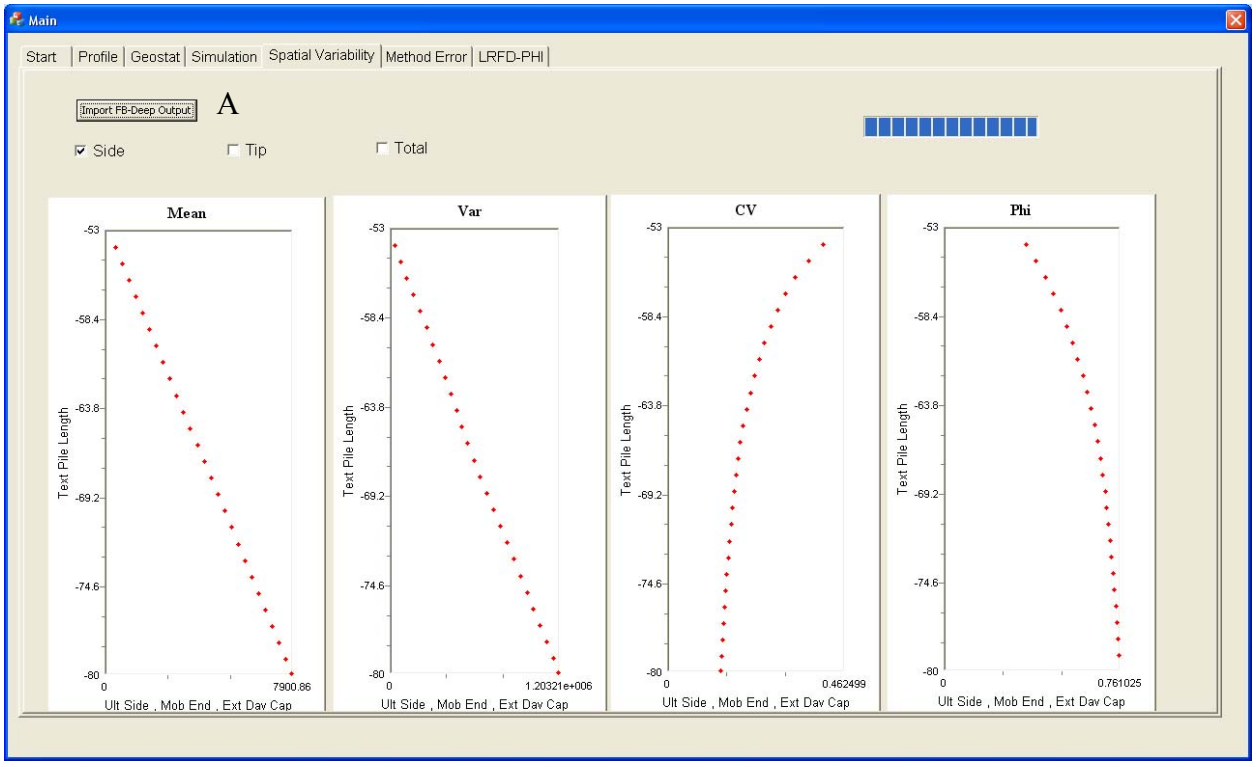

Figure 4-13. 17th Street Bridge spatial variability tab.

4.2.7 GUI: Method Error Tab

The method error tab of Figure 4-14 incorporates the errors and biases associated with the FB-DEEP's resistance calculation as well as with shaft construction. On this tab, the designer can use the results from the regression analyses given in Chapter 3 by clicking the historical data button (Figure 4-14A). Additionally, users can also import results from their own database of load test data or planned site specific load testing with regression parameters given (Figure 4-14B). Once these fields are filled out, the load test button Figure 4-14C must be clicked before

continuing. For the 17th Street Bridge example, historical data from Chapter 3 was used for the method error. The method error in this tab applies to both drilled shafts and driven piles with values used depending upon pile/shaft selected (start tab).

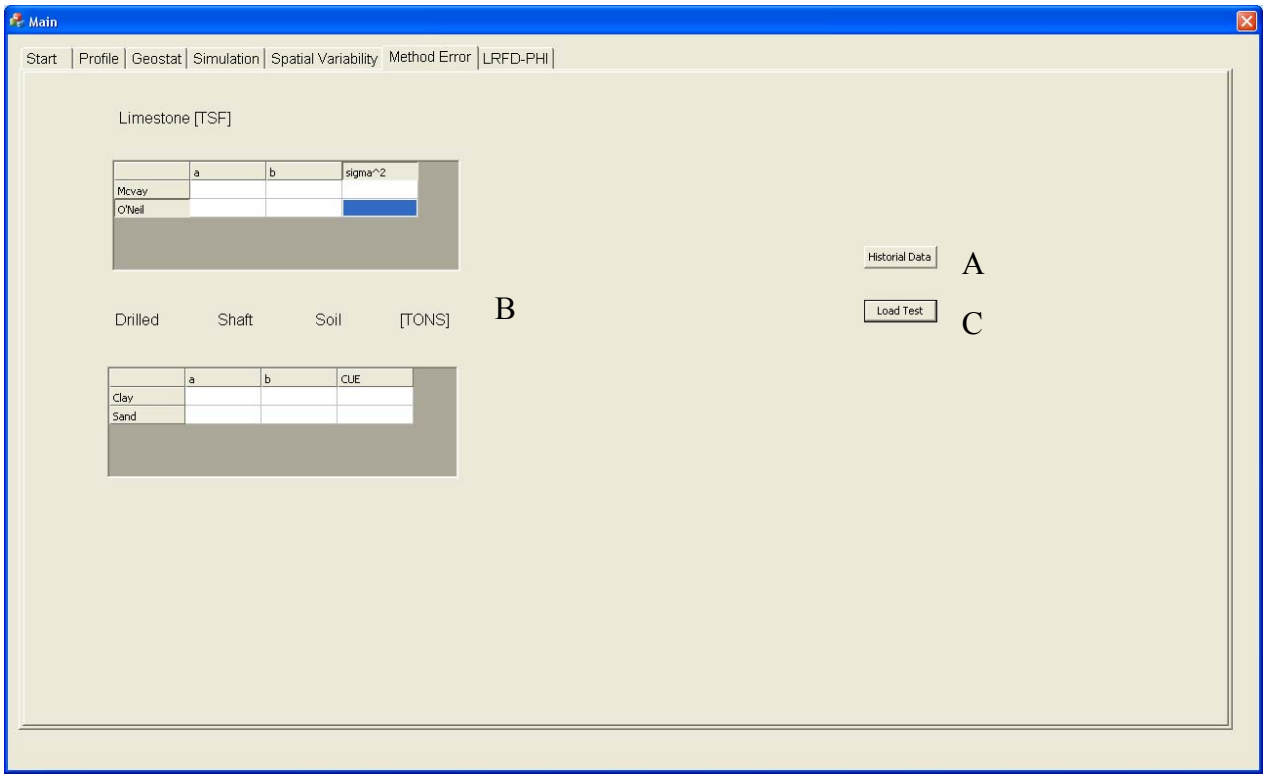

Figure 4-14. GUI method error tab.

4.2.8 GUI: LRFD PHI Tab

With both spatial and method error computed for a specific site, the final results can be computed and displayed in the LRFD PHI tab shown in Figure 4-15. Three plots are shown with the left being for side resistance only (B), the middle for tip resistance (C), and the right for total resistance (D). A pull down menu (Figure 4-15A) controls what is shown on the three plots. Four options are available: mean, CV, $\overline{\phi}$, and $\overline{\phi}$Rn may be plotted versus tip elevation of the foundation. The red line represents the results from the spatial analysis only, and the green

represents the results from both spatial and method error combined. This allows the user to see the impact that the method error has on total uncertainty with respect to spatial variability.

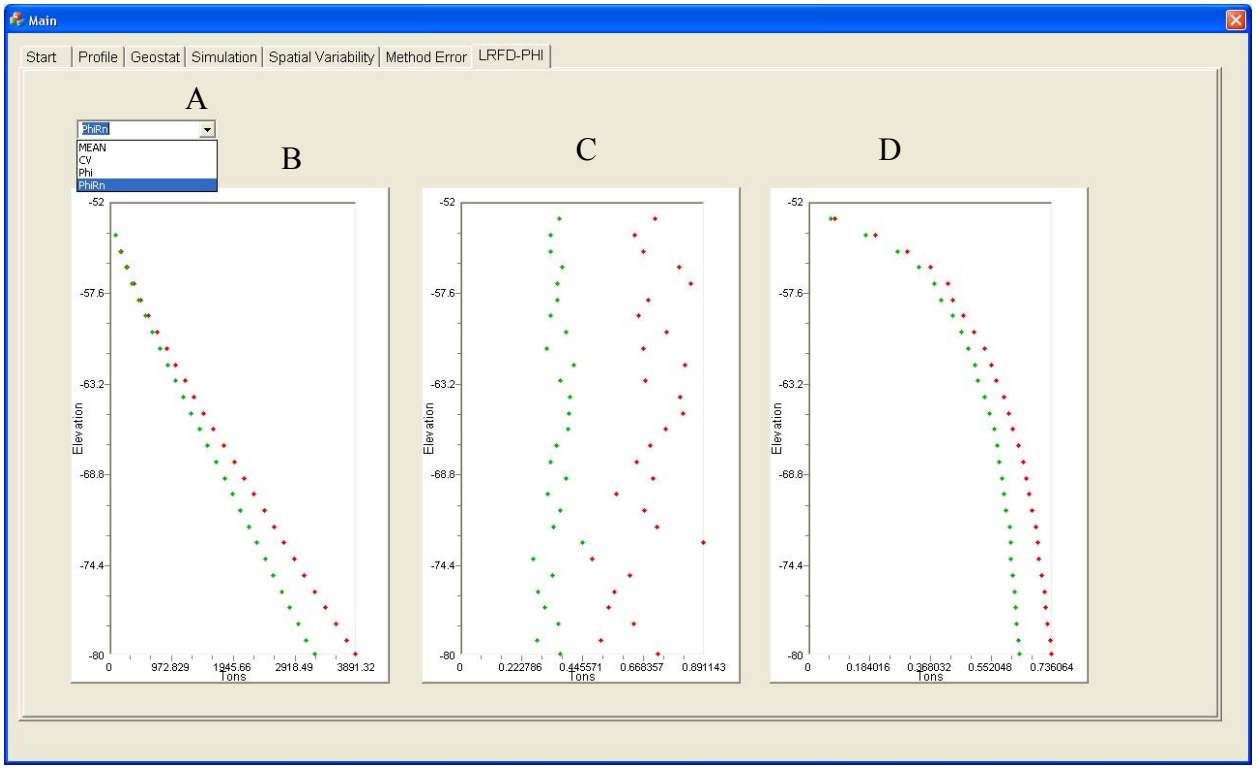

Figure 4-15. GUI LRFD PHI tab.

4.3 Unconditional Simulation Results for 17th Street Bridge in Fort Lauderdale, Florida

The first analysis reported is the unconditional simulation with results shown in Figures 4-16 through 4-18. In the plots, the blue line represents uncertainty due to spatial variability only, and the red dashed line incorporates both spatial and method error which would be used for design. The ordinate (Y) axis in the figure is the total length of drilled shaft input into FB-DEEP. Since the ground surface elevation was at 0 and the top of the limestone is located at –51.2 feet, the length of embedment in the limestone is L-51.2.

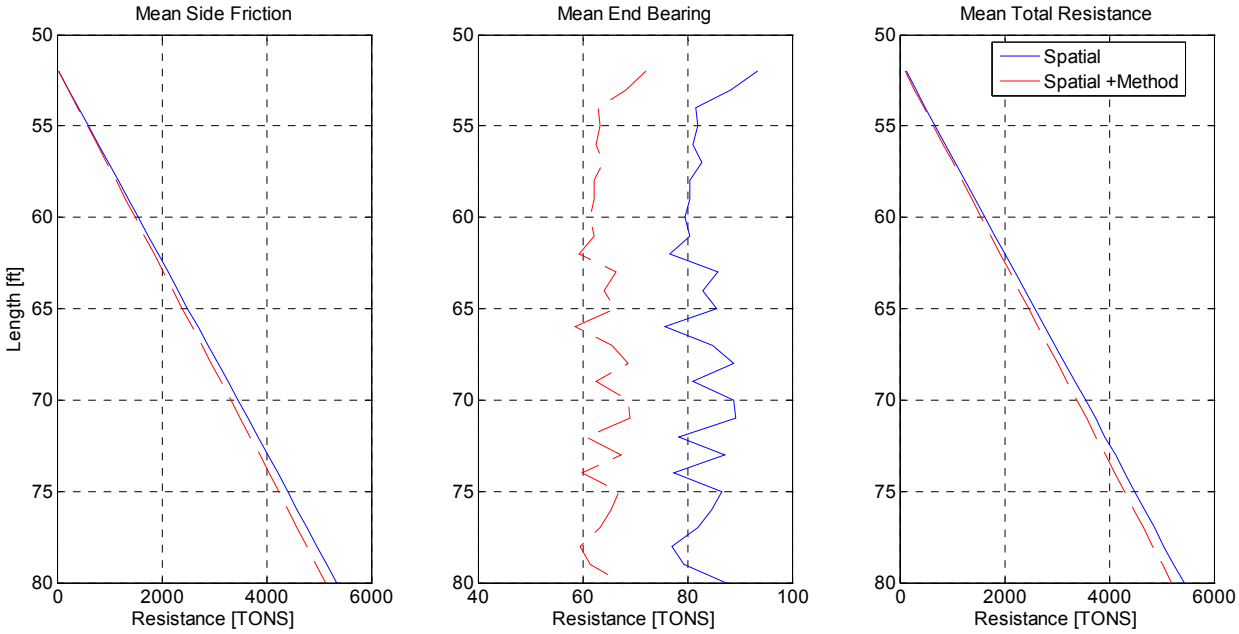

Figure 4-16. 17th Street Bridge, mean resistances – unconditional simulation.

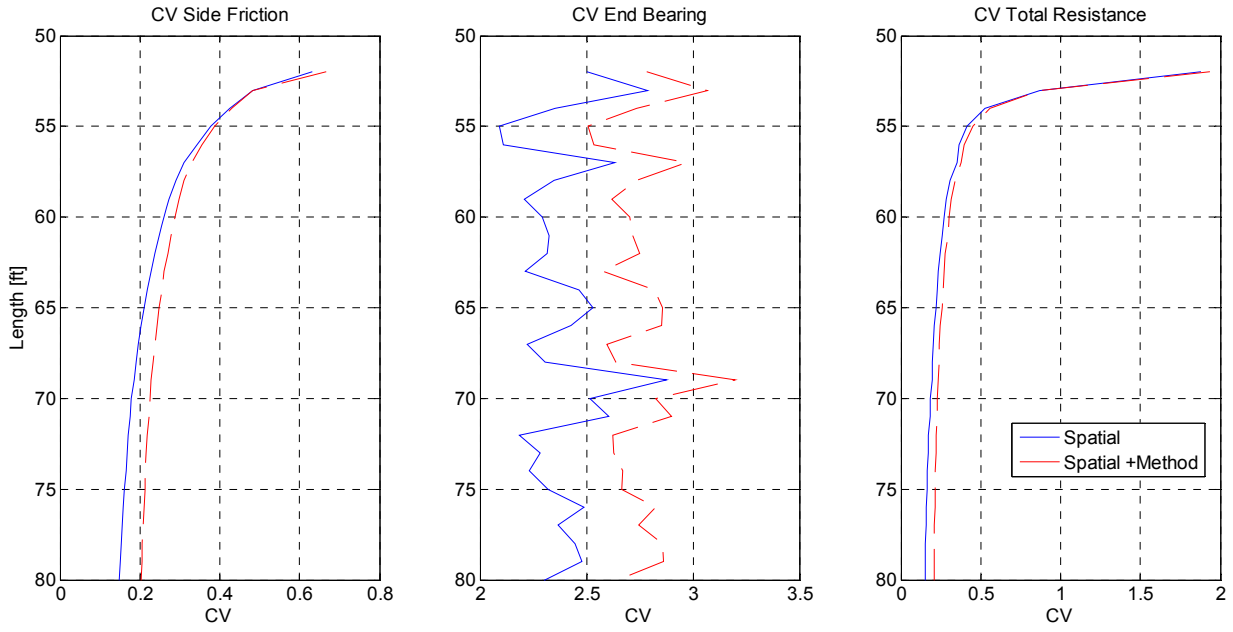

Figure 4-17. 17th Street Bridge, CV of resistances – unconditional simulation.

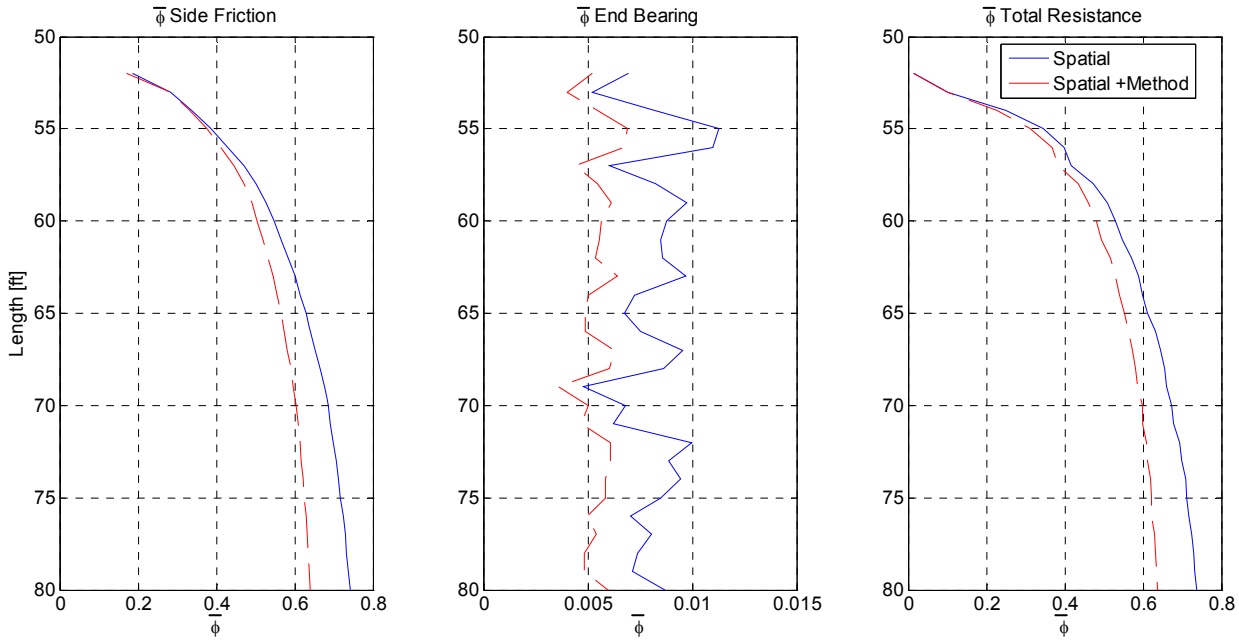

Figure 4-18. 17th Street Bridge, LRFD $\overline{\phi}$ – unconditional simulation.

Figure 4-16 plots mean capacities for just side friction, end bearing and total (side + end bearing). For side friction, it can be seen that the mean capacity increases with length of shaft at a constant slope. This is expected since unconditional simulations approach the site mean value, thus side friction becomes a function of surface area (linear with depth). However, mean end bearing is relatively constant with increasing shaft length. This is attributed to unconditional simulations reproducing the site mean over many simulations. Fluctuations with depth displayed in the end bearing figure can be attributed to simulation error, but are relatively small when compared to mean prediction, and may be neglected. For all plots, the incorporation of method error results in a mean resistance less than mean prediction from just spatial variability. This is due to regression equations used whose terms reduce the predicted resistance (Table 3-1).

Figure 4-17 plots CV for side friction, end bearing, and total (side + end bearing) resistance. The plot of side friction CV shows a decrease with depth. This is expected due to larger averaging domain of longer shaft, thus reducing the uncertainty while increasing expected

resistance. For end bearing, the CV is constant with depth as expected, and it is significantly higher than that of side friction. This is due to FB-DEEP using only one modulus value to calculate the tip resistance. This results in no spatial averaging and no reduction in variance of the measure point modulus and RQD values. Also of interest is the magnitude of contribution of spatial uncertainty (blue) and method uncertainty (difference between red and blue). Evidently, the spatial contribution is higher than the influence of the method.

Figure 4-18 plots $\overline{\phi}$ for side friction, end bearing, and total (side + end bearing) resistance. These plots have the same overall shape as the corresponding plots of CV, which is expected since $\overline{\phi}$ is a monotonic function of CV, Eq. 3.17. It should be noted that for design, $\overline{\phi}$ for spatial plus method uncertainties (red dashed line) should be used. In the plot, the difference between the spatial (blue) and spatial plus method (red) is only the influence of method error. It is evident that the influence of spatial is large. Also note that the $\overline{\phi}$ for total resistance increases with depth due to the dominating contribution of skin friction and its reduced CV due to spatial averaging.

Figure 4-19 plots design resistance $\overline{\phi}$Rn due to side, tip, and total. The design side friction can be compared with results reported in **BD545-76** for required length to support 2500 tons from spatial variability (blue line) only. **BD545-76** found that the required length for a 4-ft diameter shaft was 20 ft for an unconditional simulation. A comparable length of 19 ft was found using the GUI. The slight difference can be attributed to the GUI's use of simulating q_t from q_u rather than cohesion alone, as well as the use of randomization of RQD values.

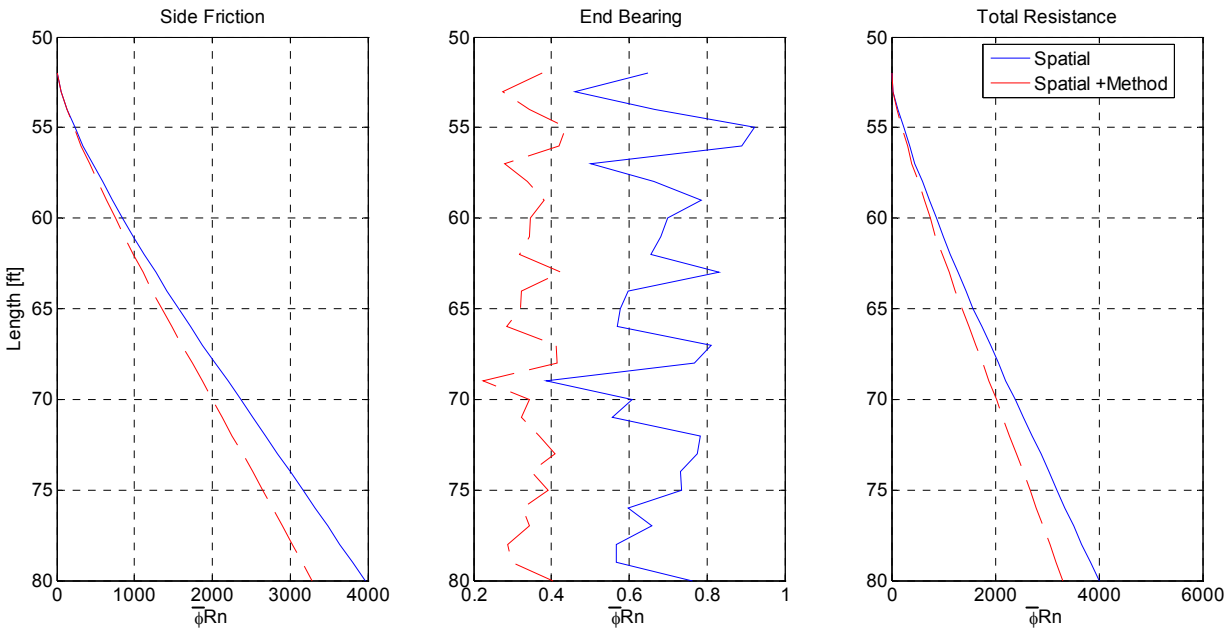

Figure 4-19. 17th Street Bridge, design resistances – unconditional simulation.

4.4 Conditional Simulation Results for 17th Street Bridge in Fort Lauderdale, Florida

Conditional simulations were performed using borings B-4 and B-6, which are assumed to be located within production shaft footprints. Results from the analyses are shown in Figures 4-20 through 4-23 for B-4 and Figures 4-24 through 4-27 for B-6. Both cases result in different mean capacities when compared to each other and to the unconditional simulation. This is due to conditioning (i.e., larger weighting) of measured q_u at each of the boring locations. This also results in a less uniform slope of increasing side friction resistance with depth. Also noticeable for the two cases is that the CV for side friction is less than the unconditional simulation, resulting in a higher $\overline{\phi}$ factor. This is a result of the shaft being within the horizontal correlation length a_h, conditioning the prediction to the measured values of the closest boring. It is important to note that use of the FB-DEEP line of input results in no averaging in the horizontal

direction, thus resulting in a conservative estimate of $\overline{\phi}$. The higher $\overline{\phi}$ for the conditional cases demonstrates the advantage of having boring located within the footprint of the foundation.

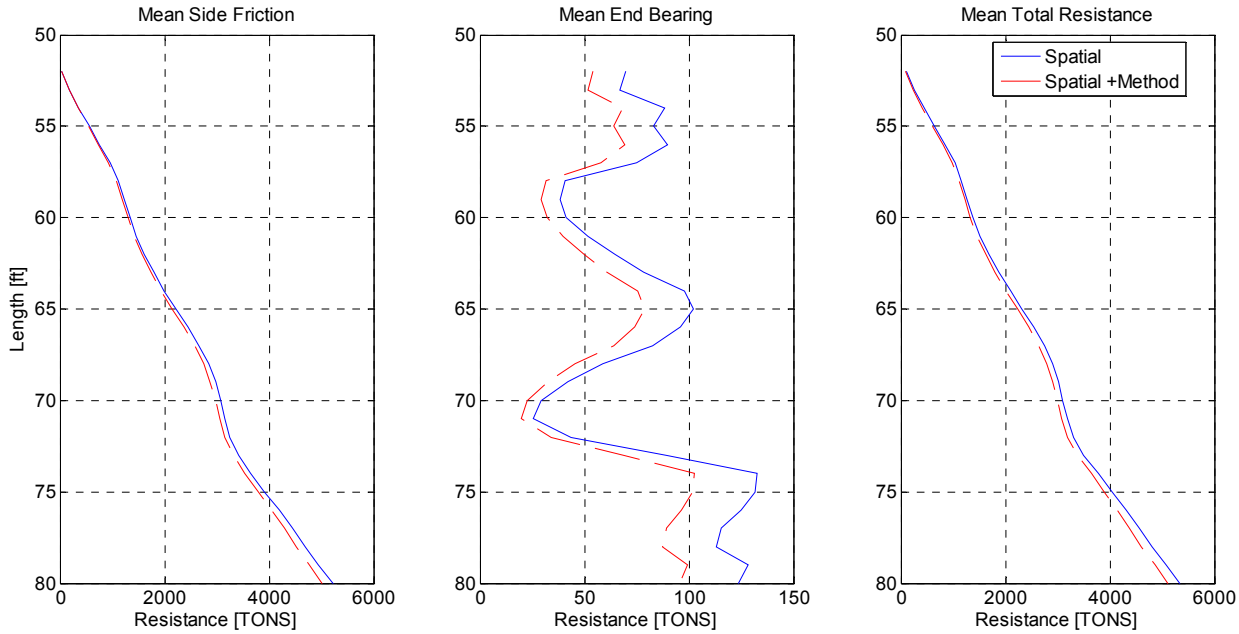

Figure 4-20. 17th Street Bridge, mean resistances – conditional simulation B-4.

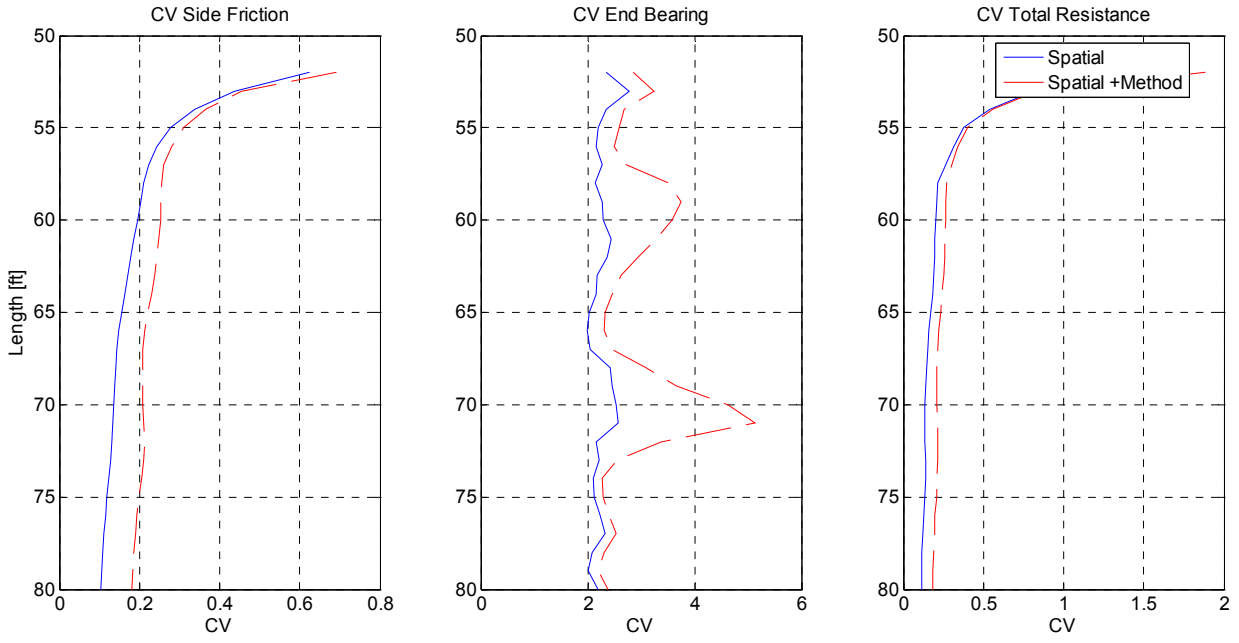

Figure 4-21. 17th Street Bridge, CV of resistance – conditional simulation B-4.

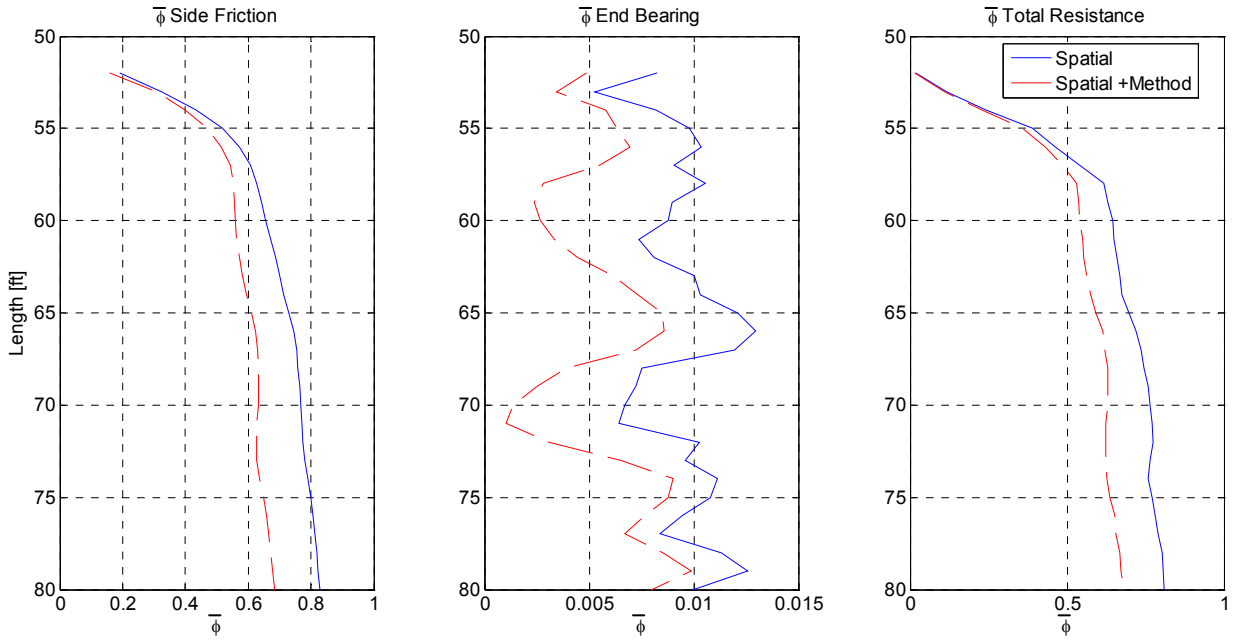

Figure 4-22. 17th Street Bridge, LRFD $\overline{\phi}$s – conditional simulation B-4.

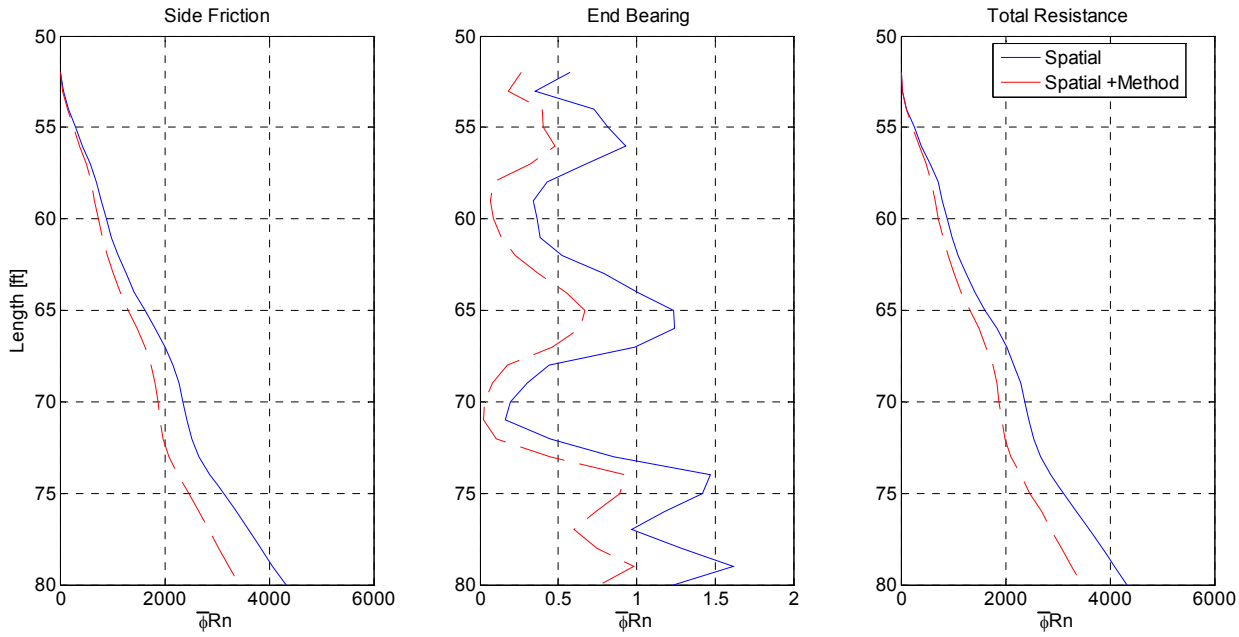

Figure 4-23. 17th Street Bridge, design resistances – conditional simulation B-4.

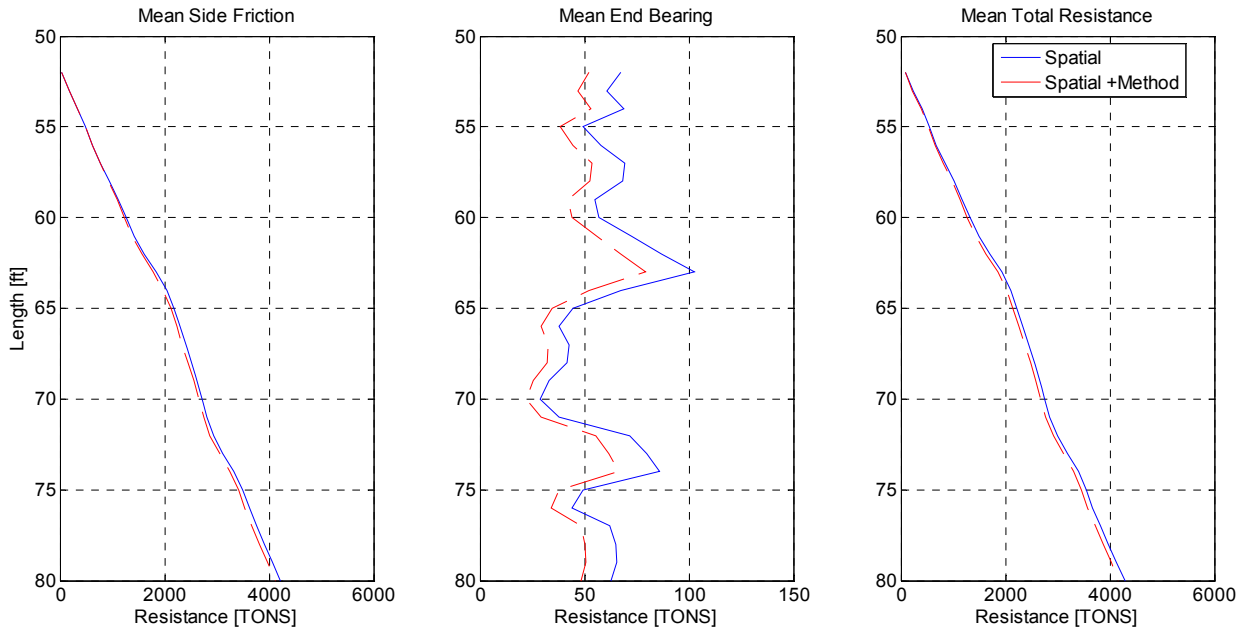

Figure 4-24. 17th Street Bridge, mean resistances – conditional simulation B-6.

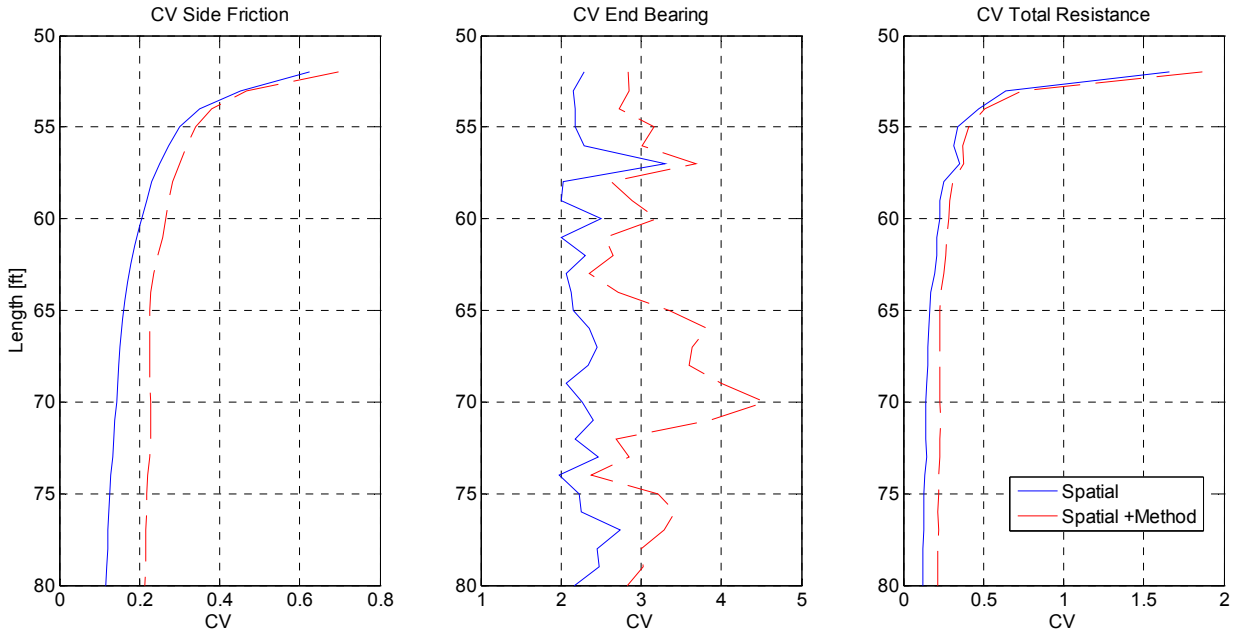

Figure 4-25. 17th Street Bridge, CV of resistance – conditional simulation B-6.

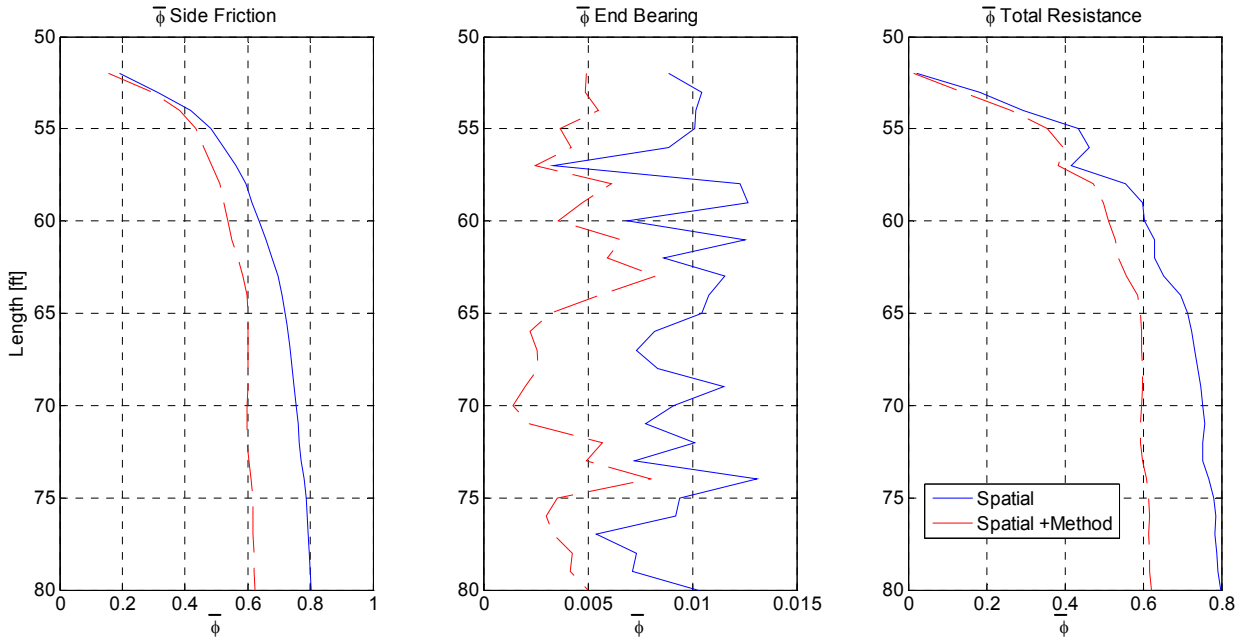

Figure 4-26. 17th Street Bridge, LRFD $\overline{\phi}$s – conditional simulation B-6.

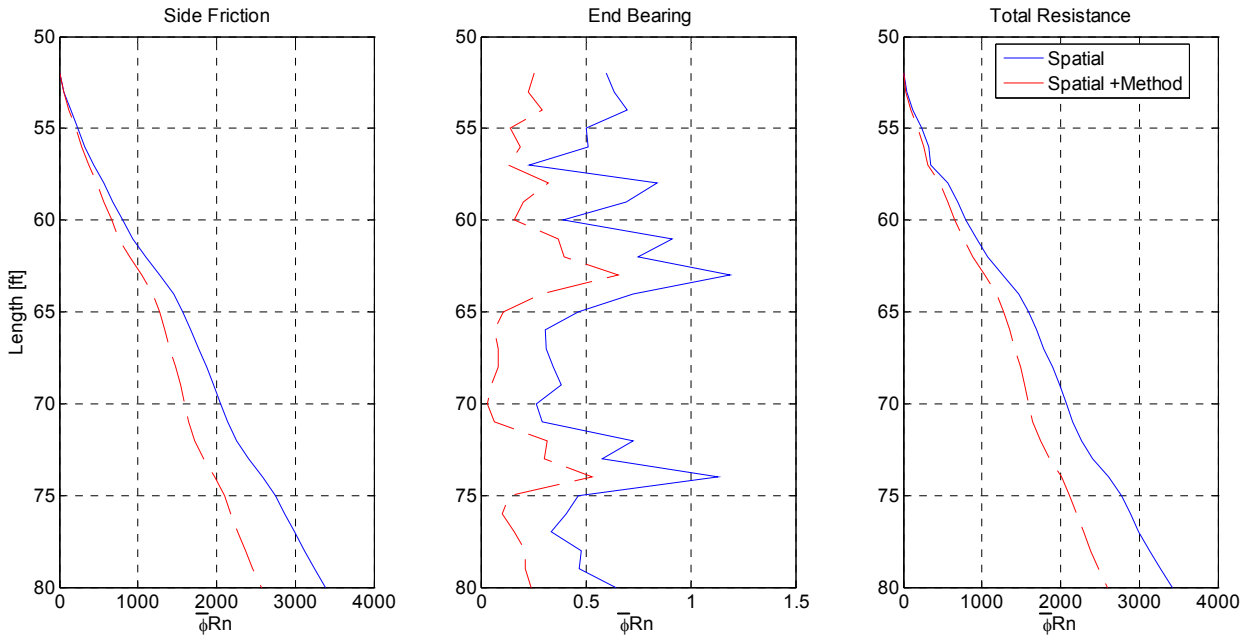

Figure 4-27. 17th Street Bridge, design resistances – conditional simulation B-6.

Note however, the design side resistance ($\bar{\phi}$Rn) is 1600 tons (B-6), 1800 tons (B-4), and 2000 tons for the whole site (i.e. unconditional) at 70 ft. Even though the conditional cases (B-6 and B-4) have higher $\bar{\phi}$, their design resistance is less than that of unconditional. This is due to conditioning to small q_u at deeper depths seen in the profile tab (Figure 4-2). This results in the smaller mean resistance determined by the simulation process.

4.5 Dixie Highway Over Hillsboro Canal in Broward County, Florida

The 17th Street Bridge example illustrates the use of the GUI for spatial and method uncertainty analysis for a drilled shaft design. Also of interest is the use of the GUI for the design of driven piles based on insitu SPT N data. A recent example of driven piles which includes static load testing is the FDOT Dixie Highway project over Hillsboro Canal in Broward County, Florida. The project had 21 SPT borings and used 24-inch prestressed concrete piles. A discussion of GUI tabs and output follows.

4.5.1 GUI: Start Tab

Figure 4-28 shows the start tab, where the user identifies type of foundation and imports boring data. The boring data is imported through the XML icon shown in Figure 4-28A. Again, the data may be entered and exported (XML) with the in situ Excel sheets used for the FDOT database (found at fdot.ce.ufl.edu/applications.html). Presently, all boring data uploaded will be considered in the unconditional simulation. Successful importing of the data will show the boring names and numbers in the boring window (Figure 4-28B). After importing the boring data and selecting foundation type, the user needs to click “Save Project Information” (Figure 4-28C).

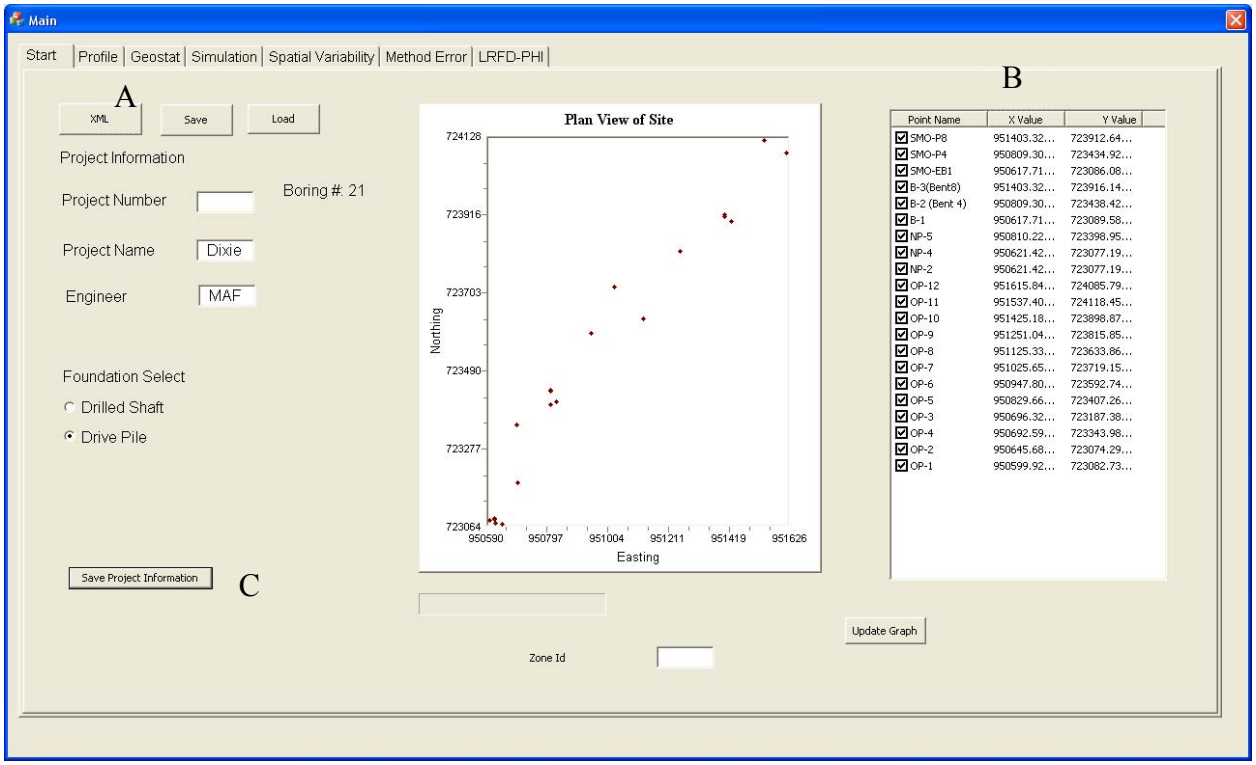

Figure 4-28. Start tab – plan view of Dixie Highway.

4.5.2 GUI: Profile Tab

With the site's in situ data loaded into the GUI, the profile is next analyzed to determine layering (Figure 4-29). The profile can be broken into layers by simply clicking within the plot window (Figure 4-29A). A layer boundary is displayed as a blue line within the window. The user should identify layers based on means, trends or variance as discussed in Chapter 2. Also, if an automatic hammer was used, a correction factor can be applied (Figure 4-29B). The correction factor is only applied to those borings that have automatic hammer identified in the XML file. For this example, a correction factor of 1.2 was used because of the rated energy of the hammer, and it was applied to three of the borings preformed by the FDOT SMO.

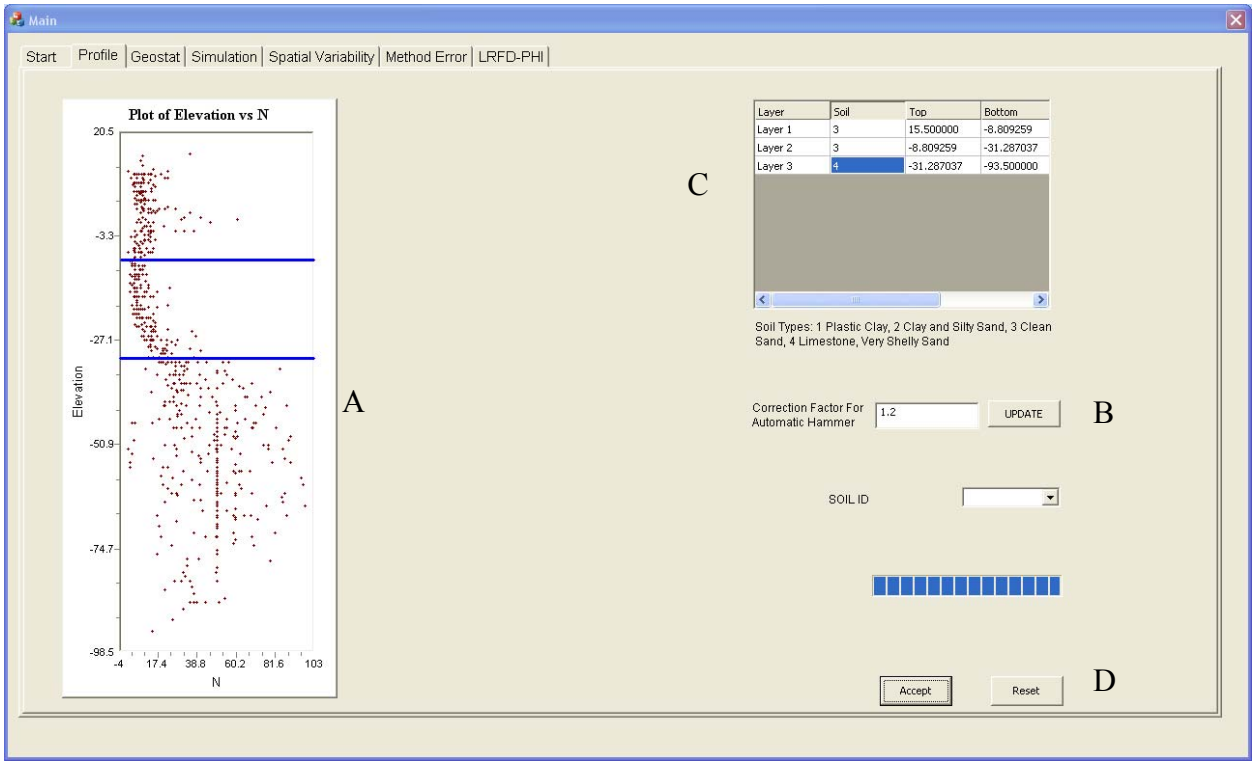

Figure 4-29. Profile tab for Dixie Highway.

After identifying layers, the user needs to input soil types in the soil summary table (Figure 4-29C). If the user does not find the layering acceptable, the profile can be "reset" by clicking the button shown in Figure 4-20D. After identifying layers and soil types, the user needs to click the "Accept" button before proceeding to the next tab.

4.5.3 GUI: Geostat Tab

For each layer indentified in the profile tab, a geostatistical analysis is needed. Shown in Figure 4-30 is the geostat tab for Dixie Highway. The geostatistical analysis should begin with detrending of any layer under analysis. Evident in Figure 4-30A, the blow count N increases with depth, particularly in layer 2, which is detrended by clicking the detrend box in Figure 4-30B and selecting the 1st order polynomial (linear detrending). This generates the blue line shown on the layer's profile plot. The detrending is performed by the GUI and applied appropriately where needed. Shown in Table 4-4 are the summary statistics for each layer. For

detrended layers CV's are evaluated from the mean of the data before detrending in combination with the standard deviation from the data after detrending.

After detrending analysis and normal score transform, the experimental variogram for both horizontal and vertical directions needs to be evaluated. For this analysis, search parameters shown in Table 4-5 were used. The lag distance of 2 ft for the vertical direction with tolerance of 1 was chosen because SPT-N's are typically taken at intervals from 2.5 to 5 ft. These parameters are recommended for SPT data in the vertical direction. For the horizontal direction, a short lag

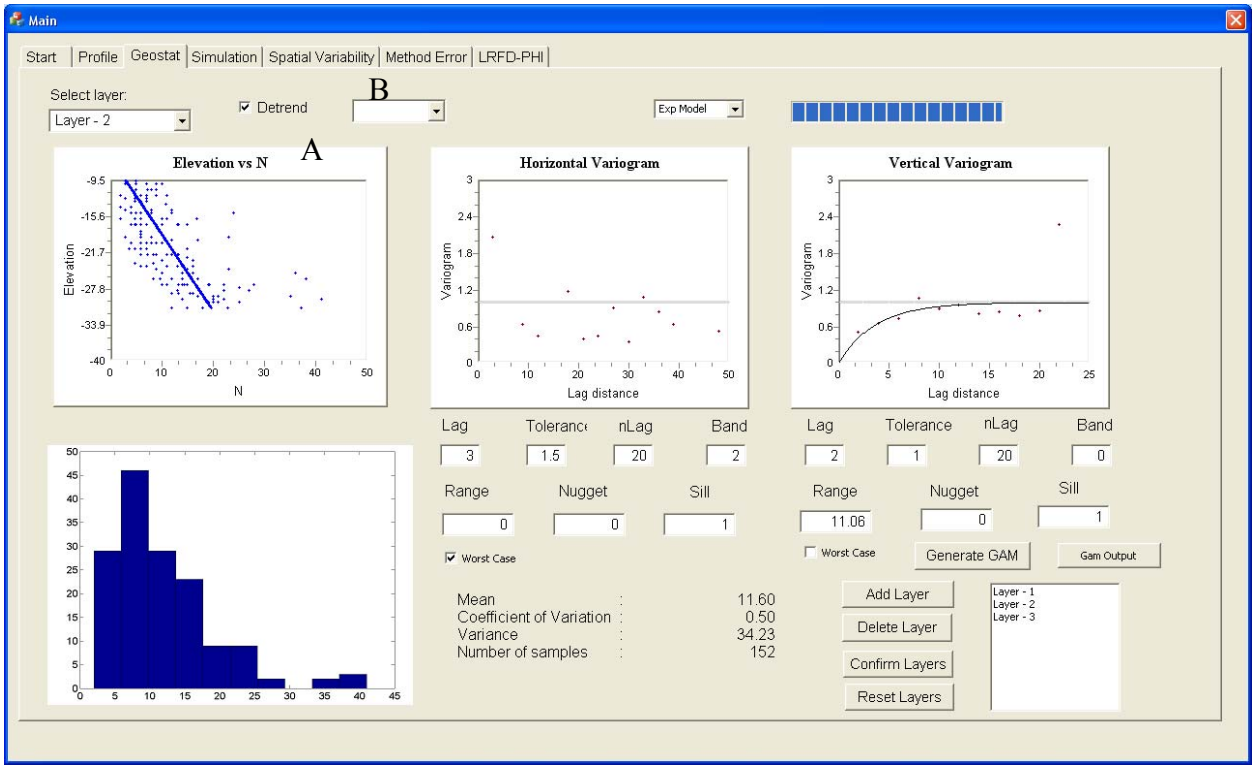

Figure 4-30. Geostat tab for Dixie Highway.

Table 4-4. Layer Summary Statistics and Performance of Detrending

Layer	Mean	CV	n	Detrend	Order
1	11.35	0.69	183	Yes	2
2	11.49	0.51	154	Yes	1
3	45.42	0.41	317	No	NA

Table 4-5. Variogram Search Parameters

Search Direction	Lag	Tolerance	Number of Lags	Bandwidth
Horizontal	3	1.5	20	1
Vertical	2	1	20	0

distance interval of 3 ft was used approximately corresponding to the shortest spacing between borings. In general, however, this parameter will vary from site to site. It is best to try multiple lag distance intervals and view the resulting variogram. Also, the Gam Output button should be clicked to see if adequate numbers of pairs (> 30) were considered in the variogram analysis. In addition, when working with SPT data, it is recommended that the vertical bandwidth for the horizontal variogram be set to 1 or 2 ft. This may help increase the number of data pairs, since all site borings may not be sampled at exactly the same elevations throughout. It is also recommended that the tolerance be set to half the lag distance.

With search parameters listed in Table 4-5, the variogram models are fitted to each layer. A summary of the models used is shown in Table 4-6. It was found for all three layers that the horizontal variogram is poorly defined due to insufficient data (n < 30 pairs). Thus for this site, the worst case analysis for a_h will be applied. For the worst case a_h, the GUI assumes $a_h = a_v$. This allows the measured values of the boring in the footprint to be weighted more during the analysis.

Table 4-6. Variogram Model

Layer	Model	a_v	$sill_v$	a_h	$sill_h$	nugget
1	SPH	6.06	1	NA	1	0
2	EXP	11.06	1	NA	1	0
3	EXP	11.08	1	NA	1	0

SPH-Spherical Model
EXP-Exponential Model

4.5.4 GUI: Simulation Tab

For the Dixie Highway 24-inch square piles were selected in Figure 4-31A. For the simulation analysis for driven piles, only one pile length is entered. This is due to FB-DEEP's limitation of only being able to calculate one pile length per file read. For future implementations, it is recommended that FB-DEEP be modified to compute driven pile resistances for a range of lengths.

Next, the user needs to identify conditional (nearest boring) or unconditional (mean boring data) simulation (Figure 4-31B). After entering the number of realizations (Figure 4-31C), the user clicks "Generate FB-Deep Files". The subsequent processes are identical to that discussed for drilled shafts above.

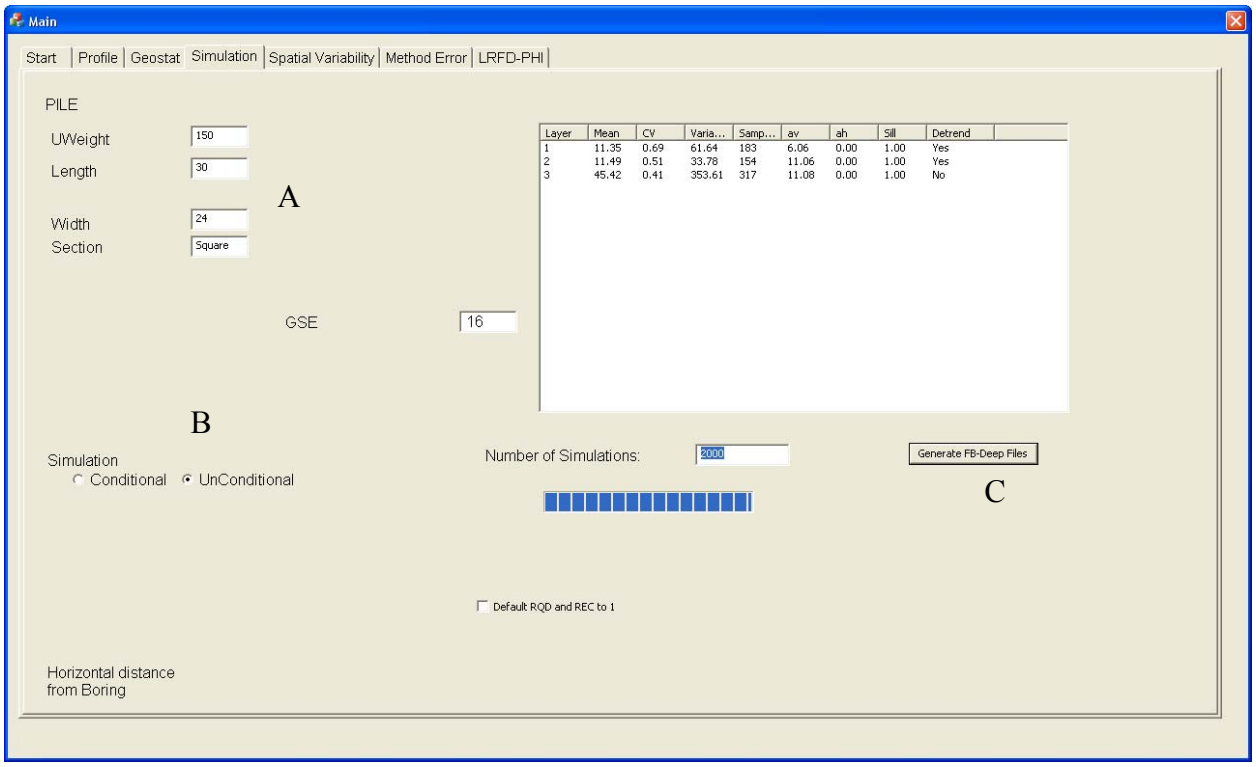

Figure 4-31. Simulation tab for Dixie Highway.

4.6 Results for Dixie Highway in Broward County, Florida

Unconditional simulation results are shown in Figures 4-32 through 4-35 and the conditional results for boring SMO-EB1 are presented in Figures 4-36 through 4-39. In the case of unconditional simulation (Figure 4-32), the mean tip resistance has a shape similar to the mean SPT-N profile for the site seen in Figure 4-30 (profile tab). The mean end bearing (FB-DEEP) becomes constant for lengths greater than 65 ft. This is due to the averaging method of FB-DEEP and the pile being embedded greater than 8 diameters into the limestone layer. Thus, no influence from the above layer affects the average end bearing computed. In all of the mean resistance plots, it can be seen that the mean of spatial plus method (red dashed line) is higher than the mean from just the spatial analysis (blue line). This is due to bias correction (exp(a)) equal to 1.19 (> 1) shown in Table 3-3. Also for the $\overline{\phi}$ profile in Figure 4-34, it can be seen that $\overline{\phi}$ for spatial plus method is smaller than that for just spatial. This is due to inclusion of method error, i.e., CV_ε, which increases the uncertainty of the prediction by increasing CV_R and lowering $\overline{\phi}$. Moreover for shorter pile lengths, $\overline{\phi}$ is smaller due to upper sand layers having a higher CV of SPT N (Table 4-3) compared to the limestone layer. Figure 4-35 plots the design resistance ($\overline{\phi}$Rn) from the unconditional simulation. Note, even though $\overline{\phi}$ between spatial and spatial plus methods (Figure 4-34) are quite different, the design resistances ($\overline{\phi}$Rn) are very similar. This can be attributed to the bias corrected mean used in Rn calculation. That is, in the spatial plus method, $\overline{\phi}$ is less than that for just spatial method, but the bias correction (> 1) increases the mean value in the case of the spatial plus method.

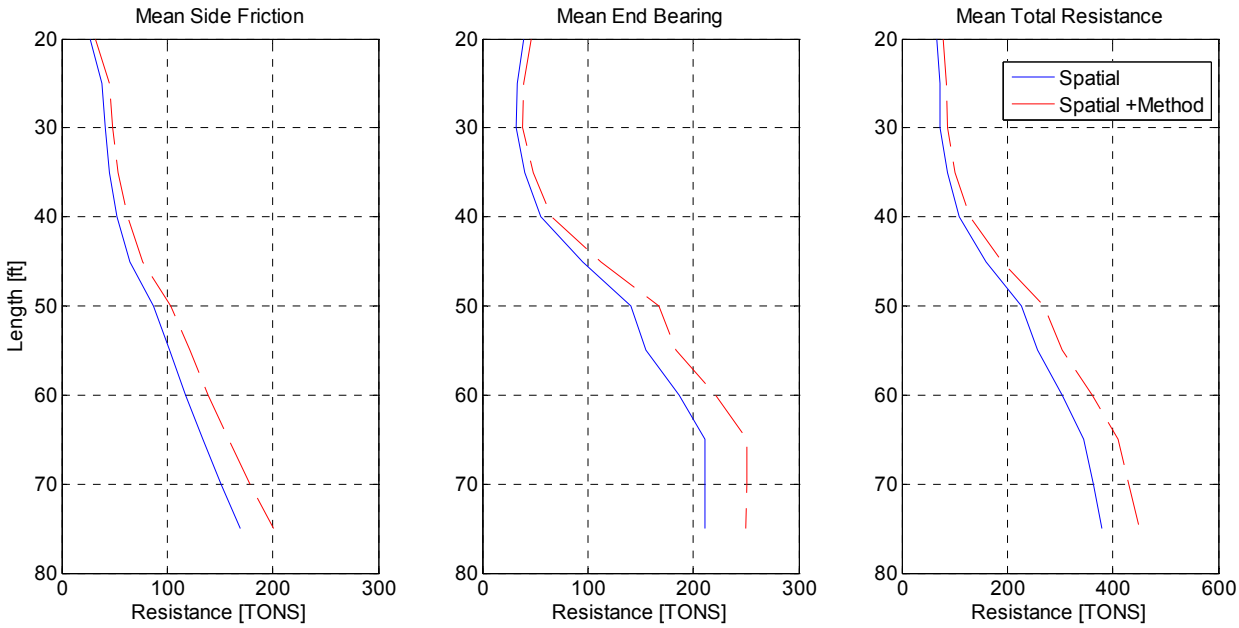

Figure 4-32. Mean resistance, Dixie Highway - unconditional simulation.

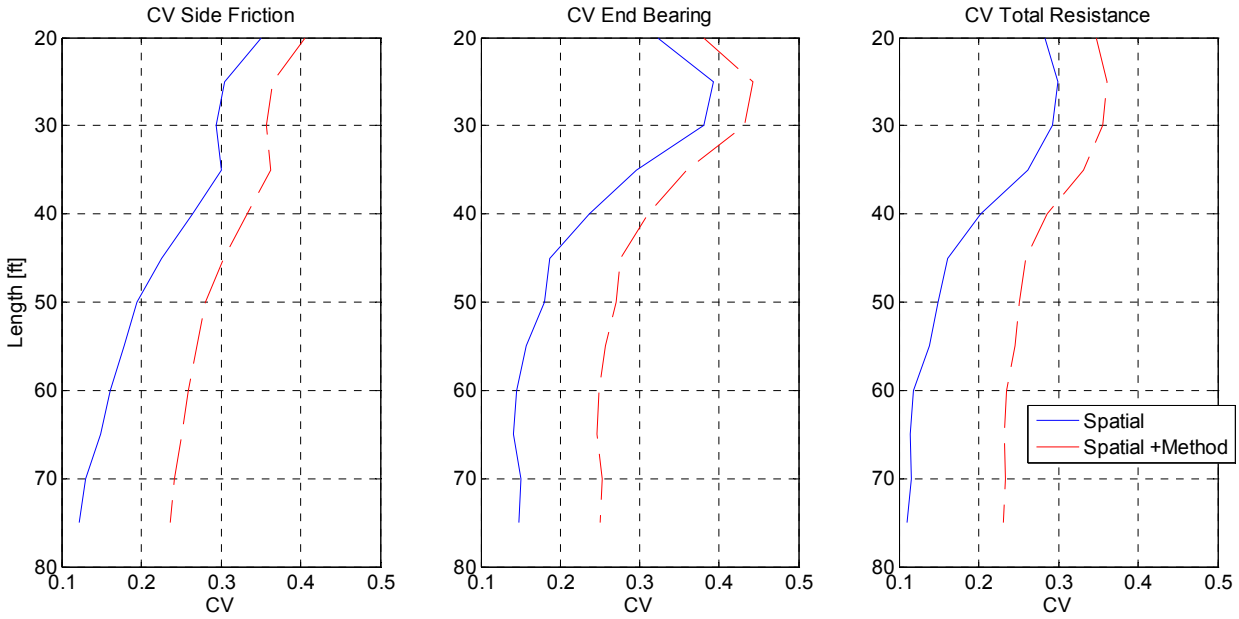

Figure 4-33. CV of resistance, Dixie Highway - unconditional simulation.

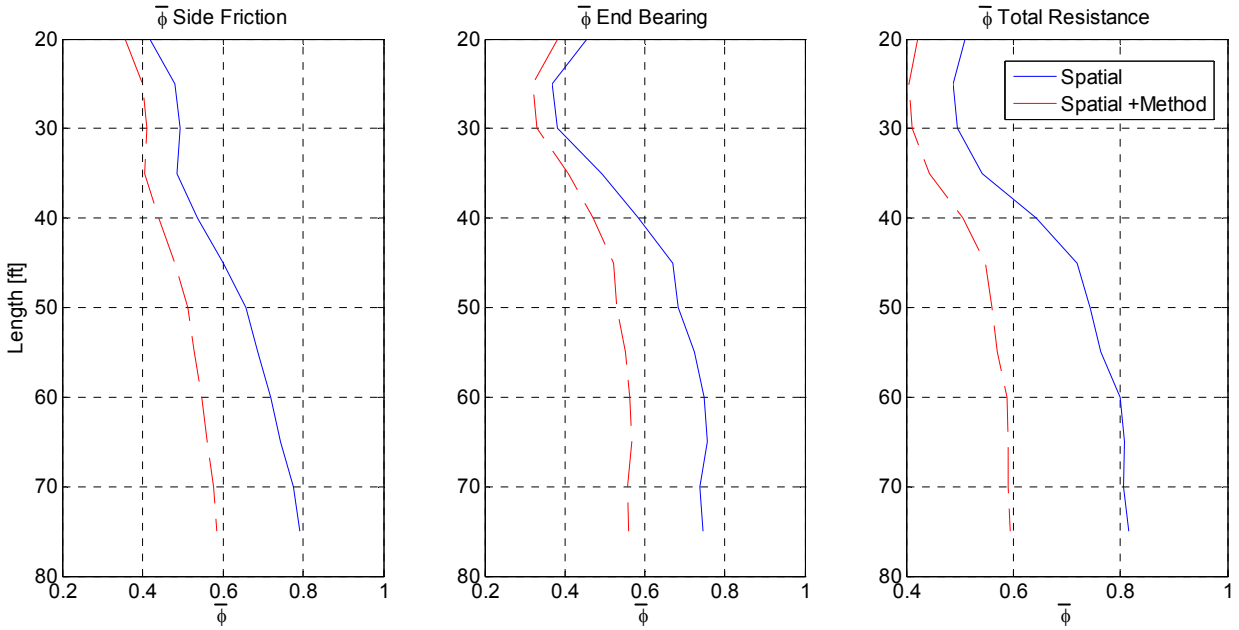

Figure 4-34. $\bar{\phi}$, Dixie Highway - unconditional simulation.

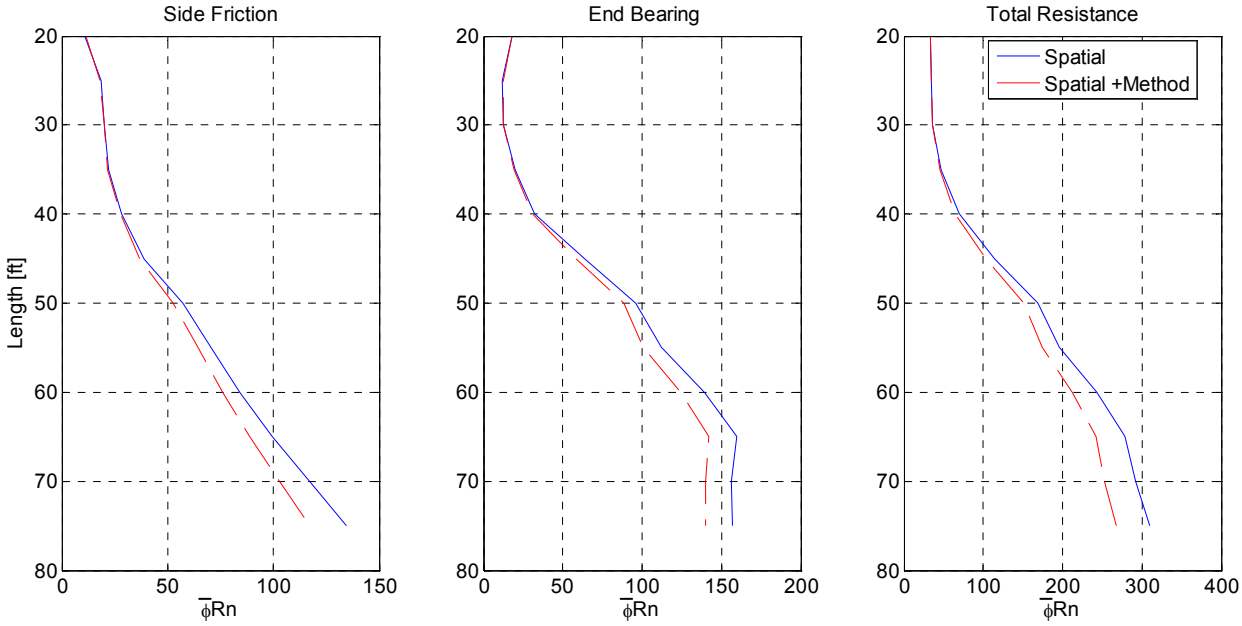

Figure 4-35. Design resistance, Dixie Highway - unconditional simulation.

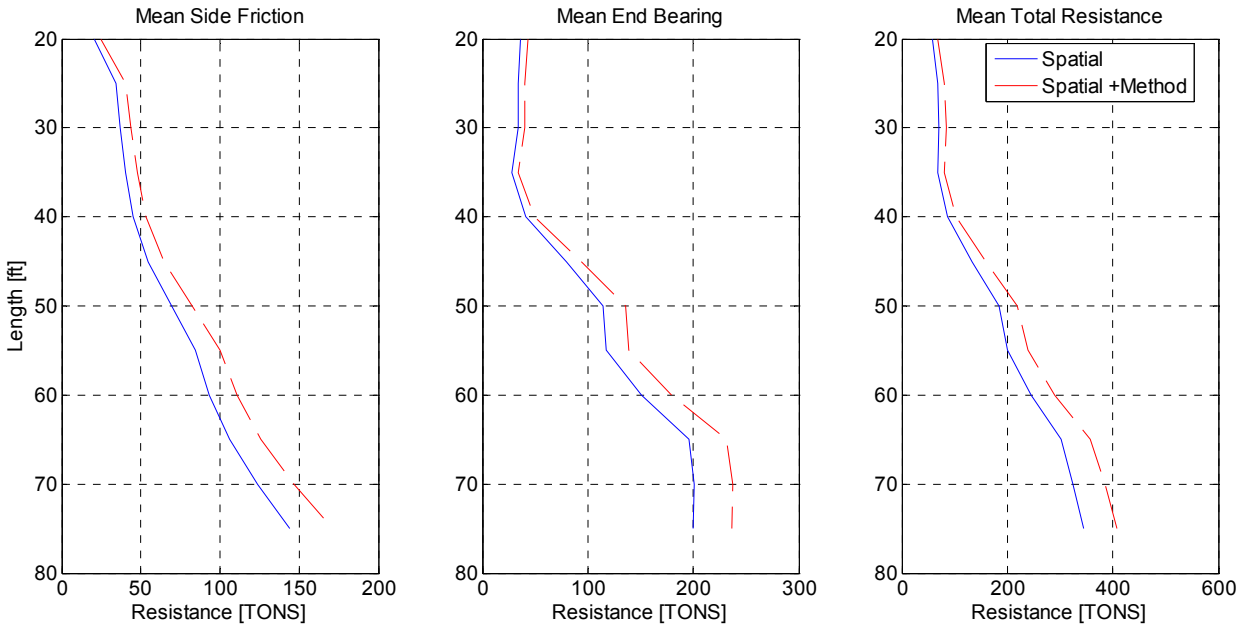

Figure 4-36. Mean resistance, Dixie Highway - conditional simulation-EB1.

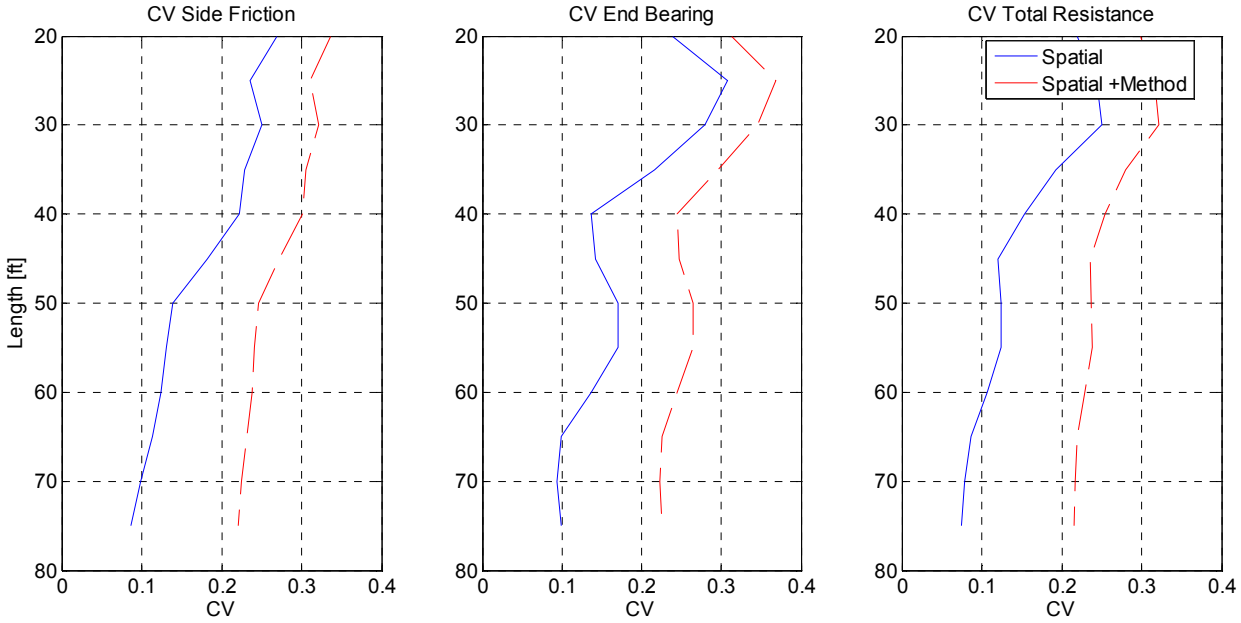

Figure 4-37. CV of resistance, Dixie Highway - conditional simulation-EB1.

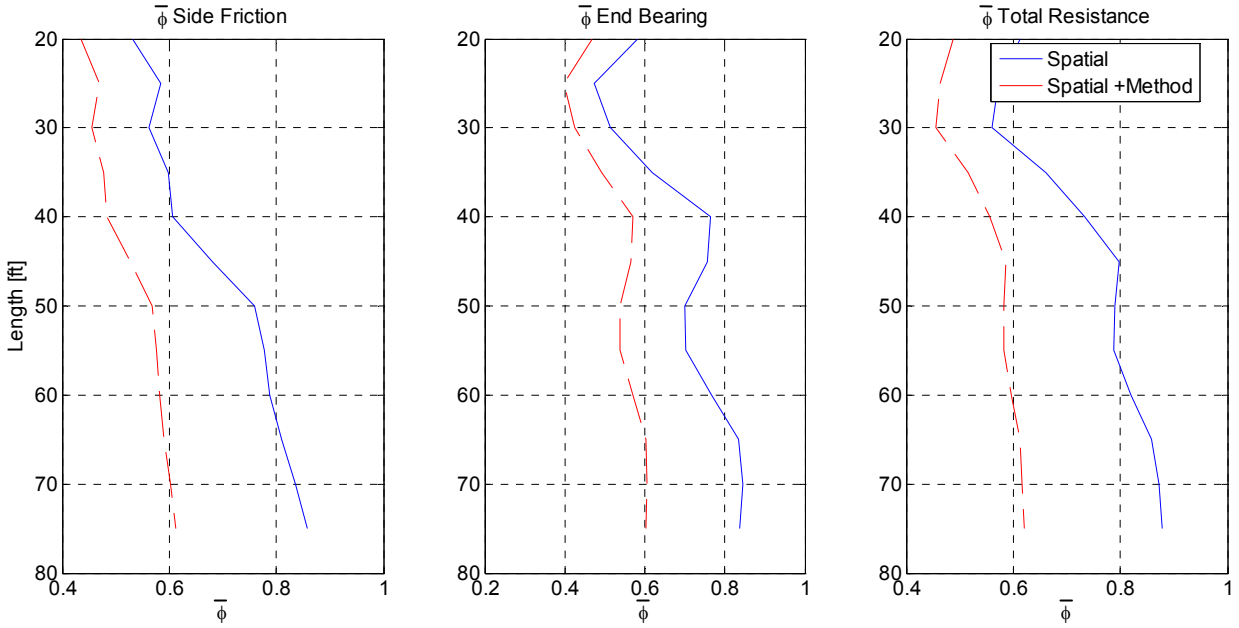

Figure 4-38. $\bar{\phi}$, Dixie Highway - conditional simulation-EB1.

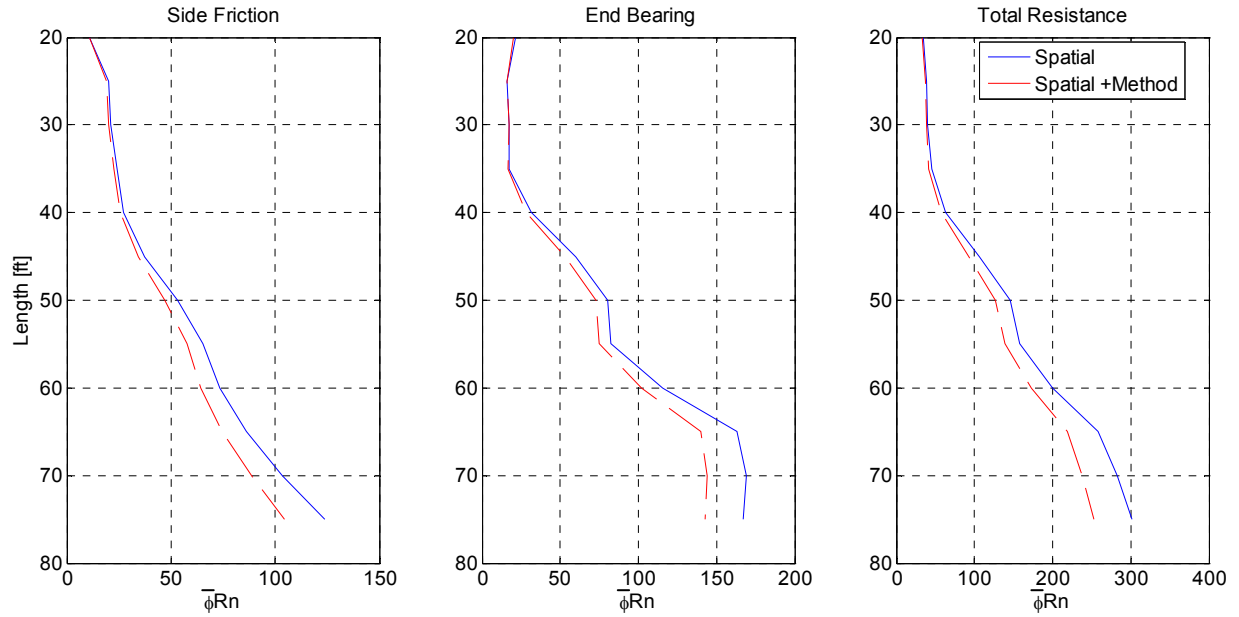

Figure 4-39. Design resistance, Dixie Highway - conditional simulation-EB1.

The conditional simulation results are shown in Figures 4-36 through 4-39. The results show similar profiles to those of unconditional simulation, however, with different means and higher $\bar{\phi}$ values with depth. The difference can be attributed to using the mean from boring

SMO-EB1 versus site mean, and the higher $\overline{\phi}$ value can be attributed to the reduction in spatial uncertainty due to the boring located within the footprint. Shown in Table 4-7 is the comparison between static load tests and the unconditional and conditional resistances for the load test piles. The difference may be attributed to method error and the use of the default CV_{ε}.

Table 4-7. Load Test versus Simulated Unconditional (UC SIM) and Conditional (CON SIM) Results

Pile	Load Test	Result (Tons)	UC SIM (Tons)	CON SIM (Tons)
End Bent 1	Compression	270	242	206
Pier 4	Tension	115	194	181
Pier 8	Compression	251	288	205

CHAPTER 5
CASE STUDIES OF FDOT BRIDGE SITES

5.1 Background

As discussed in Task 5, for acceptance of LRFD ϕ with the use of site specific spatial and method uncertainty, a comparison with existing practice is warranted. Since Task 1 involved the collection of boring, laboratory and load test data from multiple sites and foundation types, the design process (Chapters 2–4) may be readily employed at each of the sites. Table 5-1 lists the project number, site description, number of borings, number of site load tests, number of borings in the footprint, and investigative geotechnical company for each of the collected sites. Four of the sites were drilled shafts and 2 were driven piles. For each site, both unconditional and conditional analyses were performed. In the case of the unconditional, the mean and CV of all site data by layer was used for the simulation, whereas in the case of conditional, the nearest boring was used in the analysis. It should be noted the computed LRFD $\overline{\phi}$ has the bias removed, and it should be compared to ϕ/λ_R in current practice.

Table 5-1. Data Collected from FDOT Projects

Project #	Project Name	Number of Borings	Load Test	Number of Borings in FP w/ LT	DATA BY
250445-1-52-01	Jewfish Creek	98	2	2	MACTEC
256994-1-52-01	SR-686	37	2	2	Ardaman,PSI
408320-1-52-01	MIC[a] to MIA[b]	23	2	1	PSI
406800-2-32-01	MIC – People Mover Station	15	1	0	MACTEC
413485-1-31-01	CR-12A	4	0	0	FDOT
418760-2-52-01	I-4 Improvements	14	1	0	Ardaman
230656-1-52-01	Dixie Highway	22	3	3	PSI

[a] Miami Intermodal Center
[b] Miami International Airport
FP-Foot print
LT-Load test

5.2 Jewfish Creek, South Florida

Jewfish Creek project is located in both Monroe and Miami-Dade counties of District 6. The subsurface for the project is predominately limestone, which makes it an excellent site for the case of a single layer analysis. There were a total of 98 borings (Table 5-1) that were located within the design drilled shafts foundation's footprint. In addition, two more drilled shafts (not at pier locations) underwent Statnamic load testing, which had borings within their footprint.

For this site, the spatial analysis was only performed on the limestone layer, since negligible skin friction was found from the overlying thin sand layer. Shown in Table 5-2 are the summary statistics for the limestone layer's q_u values. For this site, no detrending was required. Table 5-3 shows the search parameters used to generate the experimental variograms. It was found that in the vertical direction an adequate amount of pairs ($n > 30$) was available to construct a variogram and identify vertical correlation length a_v. In the horizontal direction, only a few pairs of data were available and a variogram could not be constructed. Table 5-4 shows the variogram model parameters computed from the analysis, with worst case scenario (N/A) selected for the horizontal direction.

Table 5-2. Jewfish Creek Layer Summary Statistics and Detrend for q_u values

Layer	Mean	CV	n	Detrend	Order
1	40.19	0.77	183	No	N/A

Table 5-3. Jewfish Creek Variogram Search Parameters

Search Direction	Lag	Tolerance	Number of Lags	Bandwidth
Horizontal	20	10	20	1
Vertical	2	1	20	0

Table 5-4. Jewfish Creek Variogram Model

Layer	Model	a_v	$sill_v$	a_h	$sill_h$	nugget
1	SPH	7.25	1	N/A	1	0

The analysis was carried out on the as-built 48-inch diameter shafts of various lengths. Since no modulus values were available for the site, end bearing was neglected in the analysis. Both conditional and unconditional analyses were performed on the site. Two different cases of method error and bias correction were considered: 1) multiple site data (i.e., default, Table 3-1, Figure 3-2), and 2) Jewfish Creek load test results (Figure 3-7).

Results for unconditional and conditional simulations are shown in Figures 5-1 through 5-3 and summarized in Table 5-5 for the case of default method error. Evident in Table 5-5 for the case of 40-ft long shafts, the mean shaft resistance R_N varies (conditioning) from 3132 tons to 4595 tons. The latter corresponds to high variability in mean boring data, i.e., boring P10-S2 (low) to boring P56-S3 (high). The unconditional analysis gives a site average resistance of

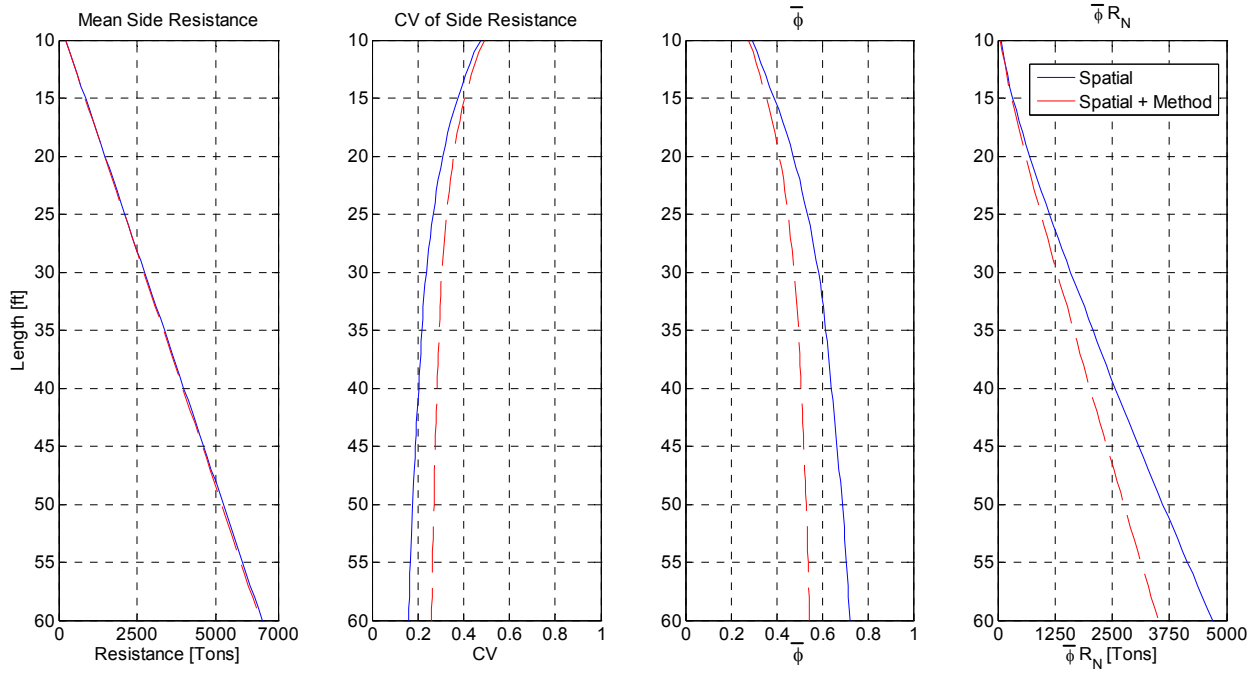

Figure 5-1. Jewfish Creek side resistance analysis unconditional simulation.

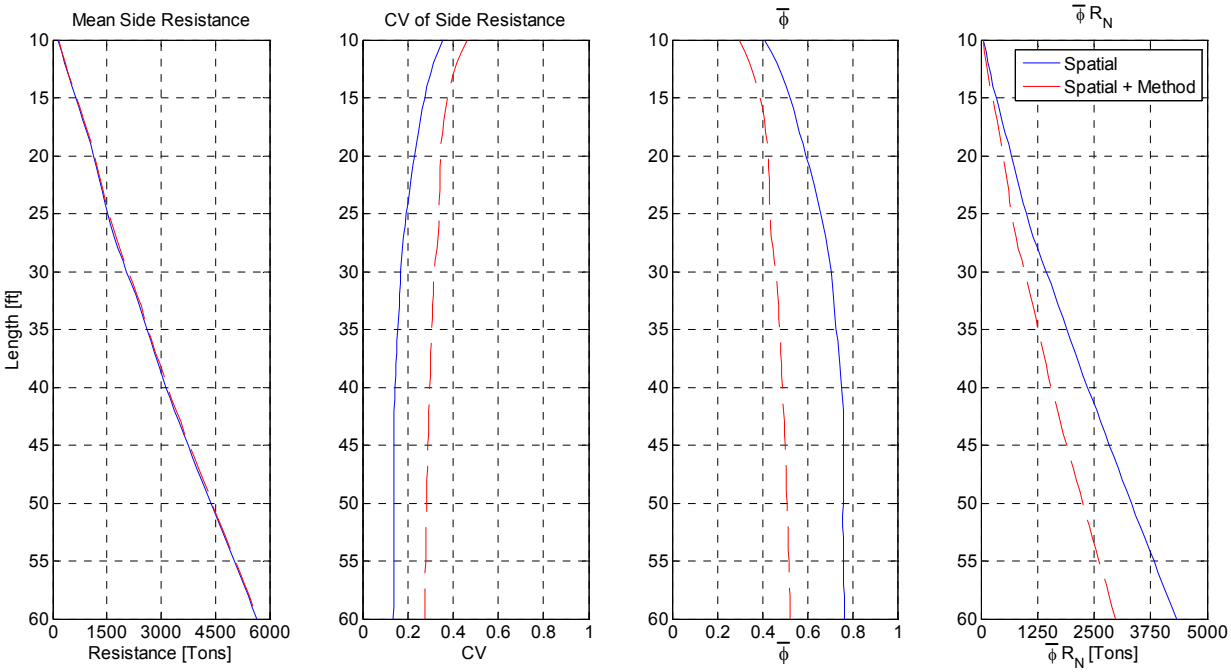

Figure 5-2. Jewfish Creek side resistance analysis P10-S2.

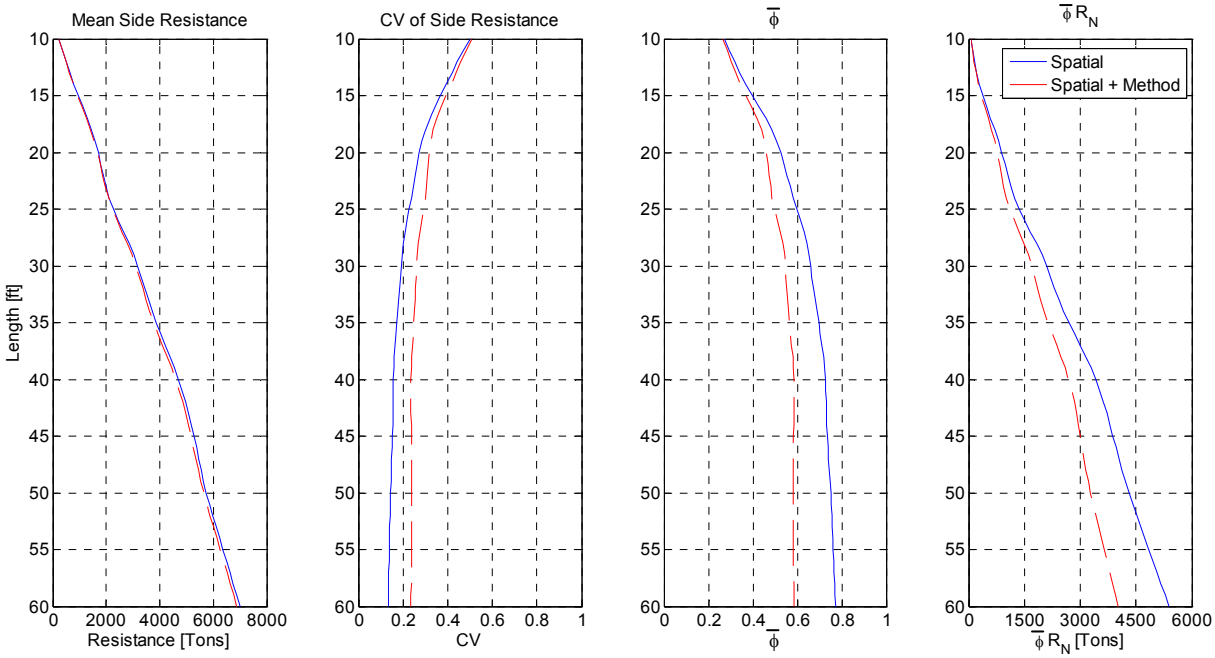

Figure 5-3. Jewfish Creek side resistance analysis P56-S3.

Table 5-5. Results for Jewfish Creek for 40-ft Long Shaft

Analysis	Spatial $\overline{\phi}$	Total $\overline{\phi}$	R_N (Tons)
Unconditional	0.64	0.51	3998
P10-S2	0.75	0.49	3132
P56-S3	0.73	0.58	4595

3998 tons using the mean of all borings. As expected in Figures 5-1 to 5-3, the conditional and unconditional uncertainties (CV- center figures) decreases with depth for both spatial and spatial plus method error. That is, for a single layer as the shaft length increases, the averaging domain increases and total side resistance variability decreases.

Also shown in Table 5-5 is the LRFD $\overline{\phi}$ as a result of spatial or spatial plus method error for both the unconditional and conditional analyses. As expected, the spatial conditional LRFD $\overline{\phi}$ values are higher than that of the unconditional due to the reduction of spatial uncertainty (horizontal $a_h = a_v$ worst case). However, in the case of total uncertainty (spatial + method), the unconditional simulation has a higher LRFD $\overline{\phi}$ than that of conditional for weak boring and a smaller value in the case of strong boring. This may be attributed to calculation of CV_R from which LRFD $\overline{\phi}$ is computed (Eq. 3.17). The numerator of CV_R is obtained from the total variance σ_R^2 given by Eq. 3.9, where a constant σ^2 is added. However, in the denominator of CV_R is the mean shaft resistance, which is smaller for the weak boring (P10-S2, Table 5-5) resulting in a higher CV_R and a lower $\overline{\phi}$ for weak boring when considering total uncertainties (Table 5-5). This issue was not as apparent for the 17th Street case (Chapter 4) due to a higher site mean for the latter case as compared to Jewfish Creek. Consequently using a fixed uncertainty of method, i.e., σ^2, has less influence on CV_R when the denominator (i.e., mean) is large.

Also evident in Table 5-5 is the predicted LRFD $\overline{\phi}$ for P10-S2 as slightly higher than that of P56-S3. This slight difference may be attributed to P10-S2 having additional rock samples in the boring. More samples resulted in less uncertainty in the boring mean (Eq. 2-15) for P10-S2. This illustrates the need to have adequate sampling, i.e., number of samples spaced relatively far apart compared to a_v when predicting resistance from a boring.

Also it should be reiterated that the use of conditional simulation using FB-DEEP results in a conservative evaluation of LRFD $\overline{\phi}$. This is due to the one-dimensional model (depth versus soil properties) that FB-DEEP requires to estimate resistance. It would be expected for a resistance estimate that considers the surface area of the shaft (i.e., three-dimensional) to result in a higher LRFD $\overline{\phi}$.

To incorporate Jewfish Creek load test results in the evaluation of $\overline{\phi}$, the evaluation process given in **BD545 -76** was used. In this process, the bias correction regression analysis from Figure 3-7 for the site specific measure versus predicted relationship was used. Specifically, the σ^2 (Figure 3-7) was reduced using α_o from Figure 2-7 (i.e., the multiple point skin friction values are up scaled to shaft layer values). For the Jewfish Creek site, a_v = 15 ft, the load test shaft length L = 30 ft, resulting in an $L/a_v = 2$ from which $\alpha_o \approx 0.33$ was obtained from Figure 2-7. Next, when evaluating CV_R, the $\sigma^2_{\varepsilon fs}$ in Eq. 3-9 is replaced with $\alpha_o\sigma^2$ due to the use of measured side versus predicted resistance values over intervals rather than single layer values assumed in default legacy $\sigma^2_{\varepsilon fs}$ analysis (Figure 3-2, Table 3-1).

Results for unconditional and conditional simulations are presented in Figures 5-4 through 5-6 and summarized in Table 5-6 for method error assessed from site load tests. Evident in Table 5-6 for the case of 40-ft long shafts, the mean shaft resistance R_N varies (conditioning) from 2601 tons to 3811 tons. The latter corresponds to high variability in mean borings data, i.e., boring P10-S2 (low) to boring P56-S3 (high). The unconditional analysis gives a site average

resistance of 3268 tons using mean of all borings. As expected in Figures 5-4 to 5-6, the conditional and unconditional uncertainties (CV- center figures) decreases with depth for both

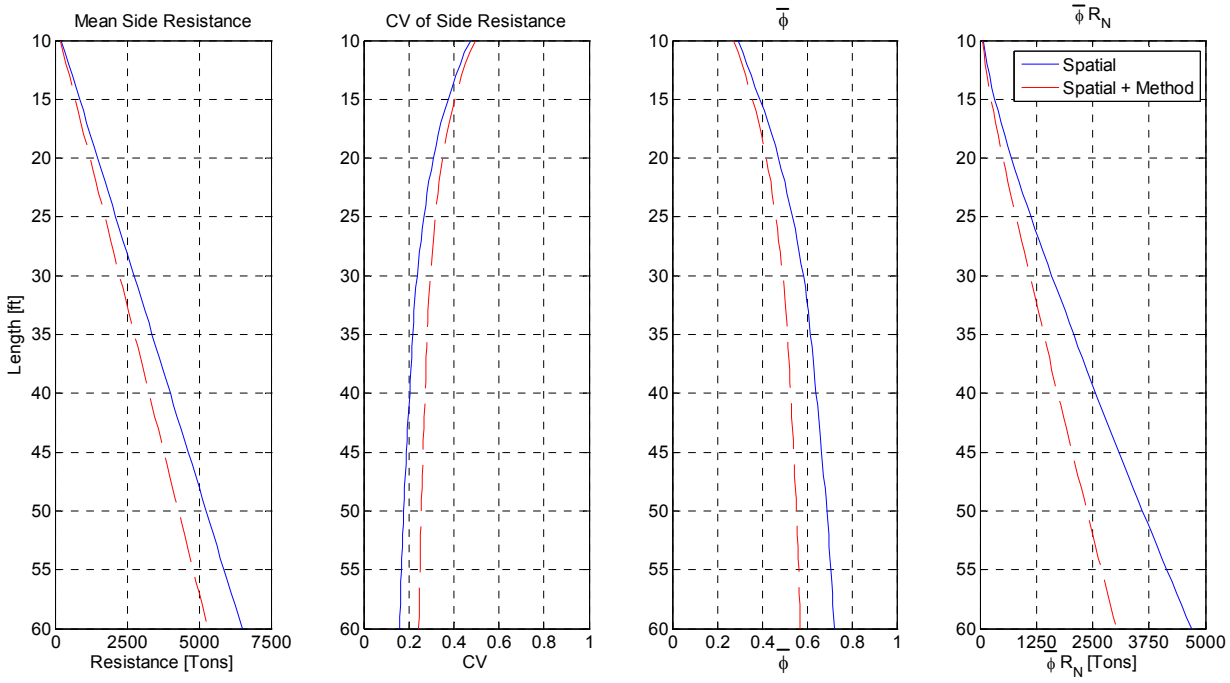

Figure 5-4. Jewfish Creek side resistance analysis unconditional simulation with load testing.

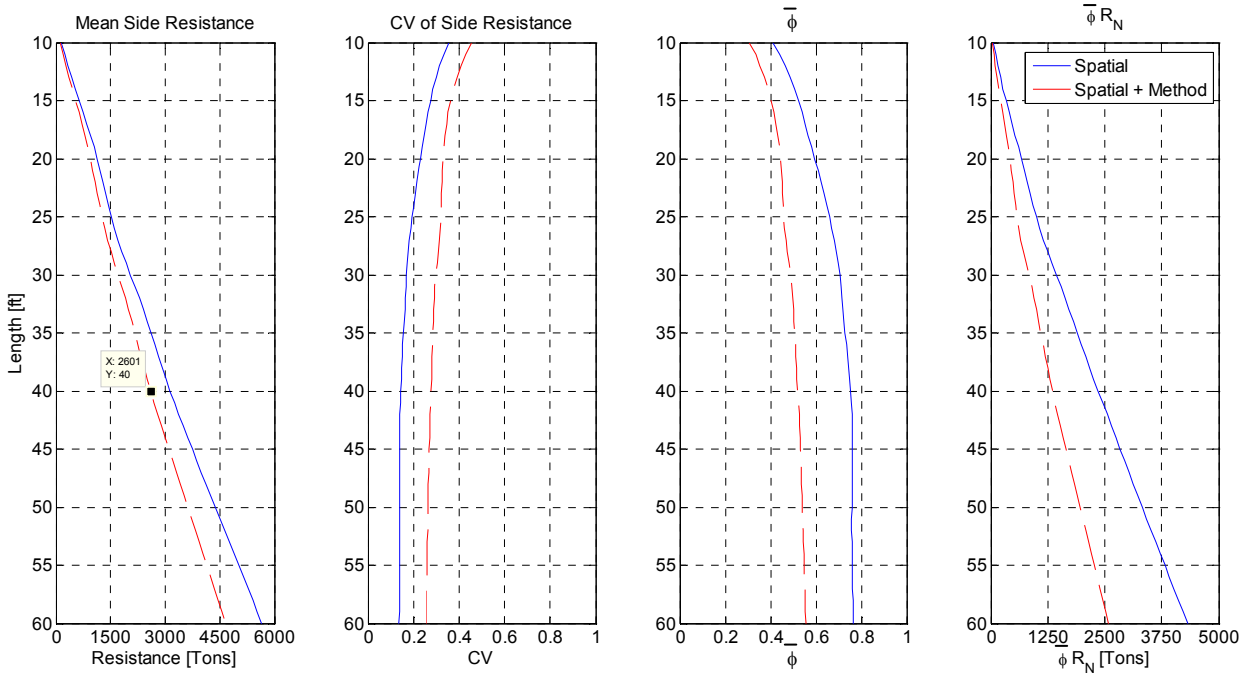

Figure 5-5. Jewfish Creek side resistance analysis P10-S2 with load testing.

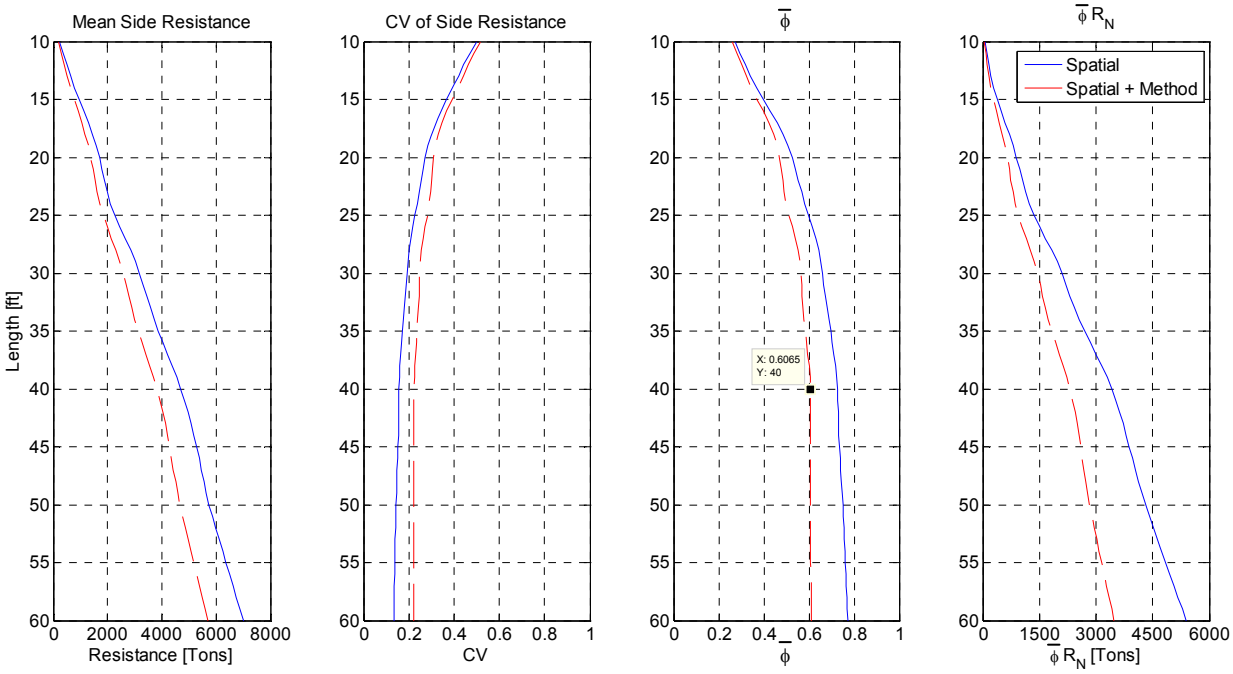

Figure 5-6. Jewfish Creek side resistance analysis P56-S3 with load testing.

Table 5-6. Results for Jewfish Creek, 40-ft Long Shaft with Load Test

Analysis	Spatial $\overline{\phi}$	Total $\overline{\phi}$	R_N (Tons)
Unconditional	0.64	0.53	3268
P10-S2	0.75	0.52	2601
P56-S3	0.73	0.61	3811

spatial and spatial plus method error. That is, for a single layer as the shaft length increases, the averaging domain increases, and total side resistance variability decreases.

Also shown in Table 5-6 is the LRFD $\overline{\phi}$ as a result of spatial or spatial plus method error for both the unconditional and conditional analyses. As expected, the spatial conditional LRFD $\overline{\phi}$ values are higher than that of the unconditional values due to the reduction of spatial uncertainty (horizontal $a_h = a_v$ worst case). However, as discussed for the legacy method error,

the case of total uncertainty (spatial + method) and unconditional simulation has a higher LRFD $\overline{\phi}$ than that of conditional for weak boring and that of a smaller value in the case of strong boring (i.e., CV_R affected by mean data).

Of interest is the comparison of total LRFD $\overline{\phi}$ reported in **BD545-76** to that in Table 5-6 or Figures 5-4 to 5-6. In the case of unconditional simulation with load testing, FDOT **BD545-76** reports a value of 0.47 for a 30-ft shaft. The numerical simulation (Figure 5-4) for unconditional simulation with spatial method error gives a very similar value, 0.48 for a 30-ft shaft. However, in the conditional simulation, i.e., in the footprint of the footing, FDOT **BD545-76** assumes all spatial uncertainty drops out (i.e., total uncertainty = method error), LRFD $\overline{\phi}$ = 0.74 for all shafts. However, as discussed in Chapters 2 and 3 for the worst case conditional simulation, the boring is generated at the wall of the shaft (i.e., radius), which always results in spatial uncertainty and reduction in LRFD $\overline{\phi}$ (0.5-P10-S2, and 0.58-P56-S3 for 30 ft).

For 40-ft shafts, the axial design resistance $\overline{\phi} \bullet R_N$ would be 1732 tons for the entire site (i.e. unconditional), 1352 tons for boring for P10-S2 (conditional) and 2325 tons for P56-S3 (conditional). Again, the unconditional falls between the high and low conditional resistance values R_N (controlled by the mean data within each boring).

5.3 MIC/MIA CONNECTOR

The elevated People Mover shuttle from the Miami Intermodal Center (MIC) Station to Miami International Airport (MIA) had 23 reported borings. Moreover, all the borings were located within the footprint of their respective drilled shaft. In addition, there were two load tests reported on this project, one Statnamic and one Osterberg-Cell; however, only one test had a boring located within the footprint of the test shaft. Unfortunately, the boring within the footprint did not have any reported rock strength data.

The MIC to MIA connector was again analyzed only for the limestone layer, due to the extent of the rock along its length and its dominating contribution to the shaft's resistance. Nonetheless, no Young's modulus values for the rock were recorded, and thus, no end bearing resistance could be evaluated. Tables 5-7 through 5-9 summarize the geospatial analysis that was performed for the limestone layer. Even though the site had fewer borings than Jewfish Creek, there were sufficient samples within the borings to generate a vertical variogram. The site is a good example of a minimal sampling strategy, which allows the generation of a vertical variogram.

Table 5-7. MIC/MIA Connector Layer Summary Statistics and Detrend

Layer	Mean	CV	n	Detrend	Order
1	67.07	0.60	66	No	N/A

Table 5-8. MIC/MIA Connector Variogram Search Parameters

Search Direction	Lag	Tolerance	Number of Lags	Bandwidth
Horizontal	10	5	20	1
Vertical	2	1	20	0

Table 5-9. MIC/MIA Connector Variogram Model

Layer	Model	a_v	$sill_v$	a_h	$sill_h$	nugget
1	SPH	6.58	1	NA	1	0

For this site, axial analysis was carried out for a 48-inch diameter drilled shaft of various lengths. Results from the GUI for side resistance are shown in Figures 5-7 through 5-9 and Table 5-10. It can be seen for this site that the LRFD $\overline{\phi}$ for boring WB9 is only slightly higher

than the unconditional simulation values and the boring's mean value is also close to the site's value. However, because the samples are spaced relatively close compared to a_v, more

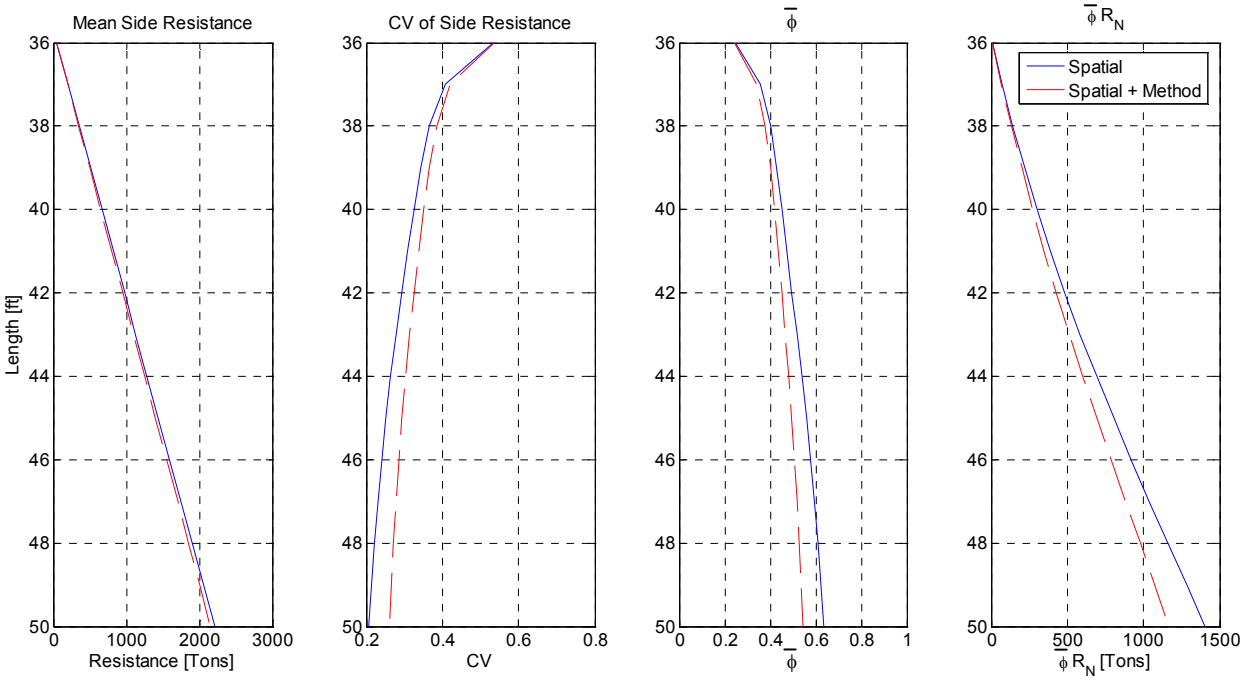

Figure 5-7. MIC/MIA side resistance analysis unconditional simulation.

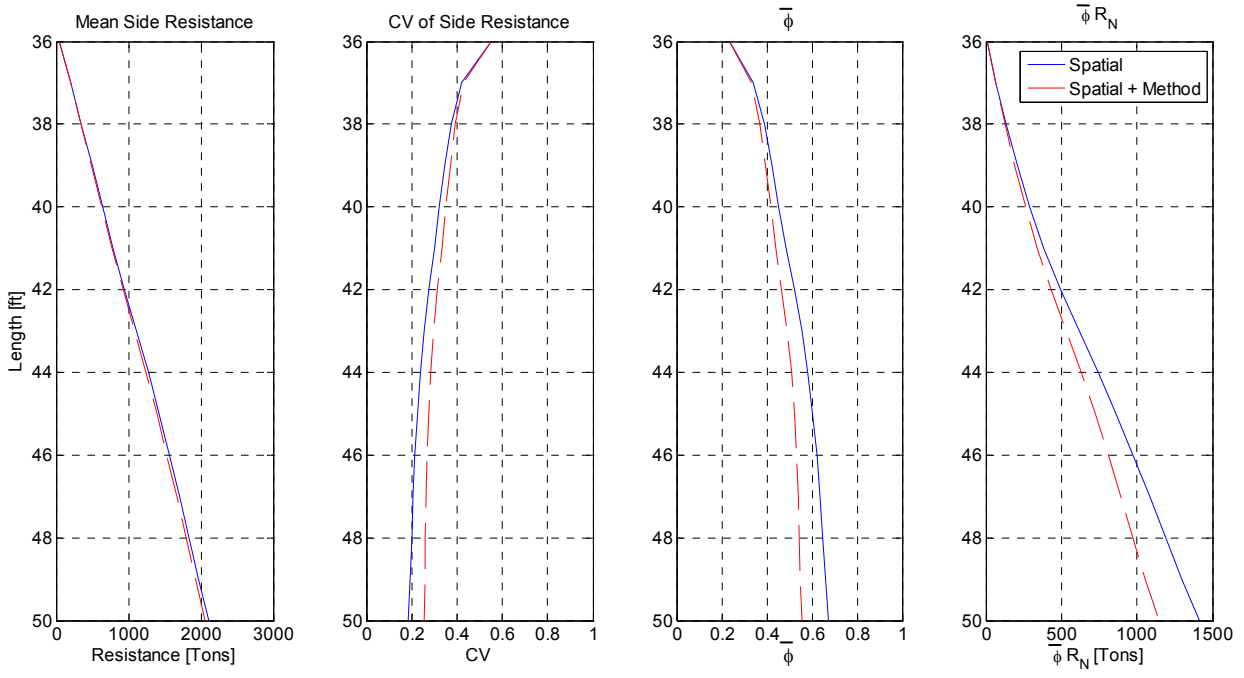

Figure 5-8. MIC/MIA side resistance analysis WB9.

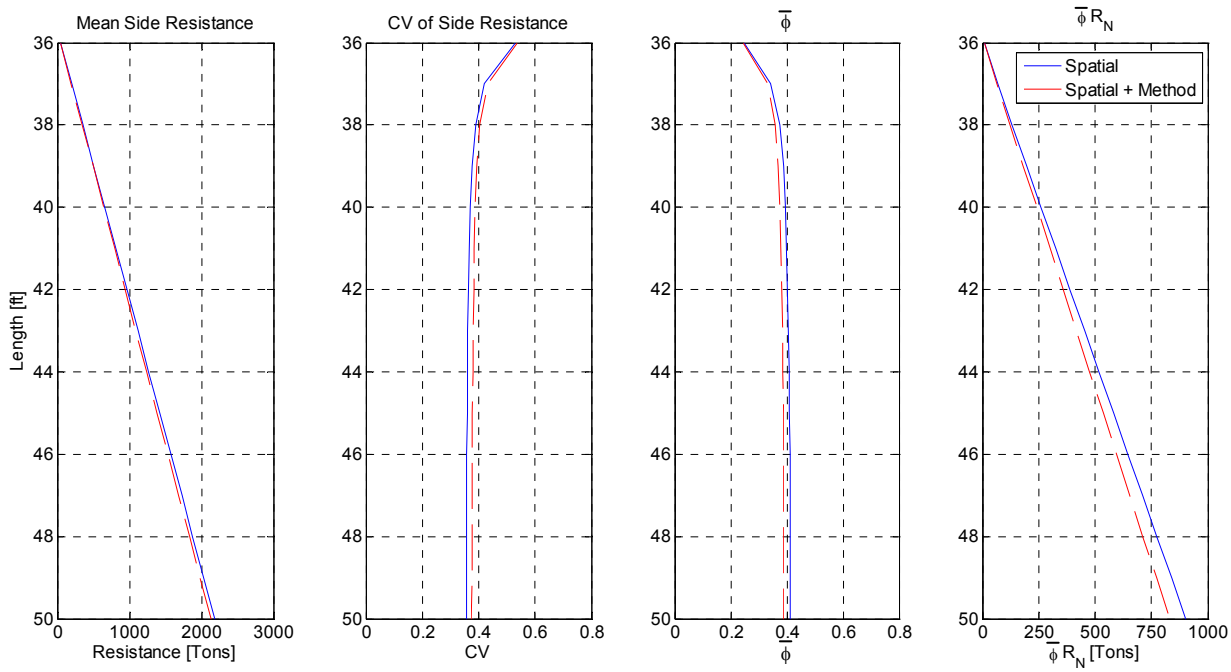

Figure 5-9. MIC/MIA side resistance analysis worst case unconditional simulation.

Table 5-10. Results for MIC to MIA for 15-ft Long Shaft

Analysis	Spatial $\overline{\phi}$	Total $\overline{\phi}$	R_N (Tons)
Unconditional	0.64	0.54	2154
WB9	0.67	0.56	2061
Unconditional, worst case a_v	0.41	0.39	2131

uncertainty is computed for the shaft's mean for this boring, which resulted in a similar $\overline{\phi}$ for the site (unconditional). Also note, the site has a higher mean value when compared to Jewfish Creek, thus the influence of σ^2 is not as great in the evaluation of CV_R (mean in denominator) when comparing the site's (unconditional) $\overline{\phi}$ to the WB9's $\overline{\phi}$.

The rock data collected for this site was able to generate an adequate variogram, however the number of pairs used to generate the vertical variogram was only slightly above 30. Consequently, a second analysis was run with the assumption that a_v was unable to be reliably determined, and the worst case a_v was used. Shown in Table 5-10 is the dramatic reduction in $\overline{\phi}$

compared to prior results. The thirty percent reduction in $\overline{\phi}$ and design resistance, $\overline{\phi} \bullet R_N$ shows the importance of sampling strategy and the need to develop a vertical variogram.

5.4 MIC – People Mover Station

Another MIC Station project available to analyze was the People Mover Station (Table 5-1). This project contains 14 borings performed by MACTEC (Atlanta, Ga; now AMEC). A majority of these borings are located within the footprint of the pier caps. The MIC-People Mover Station has one load test but it does not contain a boring within the footprint. However, the MIC Station project has the least rock strength data when compared to Jewfish and the MIA projects. This site represents a good case to investigate on $\overline{\phi}$ for a site with minimal sampling.

Table 5-11 shows the summary statistics for the site's limestone layer. The rock had a high mean strength, but with a large variability CV = 0.74. Since only 18 samples were available from the 15 borings, all variograms were considered inacurate (n < 30). Thus the worst correlation lengths were assumed in both the vertical and horizontal directions.

Table 5-11. MIC –People Mover Station Layer Summary Statistics and Detrend

Layer	Mean	CV	n	Detrend	Order
1	65.58	0.74	18	No	NA

Results for analysis of a 48-inch diameter drilled shaft are shown in Figures 5-10 and 5-11. Figure 5-11 shows the unconditional simulation results using the worst case scenario. However, it was found the unconditional simulation presented in Chapter 2 does not account for uncertainty of the measured mean in the case of a small number of samples. To incorporate the uncertainty of mean in the unconditional simulation, it was decided to run the GUI (modified LU algorithm, Eq. 2-19) in the conditional mode, but with the shaft located outside the correlation length of any of the sites borings. Being outside the correlation length results in an equivalent

unconditional simulation (no conditioning to borings, i.e., outside correlation length), and it properly accounts for uncertainty in the measured mean. The latter is accomplished through the second term in Eq. 2-15, when generating boring profiles for FB-DEEP.

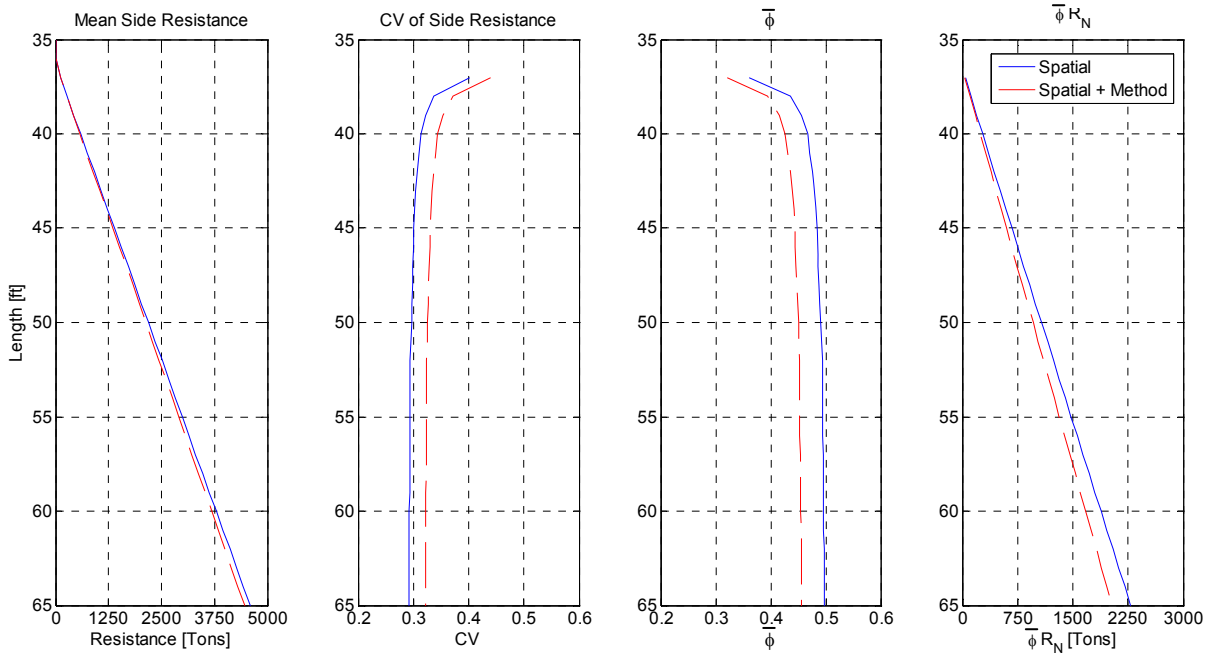

Figure 5-10. MIC Station side resistance analysis unconditional simulation.

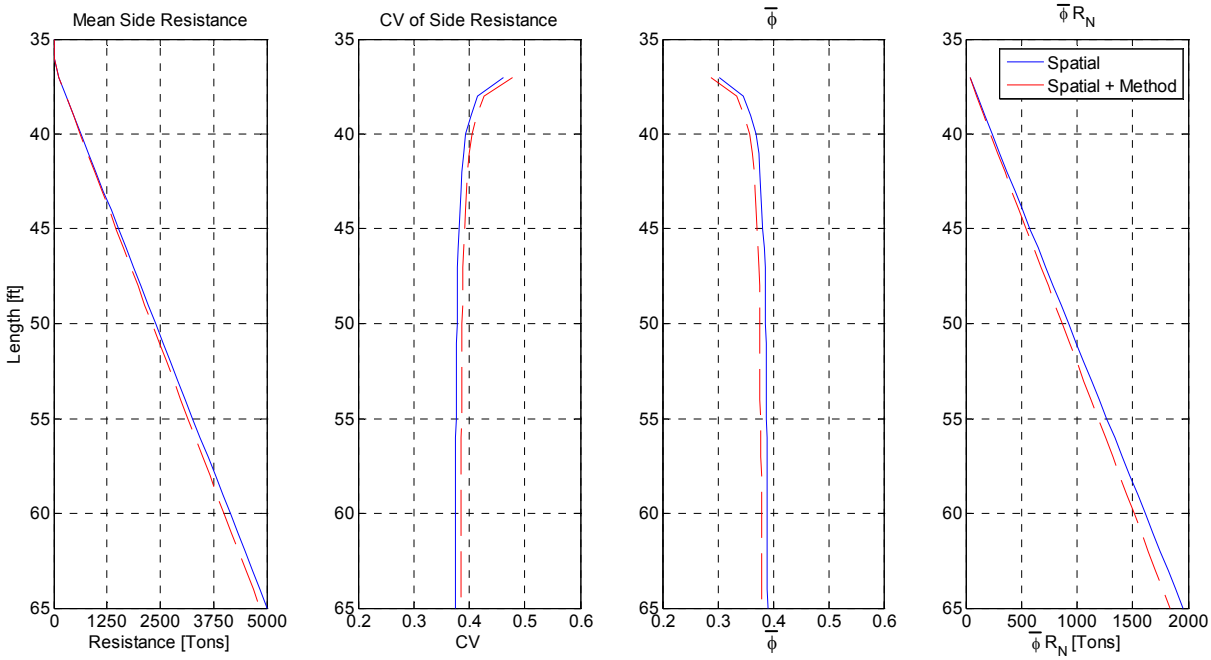

Figure 5-11. MIC Station side resistance analysis unconditional simulation, uncertainty of mean.

It can be seen from a comparison of Figures 5-10 to 5-11, poor sampling can have a significant influence on $\overline{\phi}$. The LRFD $\overline{\phi}$ went from 0.45 to 0.38 due to uncertainty of the mean (i.e., too few samples). Note, the two previous projects were checked to see if uncertainty of the measured mean had any effects on $\overline{\phi}$. It was found that there was no significant difference in $\overline{\phi}$ for those projects (i.e., sufficient sampling was performed).

5.5 County Road 12A

This is a small driven pile project in District 3 (Gadsen County) which is being designed in-house by the FDOT. The project has only four borings configured in the preliminary layout. It is unknown if there will be a boring within the footprint of the foundation element, since the final design has not been completed. It is likely that driven piles will be used, thus no load testing will be available. Both boring and lab data for this project have already been uploaded to the database. This project was used during the pilot testing of the database by FDOT personnel and was the first set of site data uploaded to the database.

The site is primary silty and clayey sand overlying weathered limestone. This site was separated into two layers with summary statistics shown in Table 5-12. The geostatistical results are presented in Table 5-13. Since Layer 1 was thin with an insufficient number of SPT N values, no vertical variogram could be developed for the layer, and the worst case scenario was considered for the layer.

Table 5-12. County Road 12A Layer Summary Statistics and Detrend

Layer	Mean	CV	n	Detrend	Order	
1	16.76	0.41	29	Yes	2	2
2	60.18	0.38	46	No	NA	4

Table 5-13. County Road 12A Variogram Model

Layer	Model	a_v	$sill_v$	a_h	$sill_h$	nugget
1	SPH	NA	1	NA	1	0
2	SPH	11.77	0.75	NA	1	0

The preliminary geotechnical report for the site recommended the use of driven piles for the foundation. Therefore, unconditional analysis (pile locations unknown) for this site with 24-inch square concrete piles was performed. Results for a range of pile lengths are shown in Figures 5-12 through 5-15 for unconditional simulations. Figure 5-12 presents the mean side, tip, and total resistance as a function of depth. Figure 5-13 shows uncertainty [spatial and spatial plus method] as a function of depth. As expected, the uncertainty diminishes with depth due to averaging. Figure 5-14 shows the LRFD $\overline{\phi}$ for skin, tip, and total resistance as a function of depth. Evidently $\overline{\phi}$ increased with depth due to the diminishing uncertainty with depth.

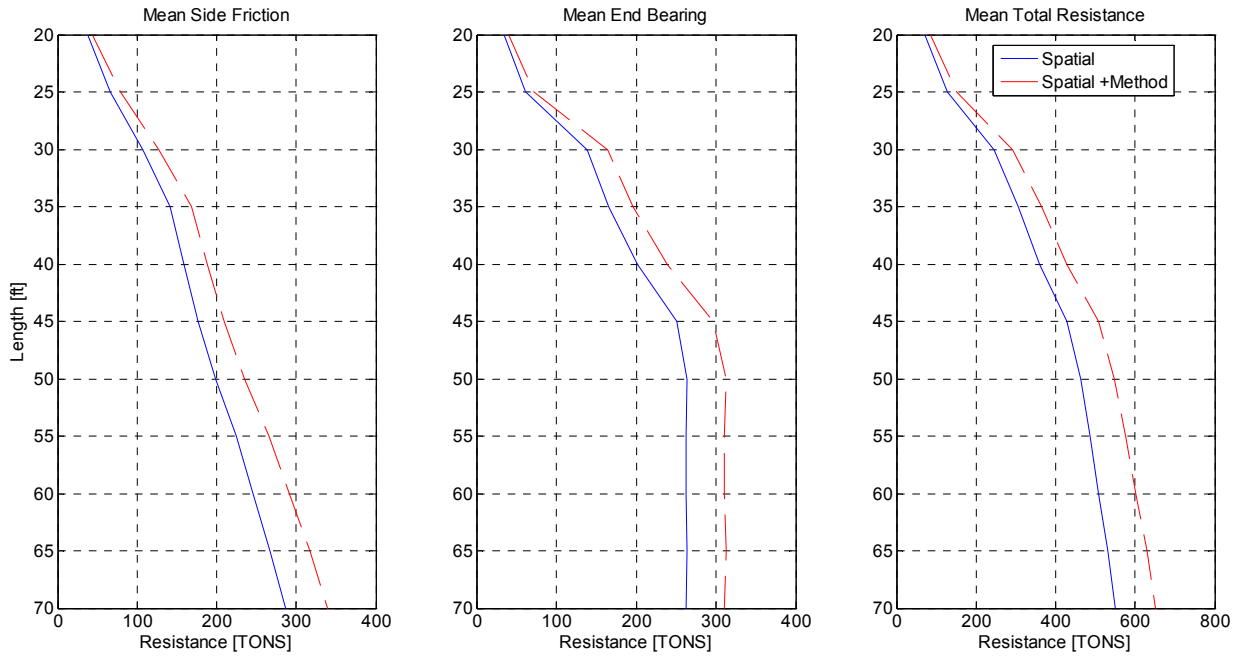

Figure 5-12. CR-12A mean resistances – unconditional simulation.

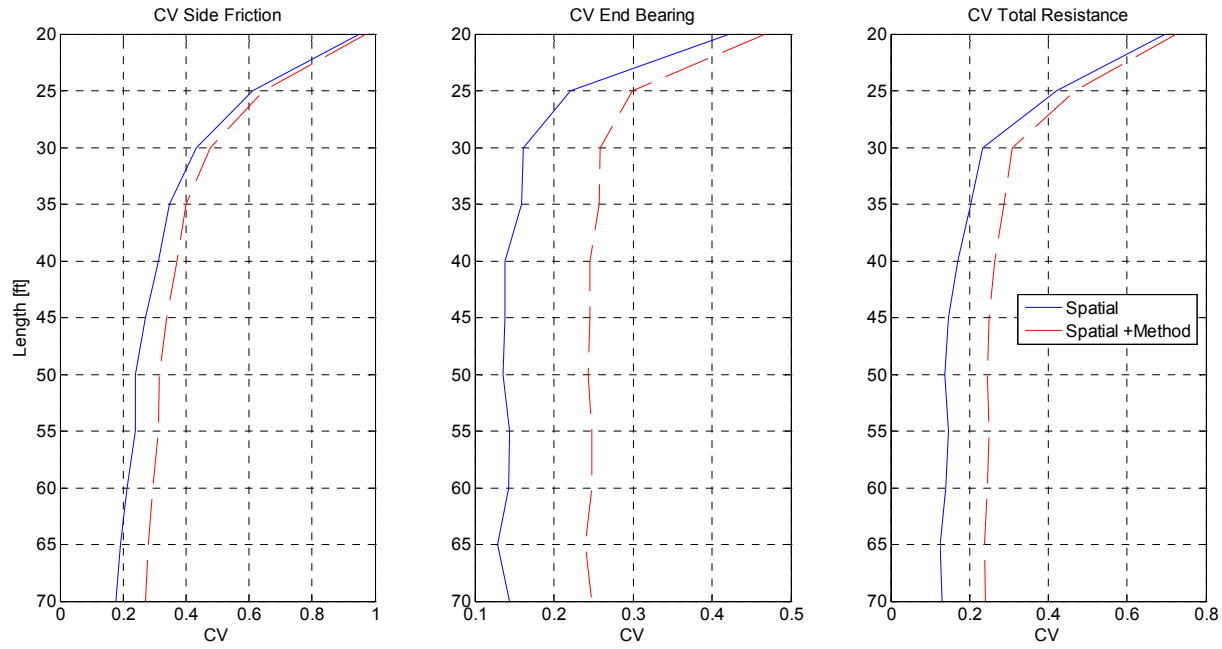

Figure 5-13. CR-12A CV of resistances – unconditional simulation.

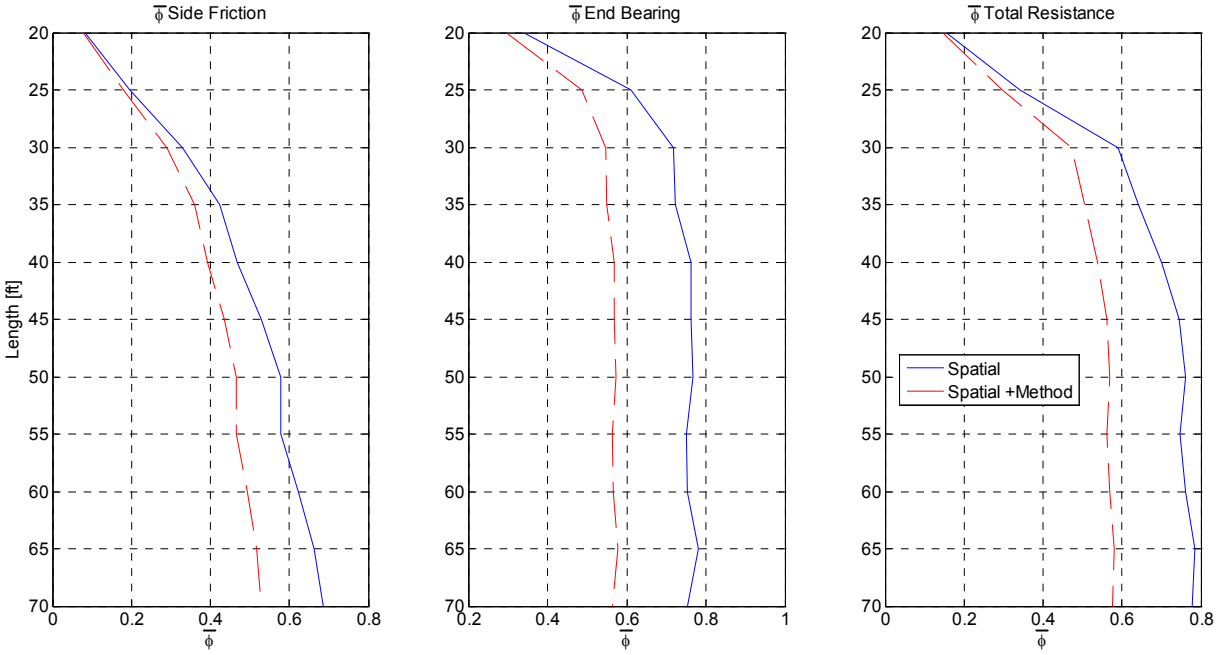

Figure 5-14. CR-12A $\overline{\phi}$ – unconditional simulation.

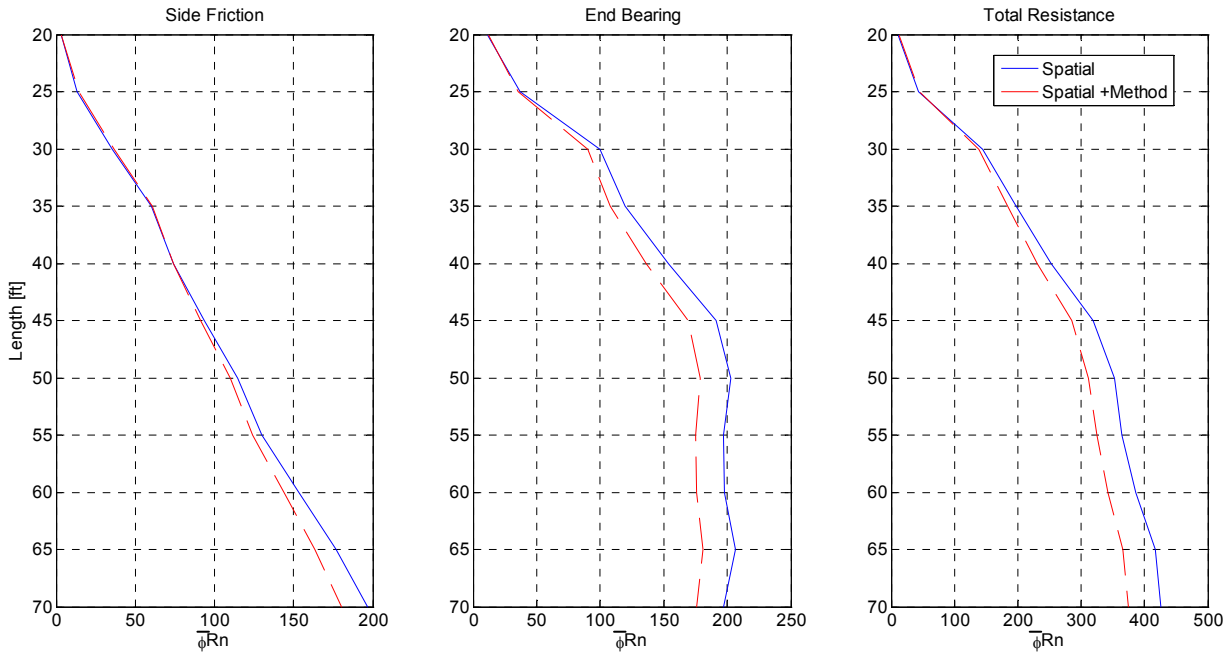

Figure 5-15. CR-12A design resistances – unconditional simulation.

However, this is not always the case, e.g., multiple layered deposits with higher CV of SPT N for lower layers, would result in lower LRFD $\overline{\phi}$. Increasing the length of the pile (i.e., averaging) in a layer will result in reduced CV_R and higher LRFD $\overline{\phi}$. Finally, Figure 5-15 displays the recommended design resistance of the piles as a function of depth.

CHAPTER 6
SUMMARY, CONCLUSIONS, AND RECOMMENDATIONS

6.1 Background

Current LRFD design codes (FDOT, AASHTO, etc.) list ϕ values for a variety of deep foundation design approaches (e.g., SPT N, CPT qc). All of the reported values were generally established from comparison of load test resistance with predictions from nearby borings. However, none of the evaluations accounted for the inherent spatial variability that exists from site to site or even within a site (e.g., by layer). This site or layer variability may be represented by coefficient of variation CV or the standard deviation of the soil/rock properties divided by the mean value. Examples of variability are shown in Table 6-1 for rock strength from multiple sites in Florida and in Table 6-2 for layer variability (SPT N) within a site. Evident in both tables, site and layer variability are quite large within Florida.

Table 6-1. Summary of CVs of Rock Data Collected

Project Name	Financial Project ID	County	q_u		
			Mean (tsf)	CV	n
17 St Bridge	WPI 4110739	Broward	98.19	0.57	99
Jewfish Creek	250445-1	Monroe	40.19	0.77	183
MIC Station	406800-2	Miami-Dade	67.07	0.66	66
MIC People Mover	408320-1	Miami-Dade	65.58	0.74	18

Table 6-2. Summary of SPT Mean N by Layers – Dixie Highway, Broward, Florida

Layer	Mean	CV	n
1	11.35	0.69	183
2	11.49	0.51	154
3	45.42	0.41	317

Besides point variability as identified in Table 6-1 and 6-2, soil/rock properties are generally spatially correlated, i.e., transitions from weak to strong or vice versa. Depending on the site's correlation structure and point variability CV, a pile or shaft axial resistance will vary over the site (by station number and pile/shaft length).

To account for site specific variability in LRFD ϕ, FDOT research project **BD545-76** was the first to incorporate the use of geostatistical analysis. Developed for skin friction of drilled shafts founded in limestone, a site specific ϕ was determined from total uncertainty σ_R^2, which was found from summing both the spatial uncertainty σ_S^2 and method uncertainty σ_ϵ^2. Computed LRFD ϕ for side friction was found to vary from 0.3 to 0.8 depending on site information, load test data, etc. Of great interest was the extension of this work to include end bearing, other types of foundations (e.g., piles), other in situ methods (CPT) and boring locations, as well as automation, i.e., assisting the engineer in assessing site characteristics (layering, summary statistics, and correlation structure).

6.2 Simulation of Boring Data at Deep Foundation Locations

To estimate pile/shaft capacity at any location, the engineer needs boring data at the planned foundation. If boring data within the footprint does not exist, it may be estimated (e.g., SPT N versus depth) from nearby borings if spatial correlation (vertical a_v and a_h) structure is known. Data kriging, from nearby borings are weighted (w_i) to estimate the boring data within the footprint of the foundation. For instance, the estimated blow count $\widehat{N}$ at depth is given by

$$\widehat{N} = \frac{1}{n}\sum_{i=1}^{n} w_i N_i \qquad \text{Eq. 6.1}$$

where N_i is the site boring data, and w_i is the weighting constants solved from Eq. 2.16 using the spatial correlation function ρ (Eq. 2.5), the spatial correlation lengths (vertical a_v and horizontal

a_h), and the distance between boring and planned pile/shaft. As important as the estimated blow count $\widehat{N}$ in the footprint is its associated uncertainty σ_s^2 given in Eq. 2.17 or

$$\sigma_s^2 = \sigma_N^2\left[\alpha_{\bar{f}_s} + \sum_{i=1}^{\hat{n}}\sum_{j=1}^{\hat{n}} \omega_i\, \omega_j \rho_{ij} - 2\sum_{i=1}^{\hat{n}} \omega_i \rho_{iA}\right] \qquad \text{Eq. 6.2}$$

where σ_N^2 is the variance of all the boring data. The terms in the bracket represent the reduction in uncertainty due to 1) averaging ($\alpha_{\bar{f}_s}$ – Eq. 2.12) over foundation surface, line, etc.; 2) number of data values defining the mean (2nd) term (e.g., MIC station too few strength data, 2nd term is appreciable); and 3) conditioning of nearby data (3rd term – 17th Street Bridge, Jewfish Creek, etc., boring inside correlation length).

Using the kriging estimate of SPT blow count N (Eq. 6.1) with a random selection of residuals (Eq. 6.2), thousands of realizations of boring data within the footprint may be simulated. Subsequently, each of these realizations may be run with pile/shaft prediction software (FB-DEEP), and the resulting mean axial resistance and variability (spatial) as a function of depth may be found. Adding the uncertainty of spatial variability to the design method error, the total uncertainty of pile/shaft CV_R may be found from which LRFD $\bar{\phi}$ may be computed (Eq. 3.17). Multiplying the LRFD $\bar{\phi}$ by mean axial pile/shaft resistance, the design resistance is found. Assisting with the steps outlined is a graphical user interface (GUI) developed for this research and available for FDOT use.

6.3 Graphical User Interface (GUI) to Assess Pile/Shaft LRFD $\bar{\phi}$ and Design Resistance

The development of the GUI has proven to be an effective tool for the application of geospatial analysis for geotechnical engineering. Of great need is software to assess summary statistics (mean and variance) and correlation structure on a site for individual layers. Also, the software has the ability to simulate thousands of realizations of hypothetical boring data used as

input for the design software. Finally, the software analyzes the results (mean and uncertainty of foundation resistance). For subsequent use, the software must be easy to learn and deliver results in a timely manner.

Options for spatial analysis in "free" software were found to have tools missing (detrending, layer separation), which are typically needed for geotechnical engineering data. Also using software in a piecemeal fashion (i.e., layers) would significantly increase time when having to manually manipulate data in Excel for input files. Consequently, it was decided to develop independent GUI (not a function of design software, e.g., FB-DEEP) for pile/shaft design incorporating spatial and method uncertainty. Note, any changes to the design methods used by FB-DEEP will not require changes to the GUI. This ability for the GUI to be impartial to FB-DEEP changes is an advantage that can be expanded to other geotechnical design methodologies. With modification, the GUI can be used to generate parameters needed for other programs (FB-MultiPier, etc.) or geotechnical designs.

An important feature implemented in the GUI is the ability to handle large amounts of data, e.g., all site boring and laboratory data. This was made possible with the XML data format developed by FDOT ("In situ" and "Lab Test" Excel sheets) (fdot.ce.ufl.edu/applications.html) for the internet based database. For instance, the case of a single layer analysis (17^{th} Street Bridge, Jewfish Creek) the geospatial analysis only took a few minutes for properly formatted data. For sites with multiple layers, the analysis takes longer depending on selection of layer boundaries and variogram analysis (10-15 min). These times include the time for the 2000 or more FB-DEEP analyses of boring logs run in batch mode.

For all boring data associated with a layer (Profile Tab – detrending, etc.), a geostatistical analysis (Geostat Tab) is performed to determine summary statics (mean and CV) and variograms (a_v, a_h). For the cases which have small numbers of samples such that variograms

may not be inferred, the engineer can still proceed with a worst case a_v and a_h (resulting in conservative $\overline{\phi}$). With summary statistics and variogram models available, a pile/shaft analysis may be performed. Two options are available to the user: conditional (nearest boring) and unconditional analysis (all site data). In the case of conditional (Eqs. 6.1 and 6.2) are used as given; however, for unconditional, all borings are used and the pile/shaft is placed outside the correlation length (last term in Eq. 6.2 is zero). Thousands of borings are generated and FB-DEEP is run to determine axial pile/shaft mean predicted resistance R_N and variance (spatial uncertainty σ_s^2) as a function of depth. The use of batch mode process was selected over analytical solution as presented in **BD545-76** due to numerous models used by FB-DEEP and associated correlations between side and tip resistances.

6.4 Uncertainty of the Design Method and Bias Correction

Important with assessment of LRFD ϕ is the contribution of method error (σ^2) to the total uncertainty. Prior work (**BD545-76**) assumed that method error was 20% of site variability. However, this work focused on collecting site specific load test data with respective boring data to assess both random method error and bias correction. Sources of error contributing to σ^2 can be associated with measurement error of in situ testing, specific empirical relationships used to develop design calculations, spatial variability of properties used to predict resistance (non-collocated boring), and construction methods (deviations from geometry or poor construction).

Data from multiple FDOT databases and reports (e.g., prestressed concrete piles, drilled shafts, etc.) of measured and predicted pile/shaft capacities were analyzed. For a number of situations σ^2 resulted in being proportional to predicted resistances, e.g., concrete piles (Figure 3-4). In other cases σ^2values was found to be independent of the magnitude of the prediction, e.g., drilled shafts (Figure 3-2). For proportional σ^2, log transforms of measured and predicted

resistances were employed and both (e.g., piles and shafts) were fit with linear regressions to establish bias corrections. Unlike AASHTO (2004) bias λ_R which is assumed to pass through zero, both intercept a and slope b (Eq. 3.5) were used. The latter requires that LRFD ϕ (Eq. 3.16) has the bias λ_R set equal to one, which is referred to as $\overline{\phi}$ (Eq. 3.17). Subsequently, to find the design resistance, $\overline{\phi}$ is multiplied by the predicted resistance, which is already bias corrected (e.g., Tables 3-1 and 3-2) through both slope b and intercept a. Finally, knowing linear regression coefficients and correlation coefficients, the uncertainty of the methods were assessed either directly (Eqs. 3.5 to 3.8) through a constant value of σ^2 (e.g., shafts in rock) or through a constant coefficient of variation CV_ε (e.g., driven piles).

As identified earlier, the uncertainty of methods developed from legacy databases contained some spatial influences (i.e., nearest boring). To reduce this uncertainty, the use of site specific load tests with borehole data in the footprint (e.g., Jewfish Creek) is warranted. In addition at sites with low rock strength, a load test may be warranted since the legacy data has a higher relative strength (a higher σ_ϵ^2 was observed).

6.5 Discussion of Results

6.5.1 Florida Spatial Correlation

Of significant importance in LRFD $\overline{\phi}$ assessment are the variance of layer properties and spatial correlation in the vertical and horizontal directions. Seven sites were investigated for correlation lengths a_v and a_h. Shown in Table 6-3 are correlations computed for the sites. Evident in the table, all sites with the exception of MIC station had vertical correlation lengths measured. They varied from 4 ft (17^{th}) up to 11.8 ft (CR-12A). This variability has a significant influence on the expected variability of pile/shaft resistance from pier to pier. In the case of horizontal correlation, only one site (17^{th}) had borings close enough to establish a variogram that

resulted in reduced variability (Eq. 6.2, 3rd term). One site had insufficient property data to establish a vertical variogram (MIC station) and the worst case scenario (i.e., a_v is large) was assumed, resulting in a low LRFD $\overline{\phi}$ (0.38).

Table 6-3. Summary of Correlation Lengths Measured

Site	a_v [ft]	a_h [ft]	In situ Property
17th Street Bridge	4.00	12	q_u
Dixie Highway (per layer)	6.06	NA	SPT N
	11.06		
	11.08		
Jewfish Creek	7.25	NA	q_u
MIC/MIA	6.58	NA	q_u
MIC Station	NA	NA	q_u
CR12A	11.77	NA	SPT N

6.5.2 Assessment of LRFD $\overline{\phi}$ for Multiple Florida Sites

Presented in Table 6-4 is the summary of LRFD $\overline{\phi}$ values for the sites and the cases presented in Chapters 4 and 5. The table begins with the identification of site, then method of analysis (e.g., FB-DEEP – pile, McVay-drilled shaft), simulation type (conditional and unconditional), information known on site (correlation lengths, and load testing), lengths of pile/shaft analyzed, and the change in LRFD $\overline{\phi}$ for the lengths considered. Note, the LRFD $\overline{\phi}$ is normalized ($\lambda_R = 1$) and should be compared to FDOT and AASHTO (ϕ/λ_R) presented in Table 3-5 (piles 0.5, shafts 0.47 to 0.57 – non-redundant and redundant).

Evident from the sites and cases in Table 6-4, the computed $\overline{\phi}$ values are quite different from site to site, method of prediction (conditional or unconditional), spatial information, and method error. Components contributing to spatial uncertainty are point variability CV, correlation lengths a_v and a_h, and sampling amount. Point variability of in situ properties is

apparent from Tables 6-1 and 6-2. In a comparison of two sites with all parameters equal except CV, it would be found that $\overline{\phi}$ is lower for sites with higher CVs. It is important to note that every $\overline{\phi}$ listed in Table 6-4 is associated with a corresponding mean resistance R_N to be used for determining the design resistance $\overline{\phi}R_N$.

Table 6-4. Summary of Case Study Results

Site	Method	Sim Type	Case	Length [ft]	$\overline{\phi}$
17th Street Bridge	McVay	UC	a_v & a_h known	52 – 80* (0.5 – 28.5)**	0.17 – 0.64
		CON(B4)			0.16 – 0.62
		CON(B6)			0.16 – 0.68
Dixie Highway	FB-DEEP Driven Pile	UC	a_h unknown	20 – 75	0.36 – 0.58
		CON(EB1)			0.44 – 0.61
Jewfish Creek	McVay	UC	a_h unknown historical data	10 – 60 (2 – 52)	0.28 – 0.55
		CON(P10-S2)			0.30 – 0.52
		CON(P56-S3)			0.26 – 0.58
		UC	a_h unknown load test data		0.27 – 0.57
		CON(P10-S2)			0.31 – 0.55
		CON(P56-S3)			0.26 – 0.61
MIC/MIA	McVay	UC	a_h unknown	36 – 50 (0.5 – 14.5)	0.25 – 0.54
		CON(WB9)	a_h unknown		0.24 – 0.56
		UC	a_v & a_h unknown		0.25 – 0.39
MIC Station	McVay	UC	a_v & a_h unknown	37 – 65 (1 – 29)	0.32 – 0.46
			a_v & a_h unknown & uncertainty in mean		0.29 – 0.38
CR12A	FB-DEEP Driven Pile	UC	a_h unknown	20 – 70	0.15 – 0.58

UC – Unconditional simulation.
CON(Boring#) – Conditional simulation
* Length of shaft/pile from ground surface.
** (## – ##) – Embedment length in limestone layer.

Spatial correlation, i.e., correlation lengths a_v and a_h, are important in the foundation design, since they represent how large a strong or weak zone is on average relative to the foundation being considered. If the engineer is unable to measure the scale of spatial correlation,

then the worst case must be selected, which assumes the weak or strong zones are of a size greater than the dimensions of the foundation. Typical correlation lengths in Florida for case studies are presented in Table 6-3. Quantifying spatial correlation increases the resulting $\overline{\phi}$ as illustrated by the MIC/MIA example, where $\overline{\phi} = 0.54$ with a_v known and $\overline{\phi} = 0.39$ with a_v unknown.

Besides the extents of weak and strong zones, the engineer must also prove that the in situ sampling was adequately performed, ensuring that the mean and variance of site data are well defined. If few samples are taken or are located relatively close to one another when compared to correlation lengths, larger uncertainty in the mean of the site results (2nd term, Eq. 6.2). This influence was illustrated by the MIC Station Case (only 18 rock strength samples). In that case, if uncertainty of the mean is ignored, $\overline{\phi} = 0.46$; however, if uncertainty of mean is accounted for, then the LRFD $\overline{\phi} = 0.38$.

For the case studies in Table 6-4, the method error σ_ϵ^2 had a varying level of influence on the final $\overline{\phi}$ computed for a site. For the site that exhibited high site variability σ_s^2 through either high CVs or worst case assumptions (e.g., MIC station), it was found that little difference in $\overline{\phi}$ was found from site variability versus total uncertainty (spatial + method uncertainty). However, for cases where spatial variability has been minimized (e.g., 17th Street Bridge), the method error has a larger impact on $\overline{\phi}$. Also, of importance are cases where mean axial resistance are small (e.g., Jewfish Creek) and a fixed legacy method error is employed σ_ϵ^2 which includes high strength sites. For low mean resistance sites, load testing should result in a reduction of σ_ϵ^2 and an improvement in $\overline{\phi}$.

For driven piles, a higher variability of $\overline{\phi}$ versus depth was observed; however, there are exceptions, e.g., piles entering layers with very high point variability CV. This is primarily due to multiple layers each having their own independent summary statistics and correlations

structures (Dixie Highway and CR12A). It was observed, however, that $\overline{\phi}$ was significantly higher when the pile was embedded in a strong limestone layer. This is due to the strong layers having lower CVs for SPT N than overlying soil.

6.6 Recommendations to Improve Design

With multiple case studies considered, the following recommendations are made for engineers to improve $\overline{\phi}$ for a site:

1. Obtain adequate number of samples to accurately quantify statistical parameters (mean and CV) for the layers significantly contributing to foundation capacity.
2. Collect enough samples at intervals of 2 to 5 ft to provide enough data pairs to accurately infer the experimental vertical variogram.
3. If spatial uncertainty still results in low $\overline{\phi}$, make improvements by either splitting the site into zones (presence of high CVs and zonal anisotropy in variograms) or using more layers for separate geospatial analysis.
4. In the case of sites with non-redundant foundations, soil/rock with high-point variability, large vertical correlation structure, and no planned load testing, use more borings spaced closer to identify horizontal correlation (e.g., identification of mean at pier, etc.)
5. With spatial uncertainty minimized, make improvements to the method error through load testing at the site of interest; however, enough measured versus predicted data points must be collected for regression analysis.
6. Consider load tests on sites where low rock strengths are recorded, since the developed method error σ_{ϵ}^2 was for the case of medium to high strength rock.

Finally, a major component of improving $\overline{\phi}$ due to spatial and method uncertainty is to make sure all data (in situ, lab, and load test) collected for a site is used in the site analysis. To help account for the many different measurements (SPT N, q_u, q_t, gamma, etc.) having data in standard format is recommended. The latter can be accomplished by uploading any data collected to the FDOT's geotechnical database and using the GUI in conjunction with the design software.

REFERENCES

AASHTO. (2004). *LRFD Bridge Design Specifications*, 3rd ed. Washington, D.C.: American Association of State Highway and Transportation Officials (AASHTO).

Bloomquist, D., McVay, M., and Hu, Zhihong. (2007). Updating Florida Department of Transportation's (FDOT) Pile/Shaft Design Procedures Based on CPT and DTP Data. (*FDOT Report BD 545-43*). Tallahassee, FL: Florida Department of Transportation.

Brustamante, M. & Gianeselli, L. (1982). Pile bearing capacity prediction by means of static penetrometer, CPT. *Proceedings 2nd European Symposium on Penetrometer Testing*, Vol. 2, 493-500.

Deutsch, C. V. (2002). *Geostatistical Reservoir Modeling*. New York, NY: Oxford University Press.

Deutsch, C. V., and Journel, A. G. (1992). *GSLIB – Geostatistical Software Library and User's Guide*. New York, NY: Oxford University Press.

Elkateb, T., Chalaturnyk, R., and Robertson, P. K. (2003). An Overview of Soil Heterogeneity: Quantification and Implications on Geotechnical Field Problems. *Canadian Geotechnical Journal*, vol. 40, pp. 1–15.

Emery,X. 2007. Conditional Simulations of Gaussian Random Fields by Ordinary Kriging. *Mathematical Geology*, vol. 39, no. 6, pp. 607–623.

Fenton, G. A., and Griffiths, D. V. (2005). Three-Dimensional Probabilistic Foundation Settlement. *Journal of Geotechnical Engineering*, vol. 131, no. 2, pp. 232–239.

Fenton, G. A., Griffiths, D. V., and Zhang, X. Y. 2008. Load and Resistance Factor Design of Shallow Foundations Against Bearing Failure. *Canadian Geotechnical Journal*, vol. 45, no. 11, pp. 1556–1571.

Goovaerts, P. (1997). *Geostatistics for Natural Resources Evaluation*. New York, NY: Oxford University Press.

Hassan, K. M., O'Neill, M. W., Sheikh, S. A., and Ealy, C. D. (1997). Design Method For Drilled Shafts in Soft Argillaceous Rock. *Journal of Geotechnical Engineering*, vol. 123, no. 3, pp. 272–280.

Isaaks, E. H., and Srivastava, R. M. (1989). *An Introduction to Applied Geostatistics*. New York, NY: Oxford University Press.

Journel, A. G., and Huijbregts, C. J. (1978). *Mining Geostatistics*. San Diego, CA: Academic Press.

Kitanidis, P. K. (1997). *Introduction to Geostatistics: Applications to Hydrogeology*. New York, NY: Cambridge University Press.

Klammler, H., McVay, M., Horhota, D., and Lai, P. (2010a). Influence of Spatially Variable Side Friction on Single Drilled Shaft Resistance and LRFD Resistance Factors. *Journal of Geotechnical and Geoenvironmental Engineering*, vol. 136, no. 8, pp. 1114–1123.

Klammler, H., McVay, M., Lai, P., and Horhota, D. (2010b). Incorporating Geostatistical Aspects in LRFD Design for Deep Foundations. In: *GeoFlorida 2010: Advances in Analysis, Modeling and Design*. E. O. Fratta, B. Muhunthan, and A.J. Puppala, eds., ASCE Geotechnical Special Publication N^{o} 199.West Palm Beach, FL: American Society of American Engineers (ASCE). ISBN 978-0-78441-095-0, CD-ROM.

McVay, M., Badri, D., and Hu, Z. (2004). Determination of Axial Pile Capacity of Prestressed Concrete Cylinder Piles. (*FDOT Report BC 354-60*) . Tallahassee, FL: Florida Department of Transportation.

McVay, M., Ellis, R., Kim, M., Villegas, Kim, S., and Lee, S. (2003). Static and Dynamic Field Testing of Drilled Shafts: Suggested Guidelines on Their Use for FDOT Structures. (*FDOT Report BC 354-08*). Tallahassee, FL: Florida Department of Transportation.

McVay, M., Klammler, H., Bloomquist, D., Otero, J., and Faraone, M. (2009). Modifications of LRFD Resistance Factors Based on Site Variability. (*FDOT Report BD545-76*). Tallahassee, FL: Florida Department of Transportation.

McVay, M., Kuo, C., and Singletary, W. (1998). Calibrating Resistance Factors in the Load and Resistance Factor Design for Florida Foundations. (*FDOT Report BA512*). Tallahassee, FL: Florida Department of Transportation.

Menard, L., Baguelin, F., and Shields, D. (1972). *The Pressuremeter and Foundation Engineering.* Trans Tech Publications, Clausthal, Germany.

O'Neill, M. W., Townsend F.C., Hassan, K. M., Buller, A., and Chan, P.S. (1996). Load Transfer for Drilled Shafts in Intermediate Geomaterials. (*FHWA-RD-95-1 72*). Washington, D.C.: Federal Highway Administration (FHWA).

Paikowsky, S. (2004). Load and Resistance Factor Design (LRFD) for Deep Foundations. (*NCHRP Report 507*). Washington, D.C.: National Cooperative Highway Research Program (NCHRP).

Poulos, H. G., and Davis, E. H. (1972). *Pile Foundation Analysis and Design*. New York, NY: John Wiley and Sons.

Schmertmann, J.H. (1978). Guidelines for cone penetration test, performance and design. (*FHWA-TS-78-209*). Washington, D.C.: U.S. Department of Transportation.

Styler, M. (2006). Development and Implementation of the DIGGS Format to Perform LRFD Resistance Factor Calibration of Driven Concrete Piles in Florida. Gainesville, FL: University of Florida.

Terzaghi, K., Peck, R.B. (1967). *Soil Mechanics in Engineering* Practice, 2nd ed. New York, NY: John Wiley and Sons.

Ueshita, K., and Meyerhof, G. G. (1967). Deflection of Multilayer Soil System. *Journal of Soil Mechanics and Foundations Division, ASCE*, vol. 93, no. SM5, pp. 257–282.